SSL-105

AFOSR SCIENTIFIC REPORT
ASOSR-69-1224TR

AD 689294

A STUDY OF THE METAL-SEMICONDUCTOR (N-TYPE) RECTIFYING CONTACT

TECHNICAL REPORT NO. 1

by

Hugh Allen Lindsey

and

Thomas A. DeMassa

May 1969

F44620-69-C-0025

JUN 20 1969

Reproduced by the
CLEARINGHOUSE
for Federal Scientific & Technical
Information Springfield Va. 22151

This document has been approved for public release
and sale; its distribution is unlimited

199

DISCLAIMER NOTICE

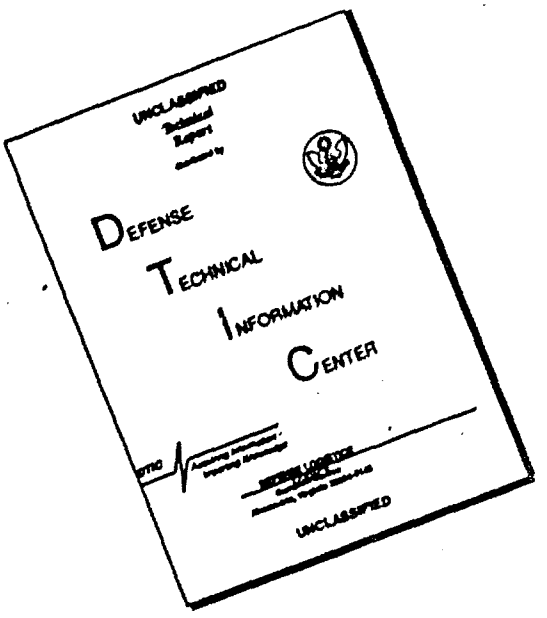

THIS DOCUMENT IS BEST QUALITY AVAILABLE. THE COPY FURNISHED TO DTIC CONTAINED A SIGNIFICANT NUMBER OF PAGES WHICH DO NOT REPRODUCE LEGIBLY.

CONDITIONS OF REPRODUCTION

Reproduction, translation, publication, use and disposal in whole or in part by or for the United States Government is permitted.

ACCESSION
CFSTI
DDC
JUSTI
BY
DISTRIBUTION
DIST.

Qualified requestors may obtain additional copies from the Defense Documentation Center, all others should apply to the Clearinghouse for Federal Scientific and Technical Information.

ABSTRACT

A theoretical study of metal-semiconductor (N-type) rectifying contacts is developed. This study begins by first analyzing previous models for this type of junction. Particular attention is given to the Schottky model and to the approximations it contains. This model is then improved upon by taking into account nonuniform impurity ionization and the free electron concentration in the depletion region. Using this more exact model a theoretical expression for the differential junction capacitance is calculated. The results indicate that the junction capacitance as a function of reverse bias can be used to accurately predict the doping concentration in the semiconductor material, but does not yield a correct measurement of the equilibrium diffusion potential or barrier height.

The current voltage characteristic for this type of contact is also discussed. An expression for the I-V characteristic of this junction is derived based upon a diffusion model. This expression is then improved upon by accounting for tunneling and quantum-mechanical reflection of carriers at the junction.

TABLE OF CONTENTS

CHAPTER		PAGE
I.	INTRODUCTION.	1
	1.1 Outline of this Study.	1
	1.2 Historical Survey.	1
II.	THEORY RELATING TO METAL-SEMICONDUCTOR SYSTEMS	6
	2.1 Energy Band Diagram of a N-Type Semiconductor.	6
	2.2 Formation of a Potential Barrier at an Idealized Metal-Semiconductor Contact .	14
	2.3 Effect of Charged Surface States on the Contact Barrier.	18
	2.4 Influence of an Externally Applied Bias Voltage on a Contact Barrier	23
	2.5 Influence of an Image Force on a Contact Barrier.	27
	2.6 Influence of Tunneling and Quantum-Mechanical Reflection on a Contact Barrier.	34
III.	THE SCHOTTKY MODEL FOR A METAL-(N-TYPE)-SEMICONDUCTOR RECTIFYING CONTACT.	40
IV.	A MORE ACCURATE MODEL FOR THE IDEALIZED METAL-(N-TYPE)-SEMICONDUCTOR RECTIFYING CONTACT	54
V.	METHODS OF DETERMINING THE EQUILIBRIUM BARRIER HEIGHTS OF METAL-(N-TYPE)-SEMICONDUCTOR CONTACTS: A COMPARISON OF THE MODELS OF CHAPTER III AND CHAPTER IV. . . .	78

CHAPTER PAGE

VI. CURRENT-VOLTAGE CHARACTERISTICS OF A METAL-SEMICONDUCTOR RECTIFYING CONTACT. 94

VII. SUMMARY, CONCLUSIONS, AND RECOMMENDATIONS FOR FURTHER STUDY 123

REFERENCES 132

APPENDIX A. The Mott Model of a Metal-Semiconductor Rectifying Contact 137

APPENDIX B. The Bethe Model of a Metal-Semiconductor Rectifying Contact 141

APPENDIX C. An Approximation for the QMTC of a Parabolic Potential Barrier. 147

APPENDIX D. Additional Comments on the Degree of Ionization (γ). 150

APPENDIX E. Verification of Equation 4.32 as the Solution to Equation 4.27. 154

APPENDIX F. The Runge-Kutta Method for Numerical Integration. 156

APPENDIX G. A Typical Computer Solution. 169

LIST OF FIGURES

FIGURE		PAGE
2.1	Energy Diagram for a N-Type Semiconductor. . . .	7
2.2	Energy Diagram for a Free (N-Type) Semiconductor Surface.	9
2.3	Summary of Depletion Region Conditions for a Barrier Formed at the Free Surface of a N-Type Semiconductor.	13
2.4	Formation of a Metal-Semiconductor Contact . . .	15
2.5	Energy Diagram for a Metal-Semiconductor Contact with Applied Bias Voltage; Image Force Neglected.	25
2.6	Potential Diagram for Image Effects.	30
2.7	Lattice Model Used to Calculate the Image Force Correction Factor at Small Distances . . .	32
2.8	Influence of Image Effects on the Energy Diagram for a Metal-Semiconductor Contact. . . .	35
2.9	QMTC Plot for an Au-GaAs Contact	39
3.1	Energy Diagram for a Metal-Semiconductor Contact.	41
3.2	Summary of Depletion Region Conditions of a Metal-Semiconductor Contact Based on the Schottky Model	49
4.1	Detailed Energy Diagram for a Metal-Semiconductor Contact Under Reverse Bias	55
4.2	Computer Solutions for the Normalized Electron Potential and Space Charge Density Based on the More Exact Model (y_o=60).	66

FIGURE PAGE

4.3 Computer Solutions for the Normalized Electron Potential and Space Charge Density Based on the More Exact Model (y_o=20). 69

4.4 Influence of Image Effects on the Normalized Electron Potential Based on the More Exact Model. 76

5.1 Energy Diagram for Photoexcitation Measurement . 80

5.2 Spectral Response of a Metal-Semiconductor Contact. 81

5.3 Photoresponse of an Au-CdSe Contact. 83

5.4 Barrier Height Measurements for an Au-Ge Contact. 86

5.5 Normalized Junction Capacitance Plot Based on the More Exact Model. 89

6.1 Energy Diagram for a Metal-Semiconductor Contact. 99

6.2 Theoretical f_q Plot for an Au-GaAs Contact . . . 105

6.3 Straight Line Approximation for the QMTC 108

6.4 Current-Voltage Characteristic for a Pt-Si Contact. 117

6.5 Equilibrium Diffusion Potential Dependence of Several Metal-Si Contacts 120

6.6 Temperature Dependence of an Au-Si Contact . . . 121

6.7 Image Force Dependence of the Reverse Characteristic of an Au-Si Contact 122

A.1 The Mott Model for a Metal-Semiconductor Contact. 138

FIGURE PAGE

B.1 The Bethe Model for a Metal-Semiconductor Contact. 142

B.2 Comparison of Junction Capacitance Plots Based on the Bethe and Schottky Models 145

C.1 Energy Diagram used for the Calculation of the QMTC 148

LIST OF SYMBOLS

A	Cross sectional area
C_j	Junction capacitance per unit area
D_n	Diffusion constant for electrons
E	Electric field strength
E_a	Activation Energy as defined by Eq. 6.6.6
E_b	Equilibrium barrier height as seen by an electron at E_{fm}
E_b'	Energy correction needed for image effects
E_c	Lowest energy of the conduction band
E_{cd}	Lowest energy of the conduction band in the depletion region
E_{co}	Lowest energy of the conduction band in the bulk semiconductor
E_d	Energy level associated with donor impurities
E_e	Kinetic energy of an electron
E_{fm}	Energy corresponding to the Fermi level in a metal
E_{fs}	Energy corresponding to the Fermi level in a semiconductor
E_g	Energy gap associated with a semiconductor ($E_g=E_c-E_v$)
E_h	Energy difference as shown in Fig. 2.2
E_i	Ionization energy for donor impurities
E_l	End-point energy as shown in Fig. 6.3
E_n	Energy level occupied by an electron

E_c Electric field strength at the metal-semiconductor interface (x=0)

E_r End-point energy as shown in Fig. 6.3

E_s Energy corresponding to eV_s, where V_s is the surface potential at the free surface of a semiconductor

E_{ss} Highest filled energy level associated with surface states at a free semiconductor surface

E_v Highest energy of the valence band

E_{vd} Highest energy of the valence band in the depletion region

E_{vo} Highest energy of the valence band in the bulk semiconductor

E_1 Arbitrary kinetic energy associated with an incident electron as shown in Fig. C.1

F_c Coulomb attractive force as defined by Eq. 2.4.1

I_n Electron diffusion current

I_o Reverse leakage current neglecting quantum-mechanical and image effects

I_{or} Reverse leakage current as defined by Eq. 6.6.7

I_o' Reverse leakage current including quantum-mechanical and image effects as defined by Eq. 6.5.2

I_o'' Reverse leakage current considering avalanche multiplication

I_r Reverse current as defined by Eq. 6.6.7

I_t Total electron current

I_{so} Reverse current ($I_o' e^{-eV_d/KT}$) neglecting avalanche multiplication

J_p Photocurrent per unit area

M Avalanche multiplication factor as defined by Eq. 6.5.2

L Length of the semiconductor

N	Experimentally determined constant for avalanche multiplication
N_c	Effective density of states in the conduction band
N_d	Density of donor impurities
N_d^+	Density of ionized donor impurities
Q_w	Stored charge within the depletion region
QMR	Quantum-mechanical reflection
QMRC	Quantum-mechanical reflection coefficient
QMTC	Quantum-mechanical transmission coefficient
R	Photoresponse
V	Potential with respect to the bulk semiconductor
V_a	Bias voltage of arbitrary polarity
V_b	Potential barrier height as seen by an electron in the metal; image force neglected
V_{br}	Reverse breakdown voltage due to avalanche multiplication
V_d	Equilibrium diffusion potential; image force neglected
V_{bm}	Potential barrier height (V_b) including image effects
V_{ds}	Diffusion potential (V_d) including image effects
V_{dso}	Equilibrium diffusion potential (V_d) including image effects
V_f	Forward bias voltage
V_j	That portion of the bias voltage which appears across the metal-semiconductor contact
V_o	Intercept voltage on a $(k_3/C_j)^2$ versus V_r plot
V_r	Reverse bias voltage
V_s	Surface potential at the free surface of a semiconductor
W	Equilibrium depletion region width

X_e	Electron affinity of a semiconductor
a	Dummy variable as used in Eq. 5.13
d	Distance of separation between the semiconductor and metal prior to contact
e	Magnitude of electronic charge
f	Frequency (cps)
f_e	Fermi probability factor for electrons
f_o	Frequency corresponding to Eb/h
f_q	Ratio of I_t to I_n
g	Lattice spacing
k_1	Constant as defined by Eq. 4.26
k_2	Constant as defined by Eq. 5.11
k_3	Constant as defined by Eq. 5.5
l_1	Lower limit of integration as used in Eq. C.4; shown in Fig. C.1
l_2	Upper limit of integration as used in Eq. C.4; shown in Fig. C.1
m	Slope of $(k_3/C_j)^2$ versus V_r curve
m_e	Electron mass
m_e^*	Effective mass of an electron
m_h	Hole mass
m_h^*	Effective hole mass
m_v	Slope as defined by Eq. 6.6.3
n	Electron density
n_c	Density of free electrons contributed by ionized donor impurities in the bulk semiconductor
n_{cd}	Density of free electrons contributed by ionized donor impurities in the depletion region

n_i Equilibrium electron density in an intrinsic semiconductor

n_o Equilibrium electron density in a N-Type semiconductor

p Hole density

r Thickness of the insulating layer in the Bethe model

s Momentum of an electron

u Normalized distance parameter as defined by Eq. 4.26

x Distance parameter as shown in Fig. 2.2

x_o Arbitrary position of an electron from a metal-semiconductor interface on the semiconductor side of the junction

x_m Distance at which $\beta(x)$ is maximum

y Normalized electron potential as defined by Eq. 4.25

y_b' Normalized image force correction factor as defined by Eq. 4.47

y_o Normalized electron potential at $x=0$

z Dummy variable as defined by Eq. 4.33

Ω Interval size used in numerical integration

Σ Dummy variable used in Runge-Kutta method

α_b Voltage dependent reduction in the equilibrium diffusion potential due to image effects

α_{bo} Variable as defined by Eq. 6.3.4

α_c' Variable as defined by Eq. 6.3.5

α_1 Dummy variable used in Runge-Kutta method

β Total negative electron potential within the depletion region with respect to the bulk semiconductor

β' Negative electron potential within the depletion region with respect to the bulk semiconductor

β'' Negative electron potential with respect to the bulk semiconductor due to image effects

β_{ij} Dummy variable used in Runge-Kutta method

β_m Maximum value of $\beta(x)$

γ Degree of ionization as defined by Eq. 4.14

δ Experimentally determined constant to account for nonideal nature of the contact; defined by Eq. 6.6.5

ϵ_o Permittivity constant for free space

ϵ_r Relative dielectric constant

ϵ_s Dielectric constant of a semiconductor, $\epsilon_s = \epsilon_o \epsilon_r$

ϵ_s' High frequency dielectric constant of a semiconductor

ϵ_s^o Ratio of ϵ_s' to ϵ_s

θ Dummy variable used in Runge-Kutta method

λ Wavelength in meters

λ_e Mean free path of an electron

ρ Space charge density

ϕ_m Thermionic work function of a metal

ϕ_s Thermionic work function of a semiconductor

$\phi_m - \phi_s$ Contact potential difference

ψ Electron wave function

CONSTANTS

Å	Angstrom: 10^{-8} cm
e	Electronic charge: $1.60(10^{-19})$ coul
h	Planck's constant: $6.63(10^{-34})$ joule-sec
$\hbar$	Planck's constant/2π: $1.504(10^{-34})$ joule-sec
K	Boltzmann's constant: $1.38(10^{-23})$ joule/^{o}K
ϵ_o	Permittivity constant for free space: $8.85(10^{-12})$ farad/m
m_e	Rest mass of an electron: $9.11(10^{-31})$ kg

CHAPTER I

INTRODUCTION

1.1 Outline of this Study.

The purpose of this study is to examine the Schottky model for a metal-(N-Type)-semiconductor contact, paying particular attention to the approximations made which limit its accuracy. The assumptions made which limit accuracy are removed and a more exact model proposed, although with great sacrifice in simplicity. Poisson's equation based on the more exact expression for space charge becomes nonlinear, but with the aid of numerical techniques solutions are obtained. These solutions result in more exact expressions for the usual contact parameters than those predicted by the Schottky model and comparisons between the two theories are made. Finally, the current-voltage relations for the contact are discussed and an expression derived for the I-V characteristic of the junction based on a diffusion model.

1.2 Historical Survey.

The earliest systematic studies dealing with rectifying systems are generally attributed to Braun.[1] Beginning in 1874, Braun used a variety of natural crystals to which he applied base electrodes of various forms and a point contact.

He then studied the dependence of the total resistance of the device on the polarity of the applied voltage and on the detailed surface conditions in the region of the point contact. It was also Braun who first noted that the rectification process was located at the contact itself, but he was unable to offer a general theory which could predict his findings.

Possibly the first studies dealing with the current-voltage character of rectifying systems were done by Pierce[2] in 1910. He too used natural crystals and studied the nature of the rectification process by an oscillographic technique. However, he was also unable to offer a general explanation for what he had observed.

Point contact rectifiers similar to those studied by Braun and Pierce found wide application in the early days of radio telegraphy as detectors, but were not generally understood and satisfactory devices could not be consistently produced. Although a wide variety of rectifying systems were known and the general properties of each categorized, their application always necessitated an adjustment of the point contact ("whisker" as it was popularly known) to find a sensitive spot and frequent readjustment in order to maintain useful rectification.

The development of a successful theory for rectifying systems was the natural result of Wilson's[3] interpretation of semiconduction based on the band theory of solids, which

was first presented in 1931. As a first attempt at a general explanation for rectification, it was believed that tunneling was responsible for the principal character. Wilson[4] was the first to offer a quantitative expression for the current-voltage relation at the contact based on tunnel theory. His results produced reasonable numerical agreement with rectification ratios observed on cuprous oxide rectifiers; however, it was later pointed out by Davydov[5] that tunnel theories predict a polarity of rectification which is opposite to the direction actually observed. This alone was sufficient cause to abandon the tunnel effect as an explanation for rectification, although other discrepencies also became apparent.

In 1932, Waibel and Schottky[6] suggested that a blocking layer of nearly stoichiometric composition at the rectifying contact on a cuprous oxide rectifier was responsible for the rectifying character. In 1938, Mott[7] incorporated a form of blocking layer along with the effects of electronic diffusion and an electric field to develop a theoretical model which could explain rectification. The Mott barrier (See Appendix A), as it became known, extended throughout the semiconducting crystal and was to be a special case of a more general theory developed by Schottky. In 1939, Schottky[8] suggested that the barrier associated with the rectification phenomena could arise from stable space charges in the semiconductor and the presence of a chemically distinct layer

was not necessary to explain its existence. Furthermore, these charges arose from the presence of the metal. Consistent with the concept of stable space charges, Schottky devised a model which could predict a voltage dependent rectifier capacitance and barrier thickness and could give reasonable agreement with experimental results. In 1942, Schottky[9] presented a final quantitative version of his theory and also assessed some of its apparent limitations. To date, the Schottky model is generally accepted as the approximate model for rectifying contacts. Also in 1942, a model was presented by Bethe,[10] which was similar to the Schottky version, but differed in that it incorporated a thin interfacial layer of insulating material and a slightly different mechanism for charge transport. (See Appendix B for a complete analysis of the Bethe model.)

The common characteristic of all models developed thus far was the strong dependence on the difference of the thermionic work function of the metal and semiconductor. However, experiments conducted on rectifying systems of silicon and germanium had failed to show this dependence. The apparent inconsistency was not explained until 1947, when Bardeen[11] proposed a different mechanism of barrier formation, which was dependent on an electrical double layer at the free-surface of the semiconductor. Bardeen's theory was able to show that the presence of such a layer tends to make the properties of the contact independent of the work

functions of the two materials. However, Bardeen's theory does not appreciably alter the properties of the Schottky model and the exact effects of Bardeen's theory will be deferred to a later section.

CHAPTER II

THEORY RELATING TO METAL-SEMICONDUCTOR SYSTEMS

2.1 Energy Band Diagram of a N-Type Semiconductor.

In order to establish a common framework in which a discussion of the Schottky model will be meaningful, this chapter will deal with the more general theory relating to metal-semiconductor systems. Also, it is of importance to note that in this chapter, as well as those which follow, all discussions will be limited to metal-(N-Type)-semiconductor systems and any reference to "semiconductor" is meant to imply N-Type unless specifically stated otherwise.

First, consider the energy band diagram of an infinitely long semiconductor as shown in Fig. 2.1. This diagram shows the relative positions of energy levels which will be of interest in future discussions. Here ϕ_s represents the energy required to transfer an electron at the Fermi level of the semiconductor (E_{fs}) into free space. The quantity ϕ_s is generally referred to as the thermionic work function and will be a function of the position of the Fermi level. Since E_{fs} is a function of other properties of the semiconductor and will, in general, not remain a constant, another energy will be defined to represent the energy

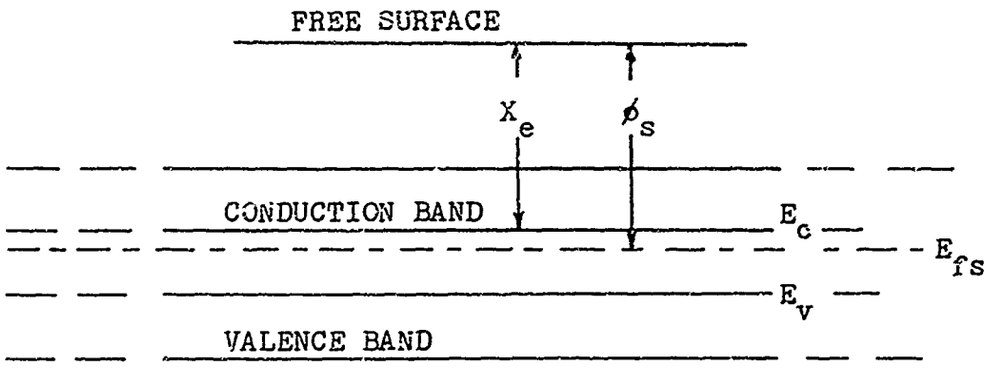

FIGURE 2.1: Energy Diagram of an Infinitely Long N-Type Semiconductor.

required to transfer an electron from the bottom of the conduction band (E_c) to free space. This quantity is called the electron affinity and will be denoted by X_e.

Next, consider the modification imposed on the band structure due to an abrupt termination of the semiconductor crystal. Figure 2.2 shows the band structure of a free semiconductor surface. The distortion noted, or band bending, is due to the presence of surface states or allowed levels of occupancy which extend into the energy gap (E_g); the levels being localized at the surface. Since the semiconductor is N-Type, the distortion in band structure at the surface has created an effective P-Type layer, i.e., the same effect could have been produced if acceptor impurities had been indiffused from the free surface. Thus, a P-N junction has been formed, and due to the polarity of the surface potential (V_s) the conduction band has somehow been depleted of electrons.

What causes the surface potential? If one examines the physical situation at an abruptly terminated crystal surface the explanation becomes apparent. Here the valence structure of the crystal is disturbed since the normal bonding pattern can no longer be maintained and "dangling bonds" or unused valences are present at the surface. Schockley[12] has made a detailed study of how these surface states arise from atomic levels and under what conditions they may be expected to appear. His general conclusion is that one discrete

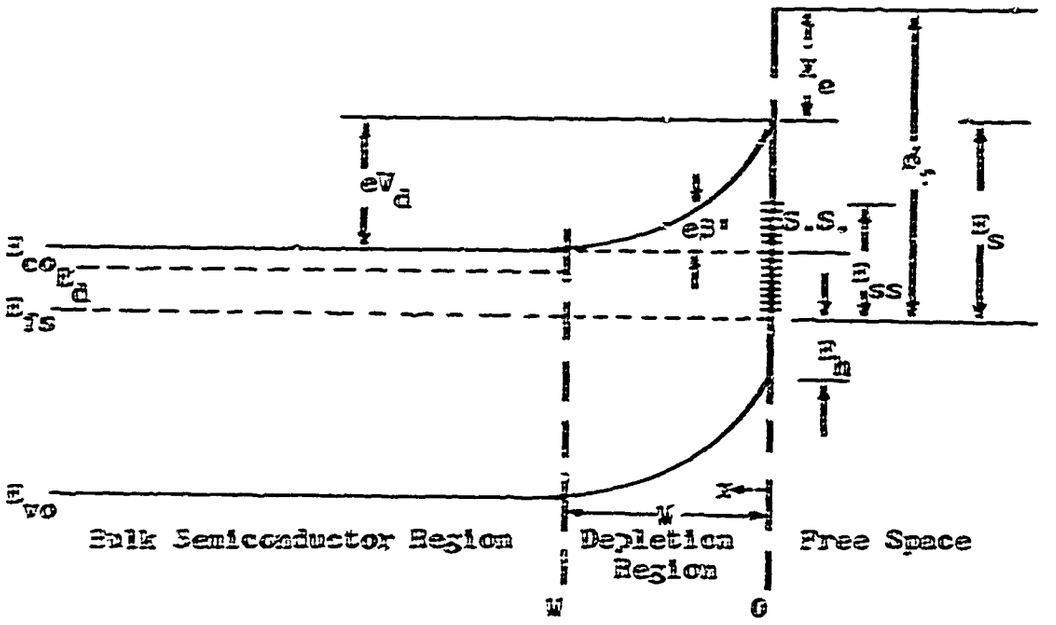

FIGURE 2.2: Energy Diagram for a Free (N-Type) Semiconductor Surface. Surface States Denoted by S.S.

surface state, or unused valence, can be expected for each surface atom if the lattice spacing of the original crystal structure is sufficiently small. These states form a quasi-continuum over an energy range within the bandgap and are half filled when the surface is charge neutral.

There are additional factors which can contribute to distortion in the bands at the free surface. One could imagine that some of the surface atoms could indeed be those of donor impurities and could thus donate electrons to empty surface states. Still another contribution could be due to any lattice disturbance at the free surface, and possibly the presence of vacancies or other lattice imperfections.

The important point to be made with regard to surface states is that they permit additional levels of occupancy within the bandgap and give rise to a potential barrier at the free surface. Under equilibrium conditions some of the electrons of the semiconductor will occupy the empty surface states at the free surface, resulting in a localized negative charge. Since some electrons are now missing from the conduction band in the vicinity of the free surface, the semiconductor must assume a net positive charge and because of the dimensions involved, this charge may be considered as localized and continuous within the region $0<x<W$. The region $0<x<W$ represents an inversion layer and is usually referred to as a depletion region since the electron concentration in this region is essentially depleted. In

addition, the positive charge associated with this region causes the band structure to become distorted as shown in Fig. 2.2. The potential denoted by V_d is commonly referred to as the diffusion potential or equilibrium barrier height and $\delta'(x)$ will be used to represent the negative potential of an electron at any point within the depletion region relative to the bulk semiconductor.

Next, consider the sources of the positive charge associated with the depletion region:

(1) The donor energy levels, denoted by E_d, within the depletion region are above the Fermi level and are either completely ionized or at least more ionized than those located in the bulk semiconductor. Within the depletion region there will be a net positive charge contributed by each uncompensated, ionized and immobile* donor site.

(2) Since the electron density in the conduction band decays rapidly with increasing energy, there will be a deminishing number of free electrons as x decreases. Furthermore, if $eV_d \gg KT$ then the region $0<x<W$ will be almost uniformly depleted of electrons, except in the vicinity of $x=W$. Thus, one must conclude that near $x=0$ (free surface)

---

*Impurities are decidedly immobile in semiconductor crystals below a temperature of 200-300 °C;[13] thus ionized donor sites can be regarded as immobile below these temperatures.

the positive space charge is essentially eN_d^+ while near $x=W$ the availability of conduction electrons would offer a compensating effect. For $x \geq W$ the net positive charge must of course be zero, since in the bulk semiconductor no net charge is observed.

(3) A final contribution of positive space charge can be attributed to the fact that in the region near the free surface there can be an additional concentration of minority carriers, since the valence band edge is relatively near the Fermi level. However, if one considers a relatively wide bandgap semiconductor and/or sufficient doping levels, then $E_h \gg kT$ and this additional contribution of positive charge by minority carriers can be neglected.

The above considerations are summarized in Fig. 2.3. The distributions shown are only approximate relationships based on the above discussion, but the concepts involved will be very useful in developing a more exact mathematical model which will be undertaken in a later chapter.

In Fig. 2.3c and Fig. 2.3d the depletion region has been divided into two approximate regions to emphasize the nature of charge distribution in these areas. Region B includes the area near the surface and in this region the ionized donor atoms are the primary contributor to space charge. Region A is an area in which the ionized donor atoms are partially compensated by electrons of the conduction band. In this region the net charge density is a function

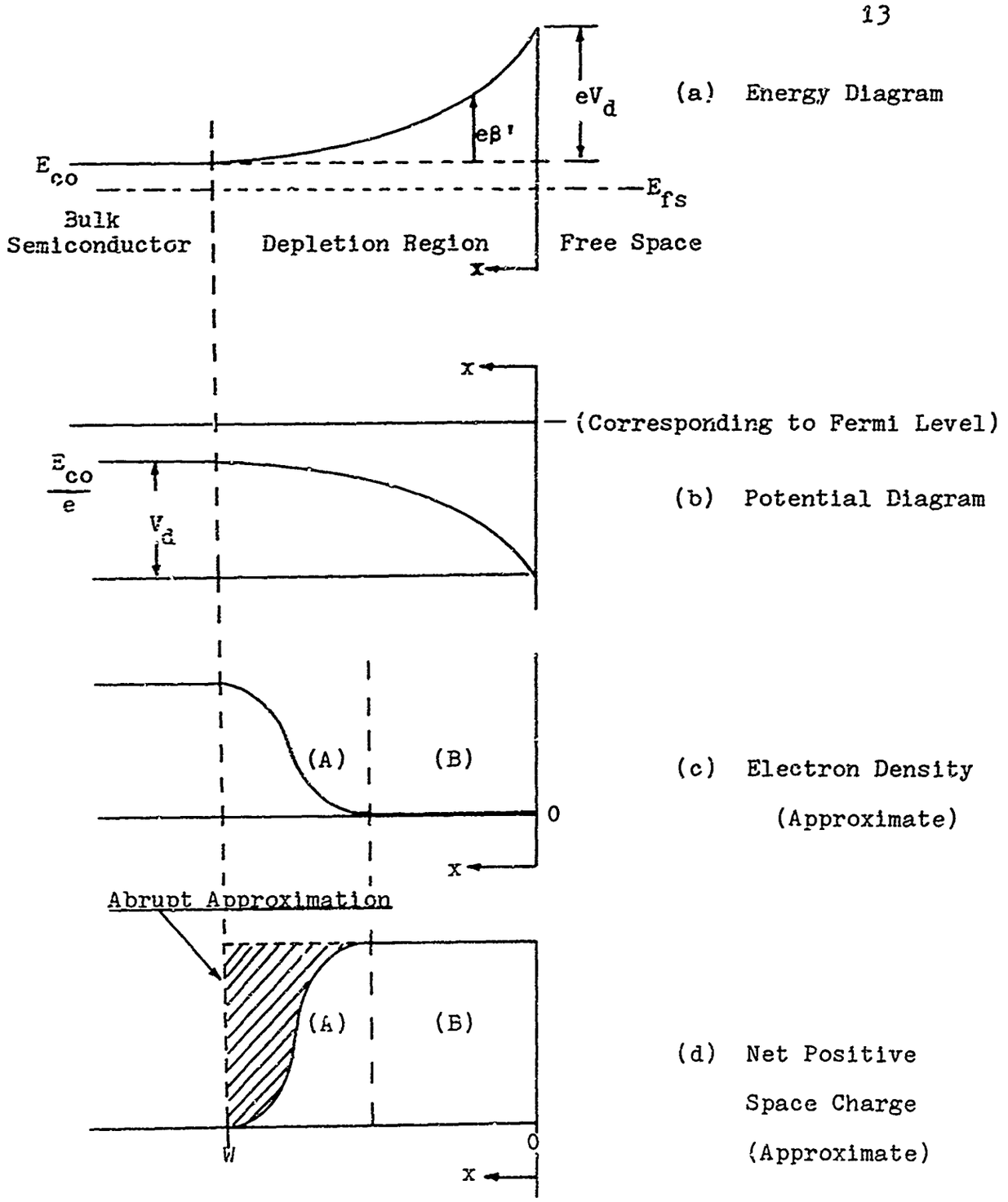

FIGURE 2.3: Summary of Depletion Region Conditions for a Barrier Formed at the Free Surface of a N-Type Semiconductor.

of the distance x. Furthermore, the barrier potential will influence this distribution since Region B may disappear entirely unless the barrier is sufficiently high. By sufficiently high it is meant that the barrier must be high enough to act effectively as a barrier to conduction electrons, i.e., $V_d \gg KT/e$.

2.2 Formation of a Potential Barrier at an Idealized Metal-Semiconductor Contact.

When a metal is brought into intimate contact with a semiconductor, a simple rectifying contact may be formed. The condition necessary for rectifying character is that the work function of the metal (ϕ_m), defined in the same manner as for a semiconductor, exceeds that of the semiconductor (ϕ_s). This situation insures the existence of a potential barrier to electrons which in turn is responsible for the rectifying nature of the contact. Also, the contact formed may be considered idealized, since the unnecessary complications introduced because of nonuniform contact, surface defects and the presence of surface contaminants will be neglected. Furthermore, for the present, the effects of surface states will also be neglected.

The formation of such a simplified, rectifying contact is shown in Fig. 2.4. In Fig. 2.4a the energy band diagrams of the two materials are shown as they would exist if both materials were freshly cut and the distance of separation (d)

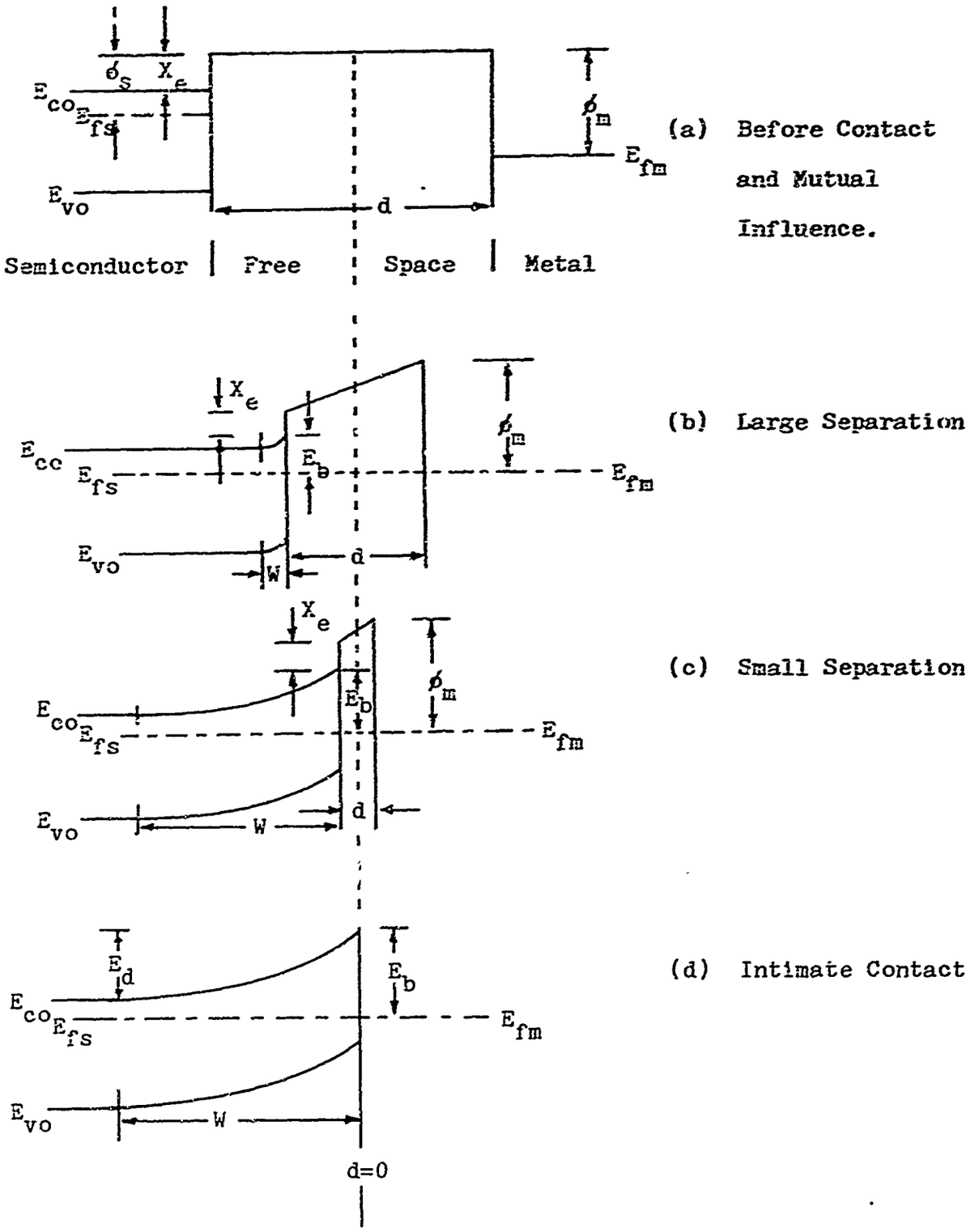

FIGURE 2.4: Formation of a Simple, Rectifying Metal-Semiconductor Contact.

is large enough so that any interaction between the metal and semiconductor is inhibited. In Fig. 2.4b the metal and semiconductor are allowed to establish thermal equilibrium with a third medium which is not shown, but would be located between the two surfaces. Once a continuum is formed and thermal equilibrium is established, the fact that no net current can flow requires that the probability of occupancy at any given energy level must be the same throughout the continuum; thus, the Fermi levels of the two materials must align.* Furthermore, if the Fermi level of the semiconductor is assumed to remain constant (an arbitrary reference point), then the Fermi level of the metal must rise relative to that of the semiconductor by an amount equal to the difference of the two work functions, i.e., $\phi_m - \phi_s$.

In Fig. 2.4c the surfaces are brought closer together. As d is decreased there will be an increasing negative charge built up on the surface of the metal. This buildup of electrons is the result of the conduction band of the

---

*From the thermodynamic point of view, the Fermi level represents the chemical potential of an electron in the solid. Thus, when a continuum is formed, the chemical potential of the mobile electrons, and hence the Fermi level of the materials involved, must be the same.

semiconductor being at a higher energy level than the Fermi level of the metal, causing some electrons of the semiconductor to diffuse into the metal. Furthermore, the electrons which leave the semiconductor will be forced to reside on the surface of the metal since the metal is already saturated with free electrons and is an equipotential medium. Thus, the electron supply of the conduction band is depleted near the semiconductor surface, which in turn produces uncompensated donor sites and a net positive space charge to form. Also, as the difference in charge between the two materials is formed an electric field is produced which opposes further electron transfer to the metal.

As d is diminished further, Fig. 2.4c, the depletion region widens (W increases) and the potential barrier is increased. One should note that E_b will remain small as long as d is fairly large, since most of the potential drop is across the gap between the two materials. Finally, as d approaches zero and intimate contact is made, Fig. 2.4d, an equilibrium state will be reached as soon as the electric field at the contact prevents any further electron diffusion from the semiconductor.

Once equilibrium is established, a limiting value of the barrier potential (V_b), diffusion potential (V_d), and depletion region width (W) will be reached; clearly, the limiting value of the barrier potential will be

$$V_b=(\phi_m-X_e)/e \qquad (2.2.1)$$

and for the diffusion potential,

$$V_d=(\phi_m-\phi_s)/e \qquad (2.2.2)$$

Thus, in the absence of surface states, the equilibrium value of the potential barrier for electrons in the metal will be the difference of the metal work function and the electron affinity of the semiconductor, whereas the height of the potential barrier to electrons in the semiconductor will be the difference of the two work functions. The quantity $\phi_m-\phi_s$ is sometimes called the contact potential difference.

2.3 Effect of Charged Surface States on the Contact Barrier.

The equilibrium model for a metal-semiconductor contact discussed in the previous section has neglected the presence of surface states at the free surface of the semiconductor. Clearly, if these surface states are present in sufficient quantity and charged to a substantial degree, one must expect some alteration in the nature of the contact, at least to the extent of altering the equilibrium barrier height at the contact.

When the barrier is formed in the same manner as discussed earlier (Fig. 2.4) an electric field will exist at the junction of the two surfaces. The establishment of this electric field requires electric charge in the two materials, which must increase as the distance of separation decreases. However, in the presence of surface states there is an additional mechanism by which this charge may be accommodated within the semiconductor. In addition to the positive charge caused by uncompensated donor sites, there may also be a charge associated with the surface charge induced in surface states present at the free surface of the semiconductor. The density of these surface states and the amount of charge they are able to accommodate will determine the amount of space charge due to donor sites and thus influence the depletion width. In addition, one can no longer expect the barrier height to be given by a simple difference of the work function and electron affinity of the semiconductor; instead, it may well be independent of these quantities and depend solely on the barrier resulting from charged surface states.

The influence of charged surface states on the potential barrier at a metal-semiconductor contact is summarized best by giving the conclusions of Bardeen[11] in a classic paper presented in 1947. His conclusions will be presented in the discussion which follows.

If the density of surface levels with energies which

fall in the bandgap is sufficiently high (greater than 10^{12} /cm^2, approximately), there will be an electrical double layer formed at the free surface of a semiconductor. This double layer is formed from the negative charge associated with the charged surface states and the positive space charge associated with the uncompensated donor sites within the semiconductor. This double layer tends to make the work function of the semiconductor independent of the height of the Fermi level in the bulk region, and thus independent of the impurity concentration.

The total strength of the double layer at a metal-semiconductor junction will be fixed by the difference in chemical potentials, and thus dependent on the bulk properties of the metal and semiconductor. As a consequence, the strength of the double layer is independent of the work functions of the material surfaces before contact is made.

The double layer consists of the following parts:

(1) A double layer of atomic dimensions at the metal surface.

(2) A double layer of atomic dimensions at the semiconductor surface.

(3) A double layer formed from the surface charges on the metal and semiconductor, both of atomic dimensions.

(4) A double layer formed from the surface charge of atomic dimensions and a space charge extending to a depth of 10^{-6} to 10^{-4} cm into the semiconductor.

The strengths of the double layers may be estimated as follows:

(a) If the density of surface energy levels is sufficiently high (greater than 10^{13} /cm^2, approximately), the double layer of (4) above will be the same as that for the free surface of the semiconductor. The rectification properties will then be largely independent of the work function of the metal, since the difference in contact potentials is compensated by the double layer of (3) above.

(b) If the density of surface energy levels is small (less than 10^{13} /cm^2, approximately), then the double layer of (3) above will be small, and the double layer of (4) above will be determined by the difference in material work functions.

(c) If the contact between the metal and semiconductor is very intimate, it may not be possible to distinguish between the double layers of (1), (2), and (3) above. The metal will then tend to broaden the surface energy levels, but if this broadening is small compared to the energy gap of the semiconductor, then conclusion (a) above will still be valid.

(d) If the broadening of the surface energy levels by the metal is large, then no conclusions about the space charge of the semiconductor can be drawn from measurements of contact potential differences. Furthermore, it is possible for all the conditions of (a), (b), (c), and (d) above to be

physically realizable.

Since Bardeen's paper, there has been extensive research done in the area of surface states, both from an experimental and theoretical approach, in an effort to be able to predict their influence on an arbitrary metal-semiconductor system. Mead[14] has compiled a great deal of the work done on surface states and concludes that an arbitrary metal-semiconductor system may be classified into two broad classes: (1) a surface state controlled system, and (2) a system in which the influence of surface states may be neglected. Furthermore, his preliminary conclusions indicate that the nature of surface state control for an arbitrary metal on an arbitrary semiconductor may be predicted from the nature of the bonding mechanism in the semiconductor.

When a metal-semiconductor system is surface state controlled, a reasonable approximation for the barrier height (E_b) would be E_{ss}, where E_{ss} is the highest filled energy level of the surface states when the free surface of the semiconductor is charge neutral. For the Group IV and III-V semiconductors the values of E_{ss} can be shown to agree quite closely to the relation[15]

$$E_{ss}=E_c-(2/3)E_g \qquad (2.3.1)$$

or the value of the barrier height is approximately two-thirds of the bandgap energy (E_g). (See Fig. 2.2)

When the metal-semiconductor system behaves as if no surface states were present then the value of E_b would be determined by the difference of the metal work function and the electron affinity of the semiconductor. In both cases it has been assumed that the metal-semiconductor contact represents an intimate contact between two clean and uniform planar surfaces.

2.4 Influence of an Externally Applied Bias Voltage on a Contact Barrier.

The discussion presented thus far has dealt entirely with equilibrium conditions. If an external voltage is applied to the device this equilibrium is upset and one would expect the potential difference between the two sides of the junction to be influenced by the external voltage. Furthermore, one would expect the depletion region to contract if the potential has been decreased and to expand if the potential difference has been increased. Clearly then, the equilibrium model is no longer applicable in the presence of an externally applied voltage and must be modified to include this influence.

When an external voltage is applied to the device a current will flow and the total voltage must be the sum of the contact potential and the voltages associated with the bulk resistance and ohmic contact of the semiconductor. In most cases, at least for reverse bias and low values of

forward bias, the electric field associated with the bulk semiconductor is small and may be neglected along with the voltage drop associated with the ohmic contact.

The following notation will be adopted in discussions concerning bias and contact voltages:

(1) V_a will be used to refer to a bias voltage of arbitrary polarity.

(2) V_f will be used for V_a when V_a corresponds to a forward biased condition of the device.

(3) $-V_r$ will be used for V_a when V_a corresponds to a reverse biased condition of the device.

(4) V_j will be used to refer to that part of the bias voltage which appears across the contact barrier. Under reverse bias conditions $V_j \approx V_r$ and under forward bias conditions $V_j = V_f -$(the voltage drops associated with the bulk resistance and ohmic contact of the semiconductor, when these are not negligible).

Figure 2.5 shows the influence of V_a on the energy diagram of a metal-semiconductor contact. If the Fermi level of the metal is taken as a reference and assumed to remain constant, then eV_a corresponds to the displacement between the Fermi levels of the respective materials. It should also be noted that the height of the barrier, as seen by conduction electrons of the semiconductor, increases when V_a is positive (relative to the metal) and decreases when V_a is negative. Since opposition to current flow increases

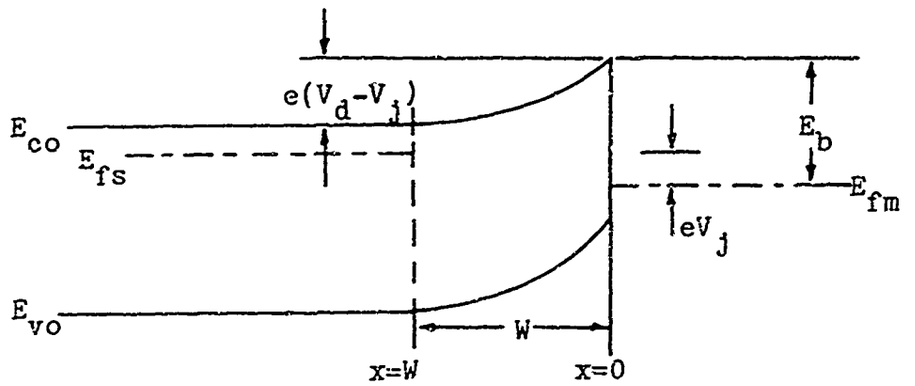

FIGURE 2.5a: Energy Diagram for a Metal-Semiconductor Barrier under Forward Bias Conditions; Image Force Neglected.

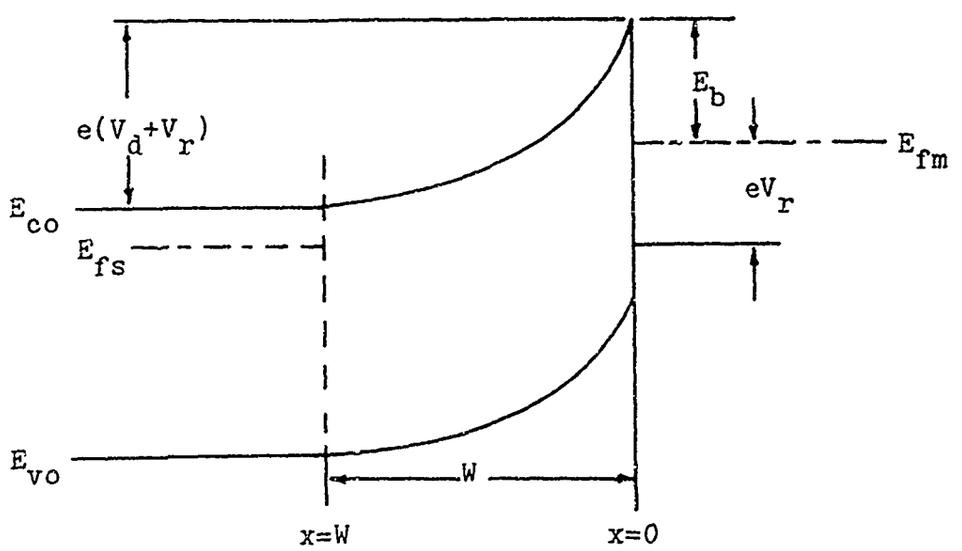

Bulk Semiconductor | Depletion Region | Metal

FIGURE 2.5b: Energy Diagram for a Metal-Semiconductor Barrier under Reverse Bias Conditions; Image Force Neglected.

when the barrier increases, a positive V_a (with respect to the metal) will correspond to a reverse bias and a negative V_a to a forward bias. The height of the barrier (E_b) as seen from the metal is assumed to remain constant since the influence of any image force (discussed in the next section) has been neglected in the diagram.

The two basic assumptions on which Fig. 2.5 is based is that the charge within the depletion region is not appreciably disturbed by the current flowing and equilibrium conditions are maintained within the bulk region of the semiconductor and in the metal. If this last assumption is valid then the Fermi levels in the bulk semiconductor and in the metal are uniquely defined. Within the depletion region the Fermi level cannot be uniquely defined, since when a current is flowing injection of free carriers prevents equilibrium from being established. The Fermi level can, however, be represented in the form of a quasi-Fermi level which represents the electrochemical potential for holes and electrons separately as a function of the distance into the depletion region. These quasi-Fermi levels can then be used to indicate a reference for holes and electrons within the depletion region; however, since the quasi-levels are not required for the analysis herein they will be omitted from Fig. 2.5 and no position for the Fermi level is indicated within the depletion region ($0<x<W$).

2.5 Influence of an Image Force on a Contact Barrier.

In order to demonstrate the influence of an image force, consider an electron approaching a metal-semiconductor contact and on the semiconductor side of the junction. This electron will be under the influence of a potential which exists inside the depletion region as well as the influence of a Coulomb attractive force as it approaches the metal surface. This attractive force arises from the presence of an electron in close proximity to the metal surface. It is a well known fact that an electron of charge -e at a distance x_o from the metal surface will induce an image charge of +e at a distance $-x_o$ inside the surface[16] and these equal but opposite charges are then responsible for the attractive force which pulls the electron toward the metal surface. This force is called, quite appropriately, an image force and is responsible for lowering the potential energy of a conduction electron in the vicinity of the metal surface. This use of the conventional image force is based on the assumption that the semiconductor is acting as a polarizable medium without free charge carriers,[17] and seems a valid assumption since the electron concentration near the junction is almost exhausted of electrons for reasons previously discussed.

The reduced potential of an electron in the vicinity of the potential barrier near a metal surface requires an alteration of the potential barrier near a metal-semi-

conductor junction. Since the potential energy is effectively reduced, the band edges must bend down in the vicinity of the metal surface and eventually the potential of the electron must remain some finite and constant value within the metal surface. It is important to note that this reduction in barrier height (eV_d) will be independent of the way in which the ultimate barrier height (without image effects) was determined, i.e., whether it was determined by the difference $\phi_m - \phi_s$, by surface states, or a combination of both. Furthermore, the presence of image effects explains the apparent discontinuity of electron potential at the metal surface, since with the presence of an image force the electron potential is no longer discontinuous but must decay over some finite distance near the junction.

The potential due to image effects can be calculated from the laws of electrostatics, if one assumes that the semiconductor acts as a polarizable medium free of charge carriers within close proximity of the metal surface. If an electron of charge -e is at a distance x from the metal surface, then by Coulomb's law the force of attraction (F_c) is

$$F_c = \frac{e^2}{4\pi\epsilon_s'(2x)^2} = \frac{e^2}{16\pi\epsilon_s' x^2} \qquad (2.4.1)$$

where ϵ_s' denotes the high frequency value of ϵ_s.* The potential energy $[e\beta''(x)]$ associated with this force is the integral of the force from the point x_o (the point at which the particle is located) to infinity, so that

$$e\beta''(x_o)=\int_{x_o}^{\infty}F_c(x)dx = \frac{-e^2}{16\pi\epsilon_s' x_c} \qquad (2.4.2)$$

One immediately notes that Eq. 2.4.2 cannot be valid as $x_o \rightarrow 0$, since it predicts an infinite potential when $x_o=0$ (see Fig. 2.6) and the potential of an electron at. or inside the metal surface must have some finite value. This apparent inconsistency arises from the approximation inherent in Eq. 2.4.1, i.e., that the distance of separation (x_o) is large compared to the atomic spacing of the metal ions. For distances of separation on the order of, or less than a few atomic diameters the electron is most strongly influenced by metal ions closest to it. The total effective induced image charge is still +e; however, the force of attraction caused by this induced charge is due to many components, each of which is derived from the neighboring metal ions.

---

*The high frequency dielectric constant must be used when dealing with image effects since electrons are moving so fast in the region near the metal surface that dipole and ionic polarization of the lattice does not occur.

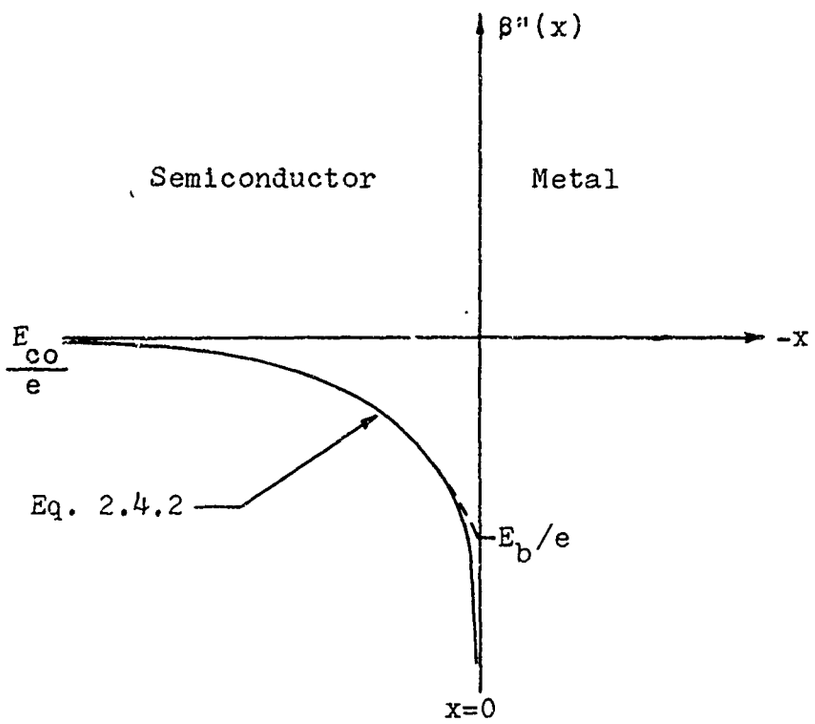

FIGURE 2.6: The Potential of an Electron Due to the Image Force at a Metal-Semiconductor Junction.

Therefore, a more accurate model for the force (Eq. 2.4.1) is needed when x becomes small and in order to model such a force the lattice structure of the metal must be known.

In order to demonstrate model dependence, consider a simple cubic structure and an electron approaching the four ions forming one face along a line passing through the mid-point of the face (see Fig. 2.7). Since the total effective charge is +e, each ionic charge component will be taken to be one-fourth of the electron charge. The total force (F_c) will then be the vector sum of the force of attraction resulting from each ion, or

$$F_c = \frac{e^2 x}{4\pi\epsilon_s'(x^2+g^2/2)^{3/2}} \qquad (2.4.3)$$

where g is the interatomic spacing as shown in Fig. 2.7. The potential energy of an electron due to image effects is again found by integration, or

$$e\beta''(x_o) = \int_{x_o}^{\infty} F_c(x)dx = -\frac{e^2}{4\pi\epsilon_s'(x_o^2+g^2/2)^{\frac{1}{2}}} \qquad (2.4.4)$$

One should note that for $x_o >> g/2$, $e\beta''(x_o)$ will reduce to

$$e\beta''(x_o) \approx -\frac{e^2}{4\pi\epsilon_s' x_o} \qquad (x_o >> g/2) \qquad (2.4.5)$$

which agrees with Eq. 2.4.2 except for a factor of $\frac{1}{4}$. This

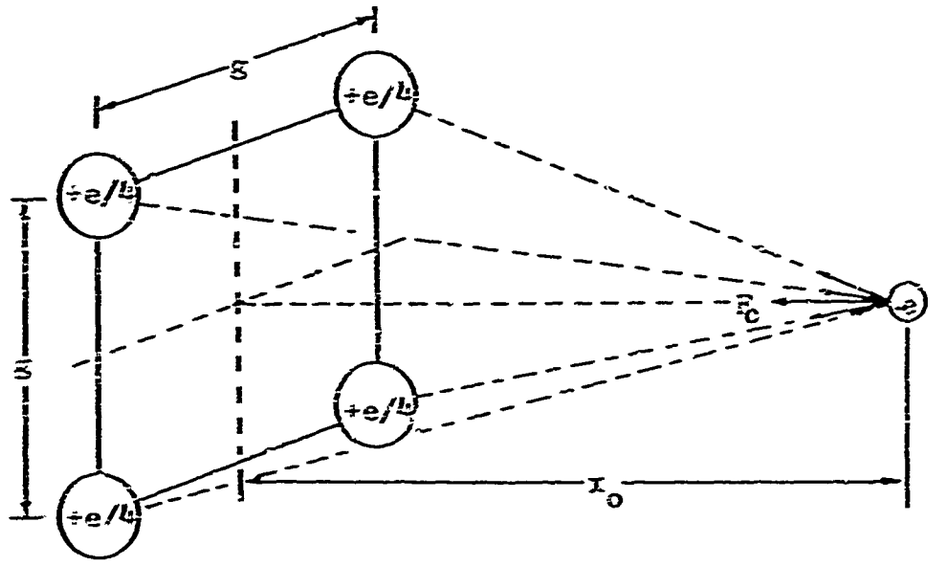

FIGURE 2.7: Lattice Model Used to Calculate the Image Force Correction Factor as $x \rightarrow 0$.

factor of $\frac{1}{4}$ arises from the approximation that only the four nearest-neighbor ions exert an influence on the approaching electron. Also of importance is the fact that Eq. 2.4.4 is finite at $x_o=0$, i.e.,

$$e\beta''(0) = \frac{-e^2}{(2)^{3/2}\pi\epsilon_s' g} \qquad (2.4.6)$$

Equation 2.4.6 states that the magnitude of the surface potential should be inversely proportional to the interatomic spacing in the metal. This point is borne out by experimental findings for the surface potential at a free surface of the alkali metals[18] (Cs, Rb, K, Na, and Li) and would indicate that Eq. 2.4.6 would be the appropriate, although approximate, expression for the potential of an electron very near ($x_o \ll g/2$) a metal-semiconductor contact.

Of primary interest is the point at which the total potential of the electron is maximum and this maximum will occur where the image force on the electron exactly balances the force on it due to the electric field which exists in the depletion region. Furthermore, this maximum should occur at a distance which is greater than g, since the major decrease in electron potential, as predicted by Eq. 2.4.4, will occur within a very few interatomic distances of the metal surface. Thus, one can conclude that Eq. 2.4.2 should be used to approximate the upper limit for the correction actually required for image effects and the corrected barrier

potential should appear as indicated in Fig. 2.8. The total electron potential $\beta(x)$, as shown in Fig. 2.8 results from the addition of $\beta'(x)$ as shown in Fig. 2.3 and $\beta''(x)$ as predicted by Eq. 2.4.2 for $x \geq x_m$, or by Eq. 2.4.4 as $x \rightarrow g$. The quantity E_b' is used to denote the approximate correction needed for image effects and x_m is used to denote the point at which the maximum value of $\beta(x)$ occurs. Appropriate expressions for these parameters will be deferred to a later section until an expression for $\beta'(x)$ has been calculated.

2.6 Influence of Tunneling and Quantum-Mechanical Reflection on a Contact Barrier.

The "tunnel effect" arises from a quantum-mechanical analysis of the situation in which a particle is incident upon an energy barrier whose height exceeds the kinetic energy of the particle. Classically, the particle would be reflected; however, quantum-mechanically the particle has a finite probability of passing through the barrier. Quantum-mechanical reflection (QMR) arises from a similar analysis of the situation in which a particle is incident upon an energy barrier whose height is less than the kinetic energy of the particle. Classically, the particle would pass over the barrier; however, quantum-mechanical analysis predicts that there is a finite probability that the particle will be reflected.

Both of these quantum-mechanical effects must be

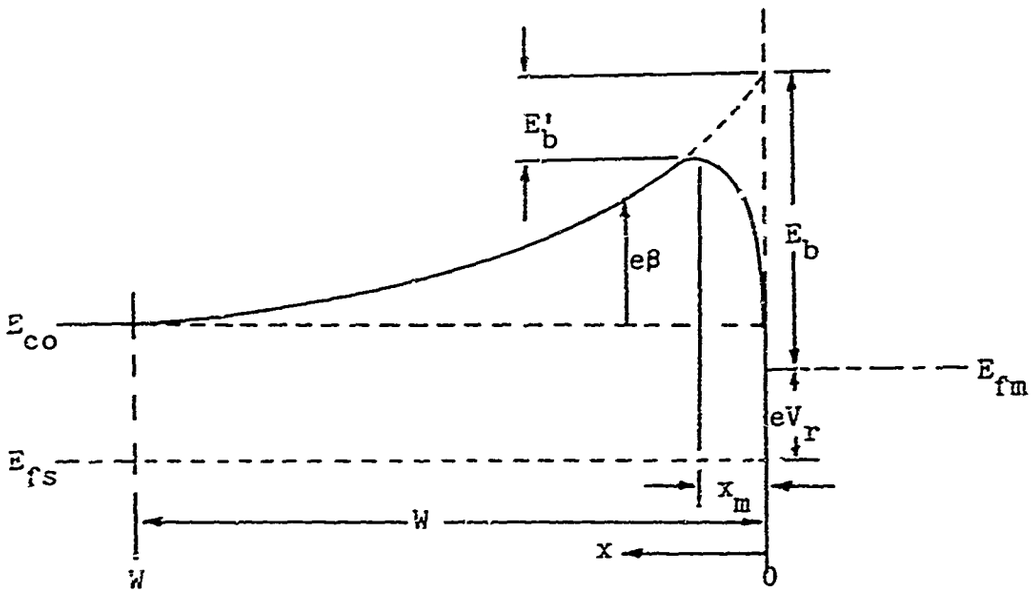

FIGURE 2.8: Lowering of the Potential Barrier Due to the Presence of an Image Force.

considered in the analysis of the carrier transport properties of a metal-semiconductor contact. The conditions which govern the behavior of an incident electron on the potential barrier associated with the contact can be determined from the solutions of Schroedinger's wave equation. These solutions would be functions exhibiting wave character and would depend on the electric potential in which the electrons are moving. The amplitudes of the transmitted and reflected waves could be inferred from the continuous nature of the wave function and its instantaneous spatial derivative and a comparison of these amplitudes would in turn provide a means of measuring tunneling and QMR.

The usual procedure when considering the influence of quantum-mechanical effects on an energy barrier is to introduce the concept of a quantum-mechanical transmission coefficient (QMTC). The QMTC for a potential barrier is defined as the ratio of the number of electrons crossing a unit area per unit time in the incident and transmitted waves. Similarly, one could define a quantum-mechanical reflection coefficient (QMRC) such that

$$QMRC = 1 - QMTC \qquad (2.6.1)$$

and would thus represent the ratio between the number of electrons in the incident and reflected waves on a per unit basis.

Kemble[19] has outlined a method for approximating the QMTC of a parabolic potential barrier in terms of the momentum of a particle incident from the side corresponding to the bulk semiconductor. The assumed form of the barrier (parabolic) could be used to account for the presence of electron image effects and would make this method directly applicable to estimating the QMTC of a metal-semiconductor contact. The results of Kemble's approximation technique are given in Appendix C.

Crowell and Sze[20] have considered the problem of calculating the QMTC of the potential barrier at a metal-semiconductor contact directly by using numerical techniques to solve Schroedinger's wave equation. The QMTC is calculated as a function of the carrier energy and effective mass, the high frequency dielectric constant of the semiconductor and the shape of the potential barrier in the vicinity of the point where the conduction band edge in the semiconductor merges into the conduction band edge in the metal. The mathematical treatment involves numerically solving the one-dimensional, time independent wave equation of the form

$$\frac{d^2\psi}{dx^2} + \frac{2m_e^*}{\hbar^2}\left[E_e(x)-e\beta(x)\right]\psi = 0 \qquad (2.6.2)$$

where $E_e(x)$ is the electron kinetic energy, m_e^* is the effective mass and $e\beta(x)$ is the potential energy perturbation introduced by the barrier. In addition to assuming that

the electrons are incident normal to the barrier (one-dimensional form of Eq. 2.6.2) it is assumed that m_e^* can be approximated as an average effective mass with different isotropic effective masses in the metal and semiconductor. Furthermore, the image potential (β'') is assumed to have the form as given by Eq. 2.4.2 so that the potential barrier can be approximated by

$$\beta(x)=\beta'(x)+\beta''(x) \qquad (2.6.3)$$

for sufficiently large x.

A typical result using the method of Crowell and Sze is shown in Fig. 2.9. Their general conclusion is that a QMTC$\gtrsim$0.5 can be expected for an electron incident on the barrier with energy greater than 0.05 ev with respect to the barrier maximum.* Furthermore, the QMTC increases slowly with increasing energy and is a rather strong function of the electric field at the metal-semiconductor interface. Figure 2.9 also shows that tunneling for this particular barrier can be appreciable for electric fields exceeding 10^4 v/cm.

Tunneling and QMR will be considered again in Chapter VI when carrier transport across the barrier is discussed in greater detail.

---

*Kemble's method[19] predicts a QMTC of approximately 0.5 for electrons with the same energy as the top of the barrier.

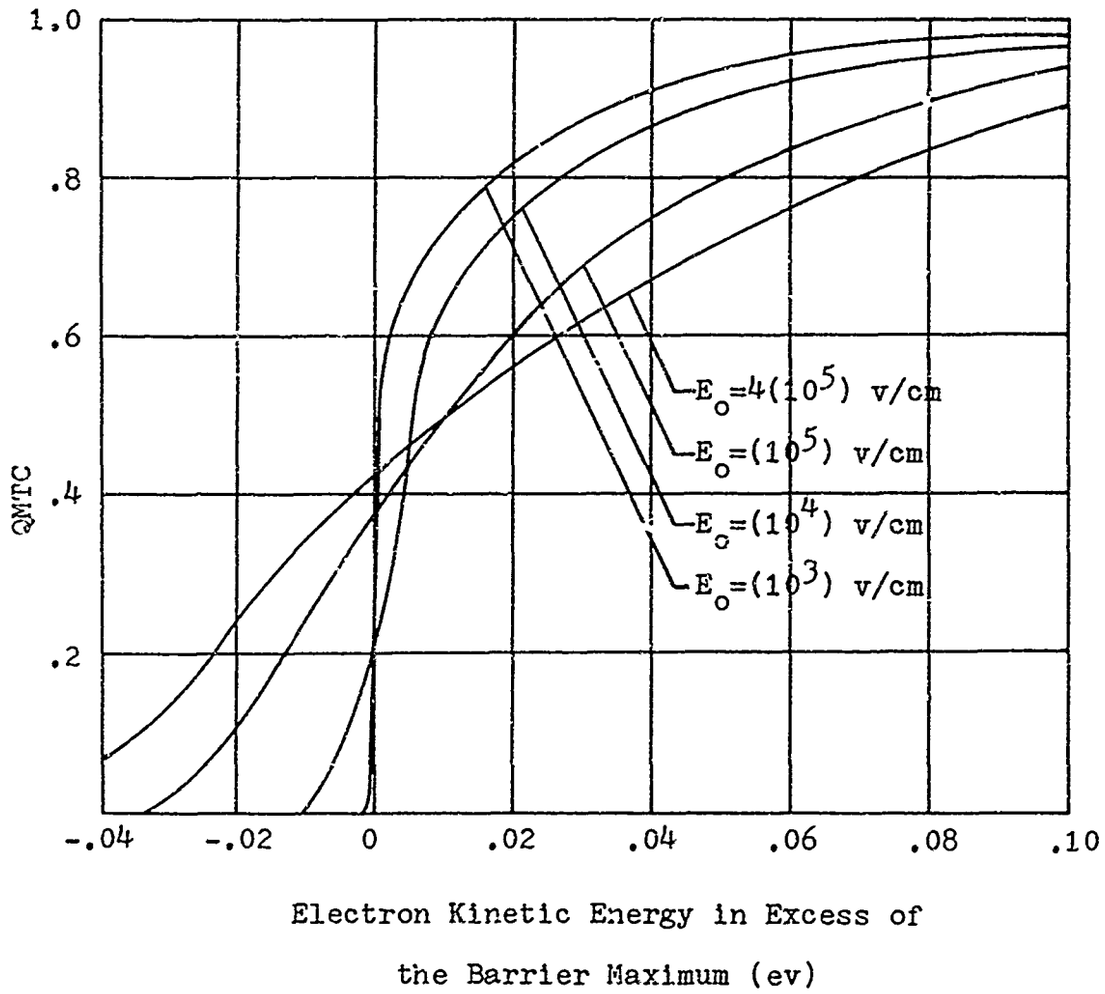

FIGURE 2.9: Quantum-Mechanical Transmission Coefficient for a Au-GaAs (N-Type) Contact as a Function of Electron Kinetic Energy Relative to the Barrier Height for Selected Electric Field Strengths at the Contact.[20]

CHAPTER III

THE SCHOTTKY MODEL FOR A METAL-(N-TYPE)-SEMICONDUCTOR RECTIFYING CONTACT

This chapter will deal primarily with a mathematical treatment of the Schottky model[9] for a metal-semiconductor contact. Basically, the model consists of assuming a constant charge density in the depletion region of the semiconductor and by using Poisson's equation an estimate of the electric field and potential can be obtained. The assumptions on which the model is based will receive particular attention as a preliminary step to the development of a more exact model which will follow in the next chapter. In addition, image effects will be introduced and an expression derived for the junction capacitance predicted by the Schottky model.

The energy band diagram for a metal-semiconductor contact is shown in Fig. 3.1a. It is basically the same as Fig. 2.5b and is repeated here for convenience. It should be noted that the influence of an image force has been neglected and also that the junction should be considered an idealized contact since the effects of lattice imperfections, nonuniform contact and the presence of surface contaminants will be neglected.

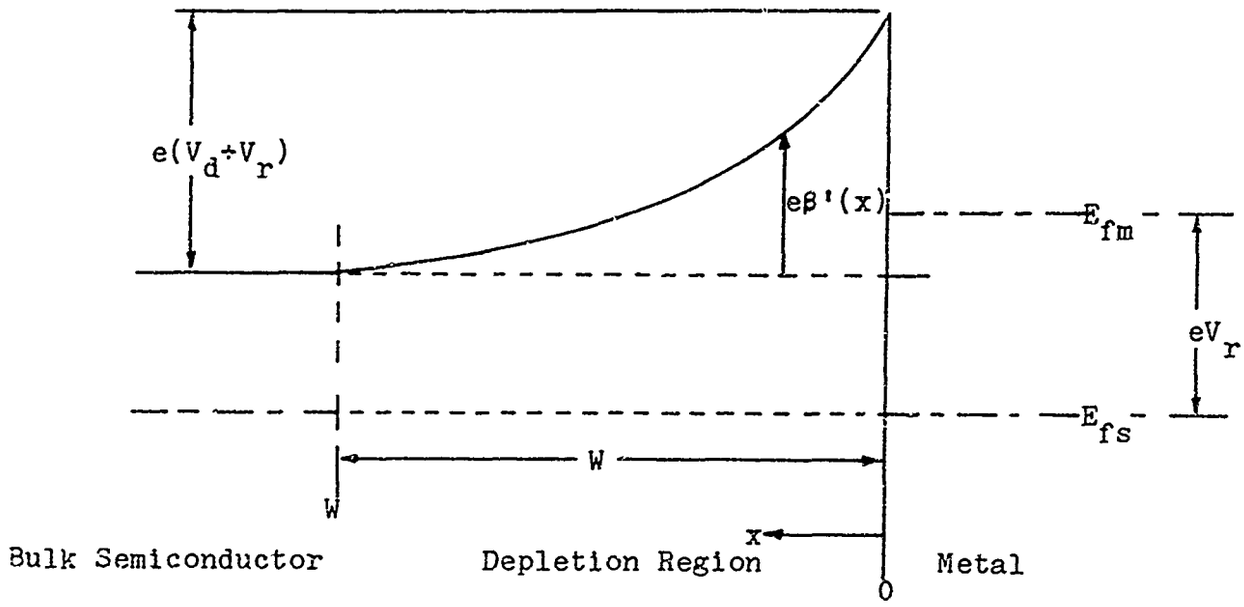

FIGURE 3.1a: Energy Diagram for a Metal-Semiconductor Contact under Reverse Bias; Image Force Neglected.

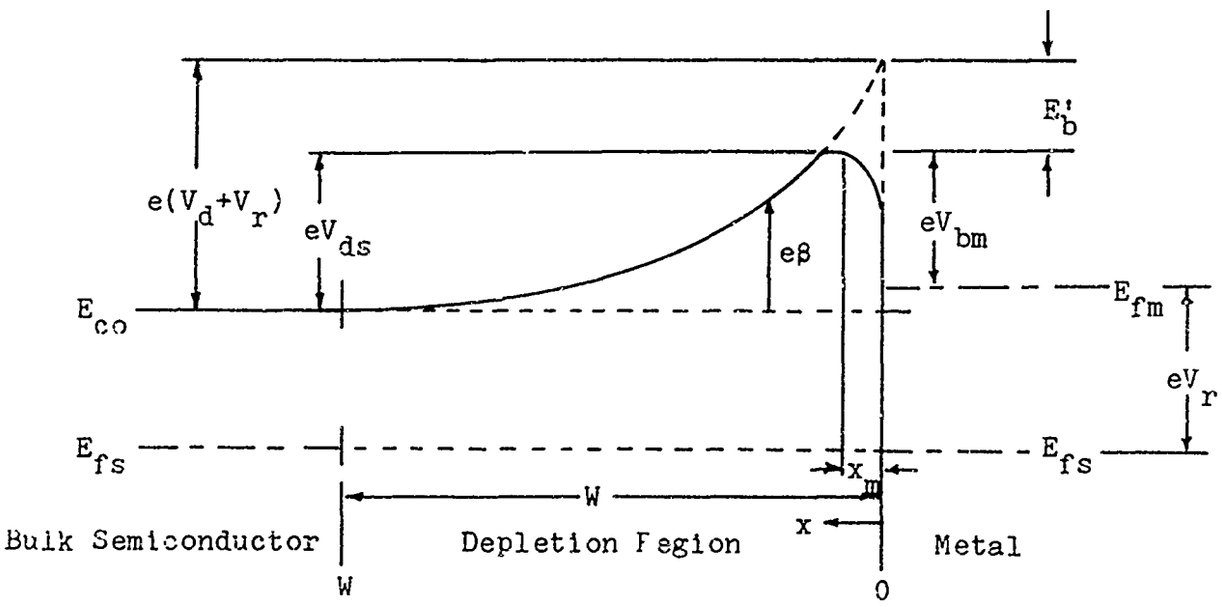

FIGURE 3.1b: Energy Diagram for a Metal-Semiconductor Contact under Reverse Bias with Image Force.

With reference to Fig. 3.1a, the following six statements describe the Schottky model for an idealized contact:

(1) The equilibrium diffusion potential (V_d) is large compared with KT/e, i.e.,

$$V_d \gg KT/e \tag{3.1}$$

This condition essentially insures that an effective barrier exists to conduction electrons of the semiconductor. If the energy barrier (eV_d) is on the order of , or less than the thermal energy of an electron (KT), then the barrier is easily surmounted by conduction electrons and it does not act as an "effective" barrier. Here "effectiveness" is meant to imply a measure of the barrier's ability to prevent electrons of the conduction band from crossing the junction. The calculations which follow will be based on the condition that an effective barrier is present, which necessarily limits application of the model to cases of small forward bias, moderate reverse bias, and the equilibrium condition stated in Eq. 3.1.

(2) The width of the barrier (W) is large compared to the wavelength of a conduction electron. This condition insures an effective barrier against tunneling, although it does not completely eliminate tunneling from taking place. Tunneling must always be considered as a contributing factor to electron transfer at a metal-semiconductor contact,

since by the very shape of the barrier its effective width becomes greatly reduced near the top.

However, if discussion is limited to barriers whose width exceeds several thousand angstroms, then tunneling may be neglected as a major contributor to electron transfer.

(3) The electron concentration on the semiconductor side of the barrier is so large compared to the hole concentration that it may be considered a constant, i.e.,

$$n(W) = N_d^+ \tag{3.2}$$

This allows E_{fs} to be uniquely specified and remain constant for the region $x \geq W$.

(4) The concentration of uncompensated, ionized, and immobile donor sites within the semiconductor is given by

$$N_d^+(x) = \begin{cases} N_d & \text{for } 0<x<W \\ 0 & \text{for } W<x<L \end{cases} \tag{3.3}$$

and $N_d^+(W)=n_o$, where n_o is the equilibrium concentration of electrons in the semiconductor.

(5) The hole concentration at the metal-semiconductor junction [p(0)] does not exceed N_d^+, i.e.,

$$p(0) \leq N_d^+ \tag{3.4}$$

(6) The space charge associated with the depletion

region is dominated by uncompensated and ionized donor sites, or

$$\int_0^W p(x)dx \ll N_d^+ W \gg \int_0^W n(x)dx \qquad (3.5)$$

Under the above assumptions one may use Poisson's equation to solve for expressions for the electric field and potential distribution within the depletion region of the semiconductor. The calculations which follow will assume the additional condition that the device is reverse biased; however, the calculations should be equally valid for a small forward bias. The limiting amount of forward bias will be determined by the point at which injection of carriers no longer allows conformance to the six statements listed above.

Poisson's equation for a planar contact has the form

$$\frac{d^2V(x)}{dx^2} = \frac{-\rho(x)}{\varepsilon_s'} \qquad (3.6)$$

in which $V(x)$ is the voltage drop associated with the contact and $\rho(x)$ is the space charge density associated with the depletion region. It is convenient to transform Eq. 3.6 into an expression involving the negative potential of an electron by the relation which follows:

$$V(x) = -\beta'(x) \qquad (3.7)$$

Thus, Eq. 3.6 becomes

$$\frac{d^2\beta'(x)}{dx^2} = \rho(x)/\varepsilon_s \qquad (3.8)$$

where $\beta'(x)$ represents the negative potential of an electron in the depletion region without image effects. (See Fig. 3.1a)

Since $\rho(x)$ represents the space charge density, it may be written in general as

$$\rho(x) = e[N_d^+(x) - n(x) + p(x)] \qquad (3.9)$$

However, for the Schottky model (statement #4) the electron and hole densities are neglected within the depletion region, so that Poisson's equation becomes

$$\frac{d^2\beta'(x)}{dx^2} = \frac{eN_d}{\varepsilon_s} \qquad (0 \leq x \leq W) \qquad (3.10)$$

The appropriate boundary conditions may be easily seen from Fig. 3.1a. These are

(1) $\frac{d\beta'(x)}{dx} = 0$ at $x=W$ (3.11)

(2) $\beta'(x) = 0$ at $x=W$ (3.12)

Integration of Eq. 3.10 once with respect to x yields

$$\frac{d\beta'(x)}{dx} = \frac{eN_d x}{\varepsilon_s} + C_1 \tag{3.13}$$

in which C_1 may be evaluated by applying the first boundary condition; thus

$$C_1 = \frac{-eN_d W}{\varepsilon_s} \tag{3.14}$$

and

$$\frac{d\beta'(x)}{dx} = \frac{eN_d}{\varepsilon_s}[x-W] \tag{3.15}$$

The second integration with respect to x yields

$$\beta'(x) = \frac{eN_d}{\varepsilon_s}[x^2/2-Wx] + C_2 \tag{3.16}$$

Using the second boundary condition

$$C_2 = \frac{eN_d W^2}{2\varepsilon_s} \tag{3.17}$$

so that the final expression for $\beta'(x)$ is

$$\beta'(x) = \frac{eN_d}{2\varepsilon_s}(x-W)^2 \tag{3.18}$$

Equation 3.18 can be used to obtain an expression for W in terms of the barrier height. Since

$$\beta'(0) = V_d + V_r \tag{3.19}$$

it follows that

$$W = \left[\frac{2\varepsilon_s(V_d+V_r)}{eN_d}\right]^{\frac{1}{2}} \tag{3.20}$$

Next, the electric field $[E(x)]$ is determined in the depletion region by noting that

$$\frac{d\beta'(x)}{dx} = -E(x) \tag{3.21}$$

Thus, $E(x)$ is given by Eq. 3.15, or

$$E(x) = \frac{eN_d}{\varepsilon_s}(W-x) \qquad (0 \leq x \leq W) \tag{3.22}$$

Also of interest is the electric field at the contact E_o and from Eq. 3.22

$$E_o = \frac{eN_dW}{\varepsilon_s} \tag{3.23}$$

However, W can also be expressed in terms of the barrier height (Eq. 3.20) so that

$$E_o = \left[\frac{2eN_d(V_d+V_r)}{\varepsilon_s}\right]^{\frac{1}{2}} \tag{3.24}$$

The results of the above calculations are summarized in Fig. 3.2.

Next, one can determine the charge per unit area contained in the depletion region by integrating the space charge density over the depletion width as follows:

$$Q_w = \int_0^W \rho(x)dx = eN_dW \tag{3.25}$$

and substitution of W from Eq. 3.20 yields

$$Q_w = \left[2eN_d\epsilon_s(V_d+V_r)\right]^{\frac{1}{2}} \tag{3.26}$$

The depletion region evidently acts as a parallel plate capacitor since for a small voltage increase additional charge will be added near the boundary at x=W. Thus, a junction capacitance (C_j) per unit area can be defined as

$$C_j = \frac{dQ_w}{dv} = \frac{\epsilon_s}{W} \tag{3.27}$$

Using Eq. 3.20, or Eq. 3.26, C_j may be expressed as follows:*

---

*For forward biased conditions (V_d+V_r) becomes (V_d-V_j) and as $V_j \rightarrow V_d$ the junction capacitance appears to increase indefinitely. This is

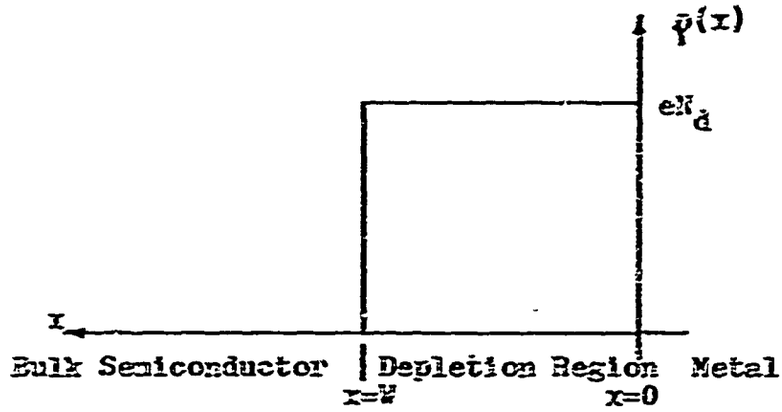

FIGURE 3.2a: Space Charge Density for the Schottky Model of a Metal-Semiconductor Contact.

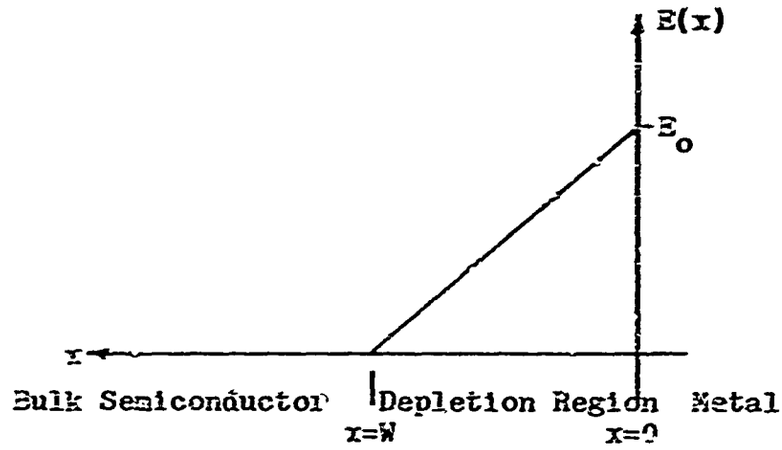

FIGURE 3.2b: Electric Field for the Schottky Model of a Metal-Semiconductor Contact.

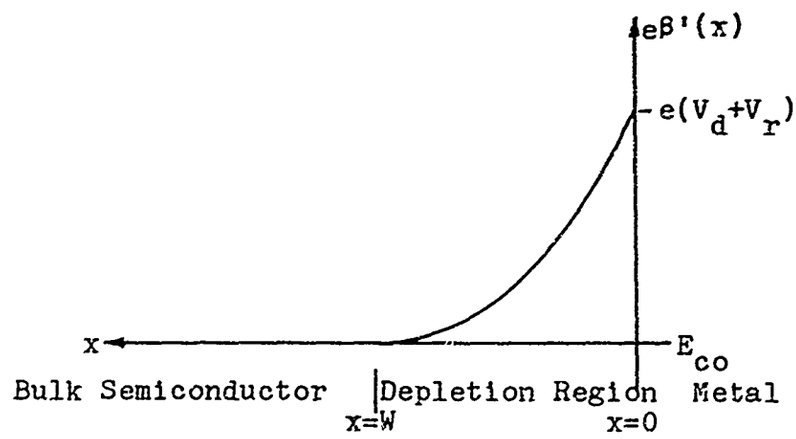

FIGURE 3.2c: Electron Potential for the Schottky Model of a Metal-Semiconductor Contact; Image Force Neglected.

$$C_j = \left[\frac{\epsilon\varepsilon_s N_d}{2(V_d+V_r)}\right]^{\frac{1}{2}} \qquad (3.28)$$

In Chapter II the effect of an image force was introduced and the electron potential due to the image effect calculated. Figure 3.1b shows this influence and the true electron potential within the depletion region. Using Eq.'s 2.4.2 and 3.18 the total electron potential, including image effects, may be expressed as

$$\beta(x) = \frac{eN_d}{2\varepsilon_s}(x-W)^2 - \frac{e}{16\pi\varepsilon_s' x} \qquad (x>0) \qquad (3.29)$$

Also, E_b' (as shown in Fig. 3.1b) may be calculated since

$$E_b' = e[V_d+V_r-\beta(x_m)] \qquad (3.30)$$

where $\beta(x_m)$ is the maximum value of the electron potential within the depletion region when image effects are included. An expression for x_m can be found from the fact that $\beta(x_m)$ will occur at the point where the image force on the electron

---

prevented by the fact that for a small forward bias sufficient current flows to prevent V_j from becoming comparable with V_d due to the voltage drop associated with the bulk semiconductor.

balances the force on it due to the electric field, or by using Eq.'s 2.4.1 and 3.22

$$\frac{e^2}{16\pi\epsilon_s' x_m^2} = \frac{e^2 N_d (W - x_m)}{\epsilon_s} \tag{3.31}$$

Assuming that $W \gg x_m$ and solving for x_m yields

$$x_m \approx \left[16\pi\epsilon_s^{\circ} N_d W\right]^{-\frac{1}{2}} \tag{3.32}$$

where ϵ_s° is the ratio of ϵ_s' to ϵ_s. Using Eq.'s 3.29, 3.30, and 3.32, E_b' can be approximated as

$$E_b' \approx e\left[\frac{eE_o}{4\pi\epsilon_s'\epsilon_s^{\circ}}\right]^{\frac{1}{2}} \tag{3.33}$$

or in terms of potential as

$$E_b' \approx e\left[\frac{e^3 N_d (V_d + V_r)}{8\pi^2 (\epsilon_s'\epsilon_s^{\circ})^2 \epsilon_s}\right]^{\frac{1}{4}} \tag{3.34}$$

by eliminating E_o using Eq. 3.24. Under normal applications of bias the lowering of the potential barrier to electrons in the semiconductor due to image effects is quite small and is usually neglected. This will be discussed in greater detail in the next chapter and a sample calculation will reveal an estimate of the magnitude of lowering due to image effects.

The potential barrier as seen by an electron on the semiconductor side of the junction (V_{ds}) may be expressed as

$$V_{ds} = V_d + V_r - E_b'/e \tag{3.35}$$

or

$$V_{ds} = V_d + V_r - \left[\frac{e^2 N_d (V_d+V_r)}{8\pi^2(\epsilon_s'\epsilon_s^o)^2\epsilon_s}\right]^{\frac{1}{4}} \tag{3.36}$$

by using Eq. 3.34. The potential barrier from the metal side of the junction becomes

$$V_{bm} = \frac{E_b - E_b'}{e} \tag{3.37}$$

and if surface states are neglected

$$V_{bm} = (\phi_m - X_e - E_b')/e \tag{3.38}$$

The results of this chapter can be stated in the form of the following equations:

(1) $\beta'(x) = \frac{eN_d}{2\epsilon_s}(x-W)^2$ (volts)

(2) $\beta(x) = \beta'(x) - \frac{e}{16\pi\epsilon_s' x}$ (volts)

(3) $W = \left[\frac{2\epsilon_s(V_d+V_r)}{eN_d}\right]^{\frac{1}{2}}$ (meters)

(4) $E_o = \left[\frac{2eN_d(V_d+V_r)}{\epsilon_s}\right]^{\frac{1}{2}}$ (volts/meter)

(5) $Q_x = \left[2e\epsilon_s N_d(V_d+V_r)\right]^{\frac{1}{2}}$ (Coulombs/meter^2)

(6) $C_j = \left[\frac{e\epsilon_s N_d}{2(V_d+V_r)}\right]^{\frac{1}{2}}$ (farads/meter^2)

(7) $E_b' = e\left[\frac{e^3 N_d(V_d+V_r)}{8\pi^2(\epsilon_s'\epsilon_s^o)^2 C_s}\right]^{\frac{1}{4}}$ (electron volts)

(8) $V_{ds} = V_d + V_r - E_b'/e$ (volts)

(9) $V_{bm} = (\phi_m - X_e - E_b')/e$ (volts)

Comparisons between the Schottky theory presented here and a more exact analysis will be presented in Chapter V.

CHAPTER IV

A MORE ACCURATE MODEL FOR THE IDEALIZED METAL-(N-TYPE)-SEMICONDUCTOR RECTIFYING CONTACT

The Schottky model, as discussed in the last chapter, is limited in exactness by the assumption that all impurity atoms within the depletion region are ionized and uniformly distributed. Furthermore, the model assumes that all free charge carriers are missing from the depletion region. These simplifying assumptions imply that the total space charge density within the depletion region is a constant and outside this region it is zero.

These restrictions on the space charge model will now be removed and a more accurate model which includes both incomplete and nonuniform ionization of donor atoms and the presence of free carriers within the depletion region will be substituted. The energy diagram for the metal-semiconductor junction is shown in Fig. 4.1 and is the same as that used for the Schottky mode. However, more quantities are defined since they are necessary for this more complete derivation which will follow. One should also note that the diagram is for reverse bias conditions, just as that for the Schottky model and one can again assume that the expressions which result will be equally valid for small forward bias.

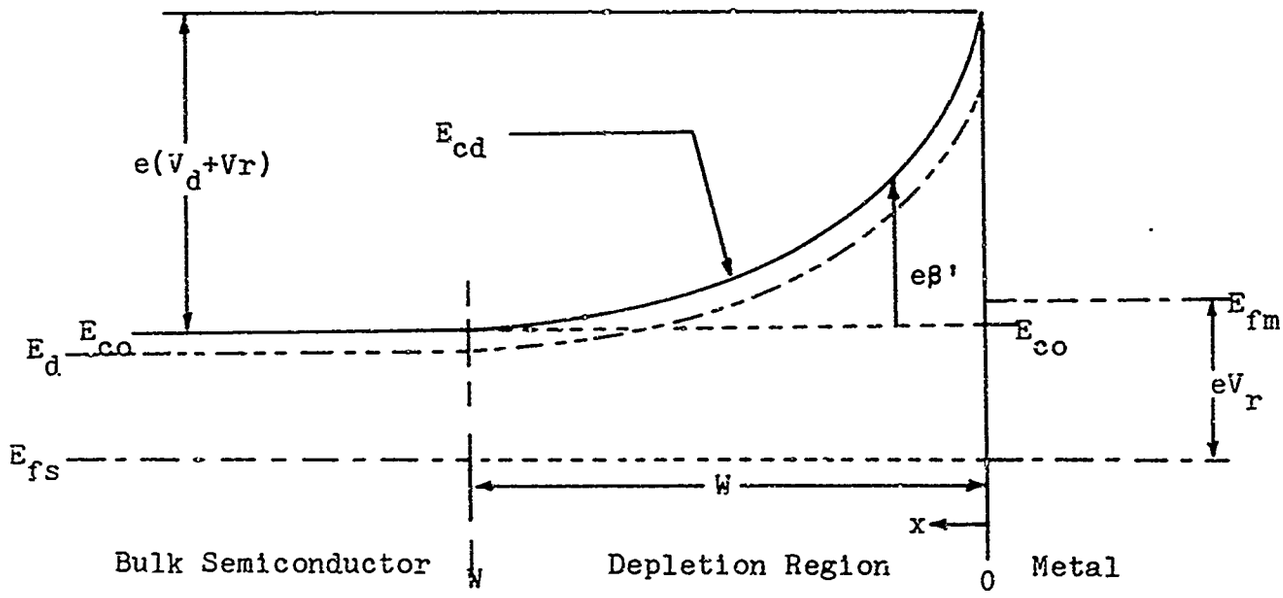

FIGURE 4.1: Energy Diagram for a Metal-Semiconductor Contact under Reverse Bias; Image Force Neglected.

In addition, it is assumed that any free carriers present in the depletion region are due to the electrons furnished by ionized donor atoms rather than injected from the metal. Then from the standpoint of an idealized junction the model should be exact, although exactness must be relative since tunneling, surface effects, and lattice imperfections will again be neglected.

When one considers incomplete donor ionization and the presence of free charge carriers within the depletion region, the total space charge density can no longer be considered a constant. Instead, one must return to the general expression for space charge density given by

$$\rho(x) = e[N_d^+(x)-n(x)+p(x)] \qquad (4.1)$$

in which $N_d^+(x)$ is the density of ionized donor sites and $n(x)$ and $p(x)$ are the free electron and hole densities, respectively.

Equation 4.1 can be immediately simplified by assuming that the positive space charge contributed by the minority carriers is negligible. This assumption is valid, since

$$p(x) \propto \exp[-(E_{fs}-E_{vd})/KT] \qquad (4.2)$$

and for N-Type semiconductors $E_{fs}-E_{vd} \gg KT$.

The electron concentration at the donor level (n_d),

which will be used to calculate N_d^+, may be obtained by forming the product of the number of available energy levels and the probability of occupancy. The donor level (E_d) actually consists of N_d narrowly spaced levels; however, since the energy is almost single valued, the electron concentration at the donor level can be expressed as

$$n_d = \frac{N_d}{\frac{1}{2}\exp[(E_d - E_{fs})/KT] + 1} \tag{4.3}$$

where the term in the denominator results from multiplication by the Fermi probability factor.* Since the electron concentration at the donor level is also the density of unionized impurity atoms, the density of free electrons contributed by ionized impurities must be

$$n_c = N_d - n_d \tag{4.4}$$

or by using Eq. 4.3,

---

*The conventional form of the Fermi probability factor for electrons is $f_e(E_n) = \left[\exp\left(\frac{E_n - E_{fs}}{KT}\right) + 1\right]^{-1}$; however, the Fermi probability factor for electrons of the donor level has an additional factor of $\frac{1}{2}$ to account for spin degeneracy. For a rigorous proof of this form see S. Wang, Solid State Electronics (New York: McGraw-Hill Book Company, 1966), pp. 143-5.

$$n_c = N_d\left\{1 - \frac{1}{\frac{1}{2}\exp[(E_d-E_{fs})/KT] + 1}\right\} \tag{4.5}$$

which may be written as

$$n_c = \frac{N_d}{2\exp[-(E_d-E_{fs})/KT] + 1} \tag{4.6}$$

Equation 4.6 may be expressed in a more useful form by the following manipulations:

(1) The ionization energy (E_i) is defined as

$$E_i = E_{co} - E_d \tag{4.7}$$

(2) By adding and subtracting E_{co} in the numerator term of the exponential in Eq. 4.6, it may be written as

$$-(E_d-E_{fs}) = (E_{co}-E_d) + E_{fs} - E_{co} \tag{4.8}$$

(3) The ionization energy can be incorporated into Eq. 4.8 yielding

$$-(E_d-E_{fs}) = E_i + E_{fs} - E_{co} \tag{4.9}$$

so that an equivalent expression for Eq. 4.6 is

$$n_c = \frac{N_d}{1 + 2\exp(E_i/KT)\exp[(E_{fs}-E_{co})/KT]} \tag{4.10}$$

Another valid expression for n_c is

$$n_c = N_c \exp[(E_{fs}-E_{co})/KT] \tag{4.11}$$

in which N_c represents the effective density of states for the conduction band. Upon substitution of Eq. 4.11 into Eq. 4.10, n_c may be expressed as

$$n_c = \frac{N_d}{1 + 2(n_c/N_c)\exp(E_i/KT)} \tag{4.12}$$

and solution of this expression for $\exp(E_i/KT)$ yields

$$\exp(E_i/KT) = \frac{N_c(N_d-n_c)}{2n_c^2} = \frac{(N_c/N_d)(1-n_c/N_d)}{2(n_c/N_d)^2} \tag{4.13}$$

Next, a new parameter will be introduced and defined as

$$\gamma = n_c/N_d \tag{4.14}$$

which may be interpreted as the degree of ionization, since it represents the fraction of donor impurities ionized in the bulk semiconductor. The degree of ionization represents an important parameter for a semiconductor and is discussed in greater detail in Appendix D. Using γ, Eq. 4.13 may be

expressed as

$$\exp(E_1/KT) = \frac{(N_c/N_d)(1-\gamma)}{2\gamma^2} \qquad (4.15)$$

Next, one can use the Boltzmann relation* to express the actual free electron density as a function of the quasi-Fermi level for electrons within the depletion region as follows:

$$n(x) = n_c \exp[-e\beta'(x)/KT] \qquad (4.16)$$

This equation represents the rearrangement of free carriers in the conduction band which occurs to establish equilibrium.

Finally, an expression for the free electron density of the conduction band valid in the depletion region must be found. Clearly, this expression will be a function of distance (x), since the potential of an electron varies with distance as shown in Fig. 4.1. Eq.'s 4.6 and 4.15 can be manipulated to show this dependence and give the desired result by making the following substitutions:

---

*The Boltzmann relation states that the free carrier density varies exponentially with carrier electrochemical potential.

(1) First, one can write

$$-(E_d-E_{fs}) = -E_d + E_{fs} \tag{4.17}$$

(2) By using Eq. 4.7, evaluated in the depletion region, the above expression may be rewritten as

$$-(E_d-E_{fs}) = E_i + E_{fs} - E_{cd} \tag{4.18}$$

(3) Adding and subtracting E_{co} yields

$$-(E_d-E_{fs}) = E_i + (E_{fs}-E_{co}) - (E_{cd}-E_{co}) \tag{4.19}$$

(4) Noting that $(E_{cd}-E_{co})$ is by definition $e\beta'(x)$, and making the above substitution into Eq. 4.6 yields

$$n_{cd}(x) = \frac{1}{1 + 2\exp(E_i/KT)\exp[(E_{fs}-E_{co})/KT]\exp[-e\beta'/KT]} \tag{4.20}$$

(5) Now if Eq.'s 4.11 and 4.13 are substituted into Eq. 4.20, the desired result is obtained, i.e.,

$$n_{cd}(x) = \frac{N_d}{1 + (1/\gamma-1)\exp[-e\beta'(x)/KT]} \quad (0 \leq x \leq W) \tag{4.21}$$

The above expression represents the free electron density due to ionized impurity atoms as a function of distance, valid for the depletion region before any rearrangement

occurs due to electrochemical potential. Furthermore, since each ionized donor site will have contributed one free electron

$$N_d^+ = n_{cd}(x) \tag{4.22}$$

which yields the needed result for the space charge density expression (Eq. 4.1).

Using Eq.'s 4.16, 4.21, and 4.22, the space charge density within the depletion region becomes

$$\rho(x) = eN_d\left\{\frac{1}{1 + (1/\gamma-1)\exp[-e\beta'(x)/KT]} - \gamma\exp[-e\beta'(x)/KT]\right\} \tag{4.23}$$

This expression represents the space charge density assuming incomplete donor ionization and the presence of free charge carriers within the depletion region. One should note that if $\beta'(x)$ is large enough the term corresponding to the free carrier concentration may be neglected. This would correspond to the Schottky approximation that the depletion region is uniformly depleted of electrons. This appears to be a good approximation for the region near x=0, but significant error is introduced in the region near x=W. Furthermore, if complete donor ionization is assumed, i.e., $\gamma=1$, then $N_d^+(x)$ reduces to N_d and yields the "abrupt" model

which was the assumed form for the Schottky expression for space charge density.

Poisson's equation will now be used to relate the space charge density $[\rho(x)]$ to the negative potential of an electron $[\beta'(x)]$, just as was done in the previous chapter. However, the relation will be considerably more complicated since both terms contributing to the space charge density are functions of distance. Poisson's equation, assuming a one-dimensional application, becomes

$$\frac{d^2\beta'(x)}{dx^2} = \frac{eN_d}{\epsilon_s}\left\{\frac{1}{1 + (1/\gamma-1)\exp[-e\beta'(x)/KT]} - \gamma\exp[-e\beta'(x)/KT]\right\} \tag{4.24}$$

This expression may be simplified by an appropriate change of variables, namely

$$y(x) = e\beta'(x)/KT \tag{4.25}$$

and

$$u(x) = \left[\frac{e^2N_d}{KT\epsilon_s}\right]^{\frac{1}{2}} x = K_1 x \tag{4.26}$$

which upon substitution into Eq. 4.24 yields,

$$\frac{d^2y}{du^2} = \frac{1}{1 + (1/\gamma-1)\exp(-y)} - \gamma\exp(-y) \tag{4.27}$$

which is a second order, nonlinear differential equation.

The appropriate boundary conditions are

$$(1) \quad \lim_{x \to \infty} \frac{d\beta'(x)}{dx} = 0 \tag{4.28}$$

$$(2) \quad \beta'(0) = V_r + V_d \tag{4.29}$$

which can be easily justified by Fig. 4.1. These boundary conditions must now be transformed to the new variables. They are

$$(1) \quad dy/du = 0 \quad \text{for } y = 0 \tag{4.30}$$

$$(2) \quad y(0) = y_o = \frac{e(V_d+V_r)}{KT} \tag{4.31}$$

It is worth noting that y_o is a function of the applied bias (V_r). Since V_d is fixed for a particular junction, y_o will in general be specified by the applied bias plus an additive constant.

The result of the first integration of Eq. 4.27 may be written as follows:

$$dy/du = -\sqrt{2}\, z^{\frac{1}{2}} \tag{4.32}$$

where

$$z = \ln[\gamma e^{y}+1-\gamma] + \gamma e^{-y} - \gamma \tag{4.33}$$

This expression is verified in Appendix E.

In order to complete the solution, one must perform a numerical integration of Eq. 4.32, since the solution in closed form is not apparent, if one exists. The numerical technique to be used here is the Runge-Kutta method of order four for finding a point by point solution; utilizing a digital computer to perform the actual calculations. A discussion of the Runge-Kutta method is presented in Appendix F along with the computer program used to integrate Eq. 4.33 and plot the results. A typical computer run is contained in Appendix G.

The computer solutions are shown in Fig. 4.2 and Fig. 4.3. In Fig. 4.2a the normalized electron potential y is plotted against the normalized distance u. It has been assumed here that the normalized barrier height is $y_o=60$. This would correspond to a combined equilibrium diffusion potential and reverse bias of approximately 1.56 volts, i.e., $V_d+V_r\approx 1.56$ volts. The degree of ionization was varied from 0.05 to 1.0 to reflect its influence on the normalized electron potential and each curve corresponding to a particular γ is shown. The curves would seem to indicate that the effect of γ is quite small, since the general shape of the curves is maintained as γ is varied. In Fig. 4.2b the normalized space charge density (normalized to unity at the contact) is plotted against the normalized distance u. For comparison purposes the equivalent Schottky

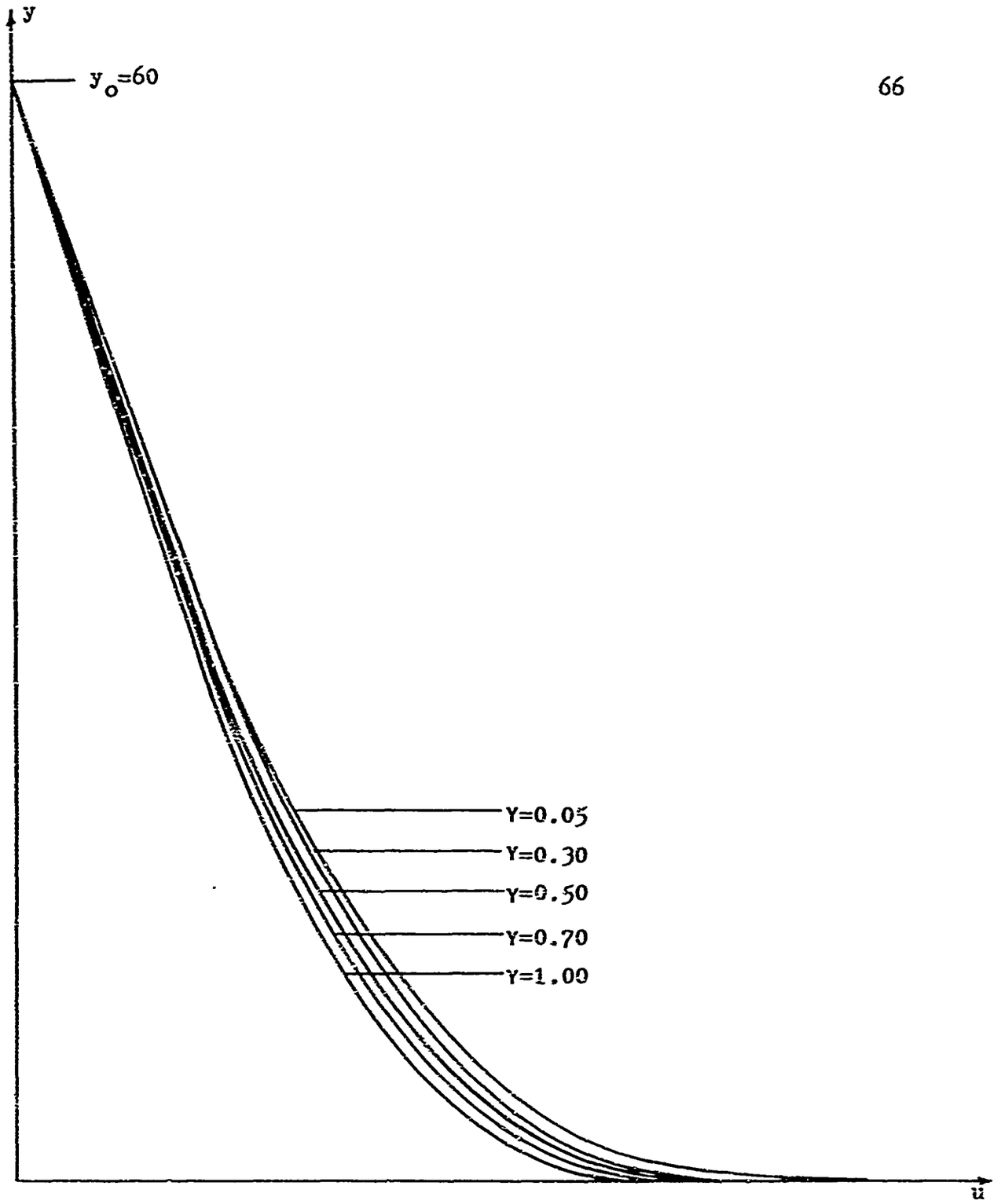

FIGURE 4.2a: Computer Solutions for the Normalized Electron Potential versus the Normalized Distance into the Depletion Region. Solution is for the Initial Condition of y_o=60.

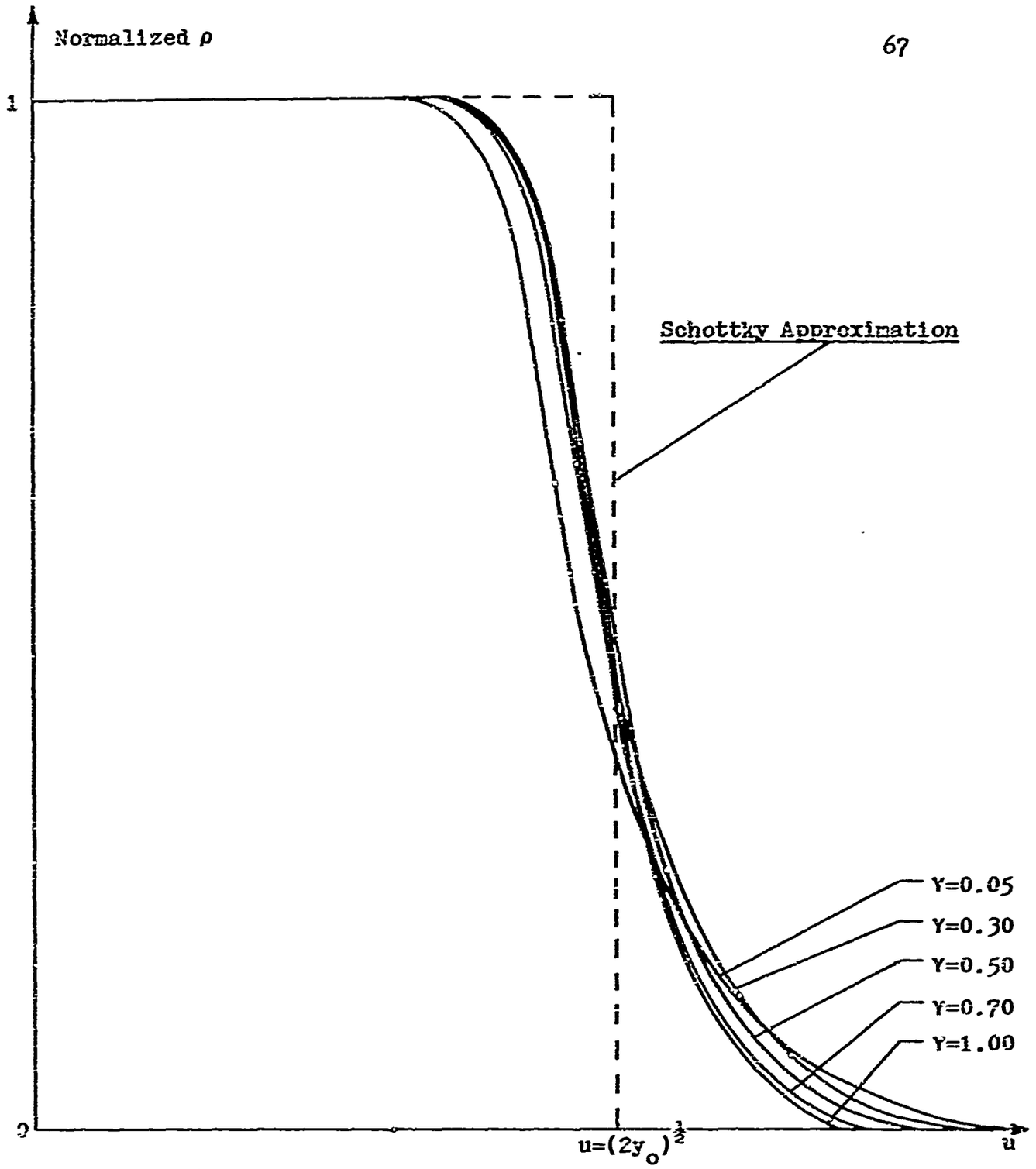

FIGURE 4.2b: Computer Solutions for the Normalized Space Charge Density versus the Normalized Distance into the Depletion Region. Solution is for the Initial Condition of y_o=60.

representation for space charge density (normalized to unity at the contact) is also plotted. The abrupt representation for space charge density remains constant to a point where $u=W$ and W in terms of the new variables y and u is $W=(2y_o)^{\frac{1}{2}}$. It now becomes apparent why the Schottky model gives useful and fairly accurate results. First, it can be noted that the Schottky and more exact model agree to a point near $u=W=(2y_o)^{\frac{1}{2}}$. After this point however, the normalized space charge density of the more exact model decays over a finite distance due to the increasing compensation offered by the increasing concentration of electrons as $x \rightarrow W$. Furthermore, W (the value of u at which $y=0$) as predicted by the more exact model is greater than that predicted by the Schottky model. However, if one compares the areas of disagreement between the two models, the additional space charge density predicted by the more exact model for $W>(2y_o)^{\frac{1}{2}}$ has a compensating effect on the reduced space charge density for $W<(2y_o)^{\frac{1}{2}}$. Thus, the Schottky model becomes a fairly accurate model for an effective space charge density and depletion width.

Similar plots are shown in Fig. 4.3. Here the value of y_o was chosen as 20, to correspond to a combined diffusion potential and reverse bias of approximately 0.52 volts.

The Schottky model predicts a voltage dependent capacitance as given by Eq. 3.28. This junction capacitance arises from the fact that the depletion region acts as a

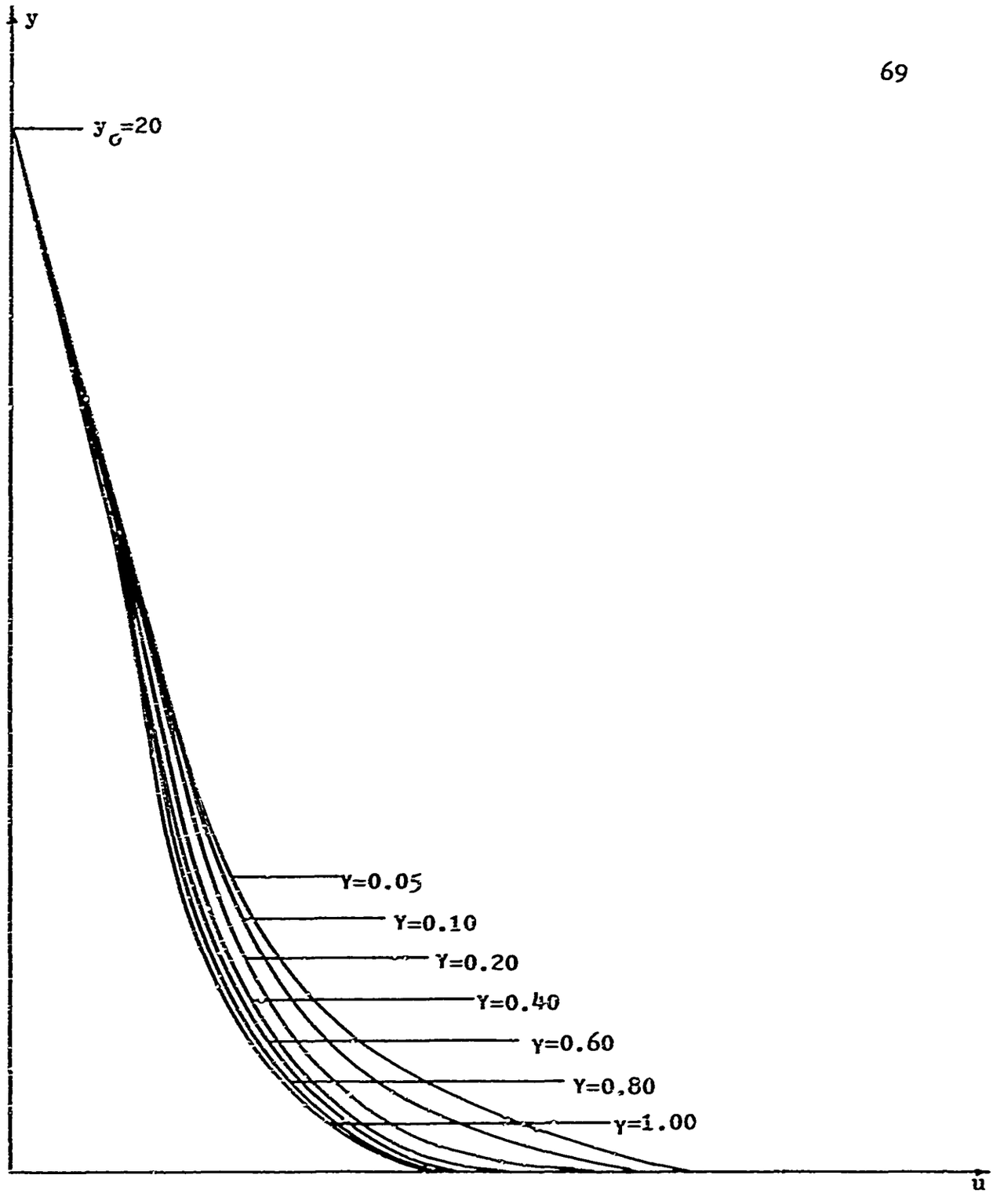

FIGURE 4.3a: Computer Solutions for the Normalized Electron Potential versus the Normalized Distance into the Depletion Region. Solution is for the Initial Condition of y_o=20.

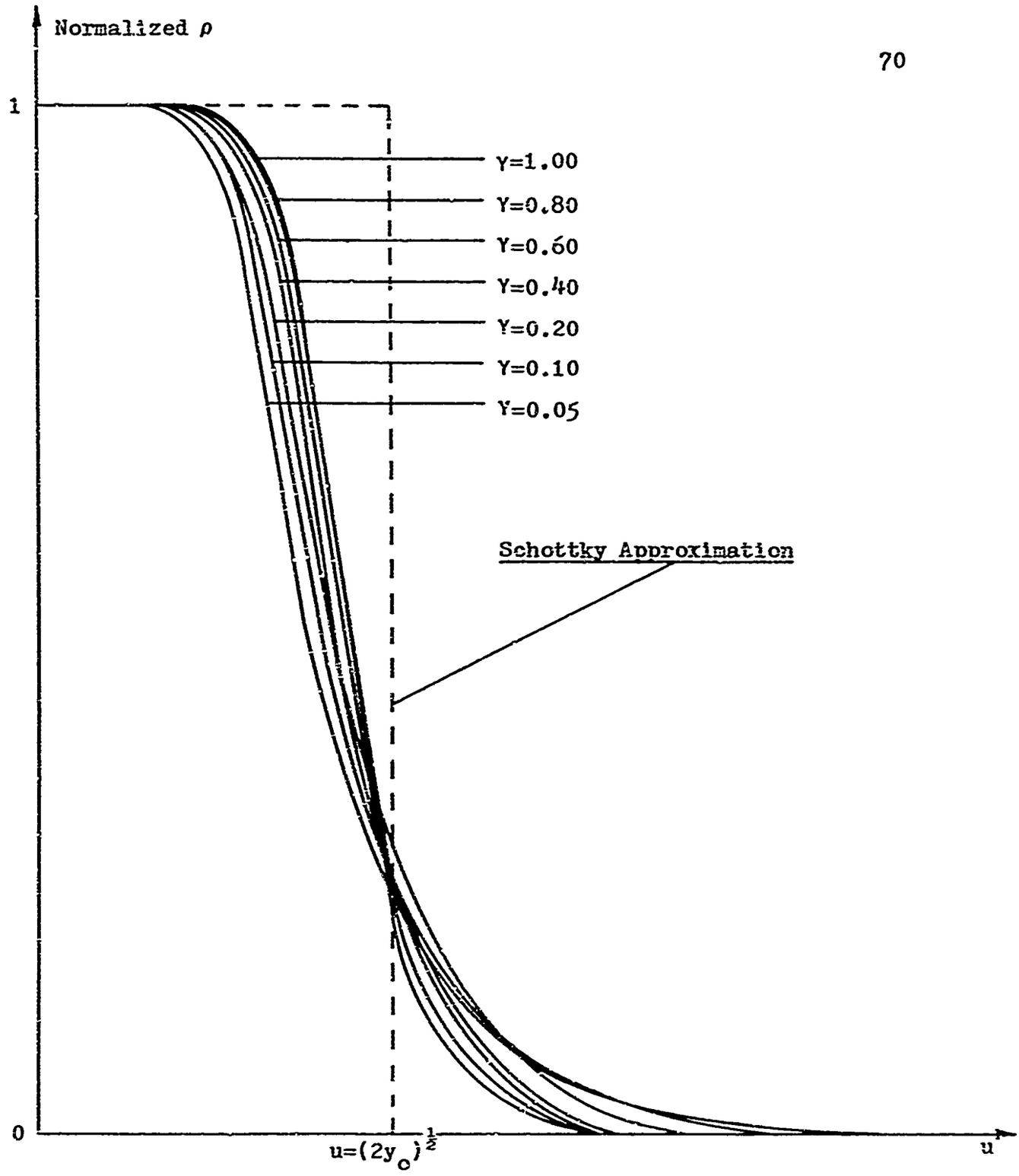

FIGURE 4.3b: Computer Solutions for the Normalized Space Charge Density versus the Normalized Distance into the Depletion Region. Solution is for the Initial Condition of y_o=20.

parallel plate capacitor since for a small voltage change a net charge is either added or substracted from the region near x=W. By Gauss's law the total space charge per unit area (Q_W) contained within the depletion region is related to the electric field at the contact (E_o) by

$$Q_W = -\varepsilon_s E_o \tag{4.34}$$

The electric field at the contact is in turn related to the slope of the potential function evaluated at the contact, or

$$E_o = \mp \left.\frac{d\beta'(x)}{dx}\right|_{x=0} \tag{4.35}$$

where

$$\frac{d\beta'(x)}{dx} = (KT/e)\left(\frac{e^2 N_d}{KT\varepsilon_s}\right)^{\frac{1}{2}} (dy/du)\Big|_{u=0} \tag{4.36}$$

in terms of the new variables y and u. Thus, by substitution Eq. 4.34 becomes

$$Q_W = -(\varepsilon_s KTN_d)^{\frac{1}{2}}(dy/du)\Big|_{u=0} \tag{4.37}$$

in which

$$(dy/du)\Big|_{u=0} = -\sqrt{2}\left\{\ln[\gamma e^{y_o} + 1 - \gamma] + \gamma e^{-y_o} - \gamma\right\}^{\frac{1}{2}} \tag{4.38}$$

by using Eq. 4.32. Finally, the junction capacitance can be calculated as follows:

$$C_j = \frac{dQ_w}{dV} = k_2\left\{\frac{\dfrac{1}{1 + (1/\gamma-1)e^{-y_o}} - \gamma e^{-y_o}}{\left\{\ln[\gamma e^{y_o}+1-\gamma] + \gamma e^{-y_o} - \gamma\right\}^{\frac{1}{2}}}\right\} \tag{4.39}$$

where

$$k_2 = \left(\frac{e^2 \epsilon_s N_d}{2KT}\right)^{\frac{1}{2}} \tag{4.40}$$

$$y_o = \frac{e(V_d+V_r)}{KT} \tag{4.41}$$

The calculations made in this chapter thus far have neglected image force effects. If one were to include image effects, Poisson's equation (Eq. 4.24) would have to be modified by replacing $\rho'(x)$ by $\rho(x)$ where

$$\rho(x) = \rho'(x) + \rho''(x) \tag{4.42}$$

Since the discussion of Chapter II indicates that a single expression for $\beta''(x)$, valid for the entire depletion region, is not possible because of model dependence near the metal surface, then Eq. 4.42, at best, would have to be approximated by assuming two expressions, one valid for $x > x_m$ and the other valid as $x \longrightarrow 0$. In addition, a simple transformation of variables could no longer be used to make the solutions of Poisson's equation independent of the particular materials used to form the contact, and no general results could be obtained. In short, the addition of image effects would hopelessly complicate Eq. 4.24.

Fortunately, there is an alternate approach which can give a reasonably accurate approximation to the maximum correction of barrier height needed because of image effects. It has already been established that the Schottky model is quite accurate in the region near the junction and that the influence of image effects predominates in this region. Furthermore, if one assumes that β_m occurs in this region and that x_m is large enough to permit $\beta''(x)$ to be approximated by

$$\beta''(x) = \frac{-e}{16\pi\epsilon_s' x} \qquad (4.43)$$

then one can use the results obtained in Chapter III to estimate the maximum correction needed for image effects by

E_b'. In order to show the influence of image effects on the result obtained for the normalized electron potential as shown in Fig. 4.2a, E_b' will be normalized to y_b'. This can be done by using the approximate expression for E_b' based on the Schottky model, or

$$E_b' \approx e\left(\frac{eE_o}{4\pi\epsilon_s'\epsilon_s^o}\right)^{\frac{1}{2}} \tag{4.44}$$

where E_o is given by

$$E_o = \left[\frac{2eN_d\beta'(0)}{\epsilon_s}\right]^{\frac{1}{2}} \tag{4.45}$$

In terms of the normalizing variable y, $\beta'(0)$ may be expressed as

$$\beta'(0) = \left(\frac{KT}{e}\right)y_o \tag{4.46}$$

Combining Eq.'s 4.44, 4.45, and 4.46, the normalized correction for image effects may be written as

$$y_b' \approx (e/KT)\left[\frac{e^2N_dKT}{8\pi^2(\epsilon_s'\epsilon_s^o)^2\epsilon_s}\right]^{\frac{1}{4}}(y_o)^{\frac{1}{4}} \tag{4.47}$$

which represents a "worst case" estimate to the modification imposed on the normalized electron potential near the contact due to image effects. The reduction in the barrier height y_o is usually quite small under normal applications of bias

voltage and for the purpose of illustrating this reduction the following situation will be assumed:

The contact is a metal-(N-Type)-Si contact with $V_d+V_r=1.56$ volts, $\gamma=1.0$, $T=300\ ^oK$, $N_d=10^{16}\ cm^{-3}$, and $\epsilon_s'\approx\epsilon_s=12\epsilon_o$ farad/m.* Under the assumption that $V_d+V_r=1.56$ volts Fig. 4.2a is applicable and one may proceed to calculate the reduction factor y_b' as follows:

$$y_b' \approx (e/KT)\left[\frac{e^2N_dKT}{8\pi^2(\epsilon_s'\epsilon_s^o)^2\epsilon_s}\right]^{\frac{1}{4}}(y_o)^{\frac{1}{4}}$$

$$y_b' \approx 38.6\left[\frac{(2.56)(1.38)(3)(10^{-37})}{8(9.87)(1.2)(10^{-30})}\right]^{\frac{1}{4}}(60)^{\frac{1}{4}}$$

$$y_b' \approx (3.86)(1.03)(2.78)(10^{-1})$$

$$y_b' \approx 1.1$$

$$y_b' << y_o = 60$$

The result of this calculation is shown in Fig. 4.4.

The quantity y_b' seems quite negligible in comparison to $y_o=60$ and would be even smaller for a lower doping concentration, i.e., $N_d<10^{16}\ cm^{-3}$. Although this seems sufficient justification for neglecting image effects, one must be

---

*For silicon $\epsilon_s^o\approx1$ since lattice polarization is purely electronic.[21]

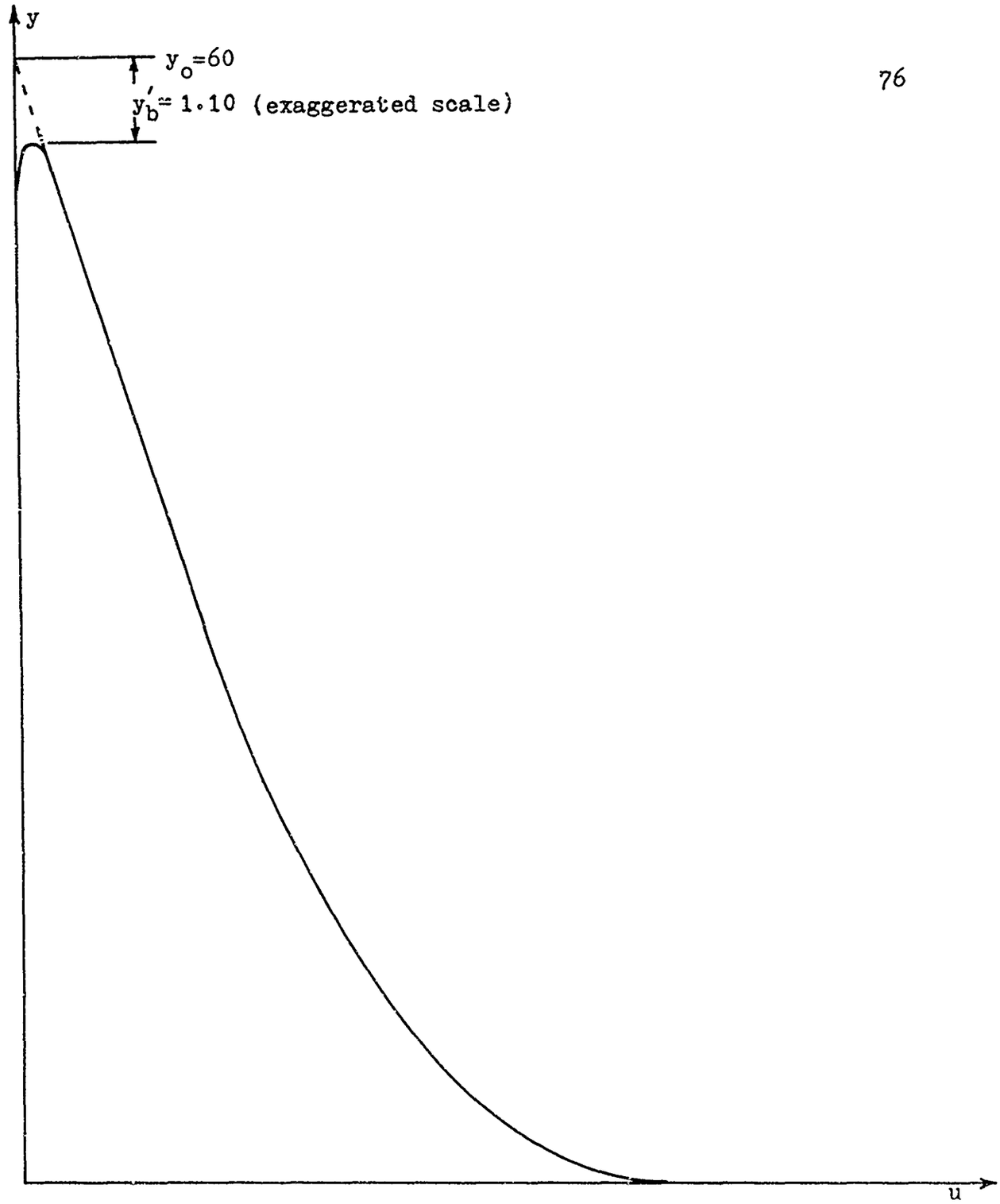

FIGURE 4.4: Normalized Electron Potential versus Normalized Distance into the Depletion Region Showing the Influence of an Image Force. Not to Scale.

cautious in doing so. Since y_b' is a function of the reverse bias voltage image effects can be expected to become more important at higher voltages. In addition, it has been shown in Section 2.6 that a small change in the barrier height would significantly alter the transport properties of the barrier due to quantum-mechanical effects. As it turns out, image effects can usually be neglected except under reasonably large reverse biases, when the reduction in the barrier potential accounts for the voltage dependence of the reverse saturation current. Image effects will be discussed again in relation to the I-V characteristic of the contact in Chapter VI.

CHAPTER V

METHODS OF DETERMINING THE EQUILIBRIUM BARRIER HEIGHTS OF METAL-(N-TYPE)-SEMICONDUCTOR CONTACTS: A COMPARISON OF THE MODELS OF CHAPTER III AND CHAPTER IV

The most commonly used experimental methods to determine the energy barrier heights E_b and eV_d are by the photoresponse method and by an extrapolation of data obtained from a capacitance versus voltage plot. In this chapter both methods will be discussed; however, major attention will be focused on the capacitance method since the results obtained are dependent on the particular model used for the metal-semiconductor contact. Furthermore, since the photoresponse method provides a direct measure of the barrier height, a comparison of the results predicted by the two methods will provide a means of comparing the accuracy of the contact models discussed in Chapters III and IV.

The photoresponse method uses a monochromatic light source to induce a photocurrent in the device under investigation. The source may be incident upon either the semiconductor or metal side of the contact. To provide a direct measurement of eV_d the source must be incident upon the semiconductor and to measure E_b the source must be incident upon the metal; in either case, the material upon which the

light source is incident must be as thin as possible to enable sufficient light for electron excitation in the immediate vicinity of the contact. Generally, the light source is incident on the metal since the most common method of preparing metal-semiconductor contacts is by vacuum evaporation of the metal onto a doped, single crystal substrate. This method allows very accurate control of the metal thickness and evaporation of a metal has the additional advantages of lower evaporation temperatures while avoiding the problems of doping and crystal structure. Assuming that the light source is incident on the metal, Fig. 5.1 defines the relevant parameters involved in measuring E_b by the photoresponse method.

When light is directed onto the metal surface the free electrons in the metal are excited and if sufficient energy is acquired, they will overcome the energy barrier (E_b) and produce a current in the semiconductor. If the photoelectric current per incident photon is defined as the photoresponse (R), then the spectral distribution of R will reveal the barrier height (E_b) as seen by an electron leaving the metal. A typical spectral response is shown in Fig. 5.2. Figure 5.2 also shows that there are two distinct regions of the photoexcitation process:

(1) The photoemission of excited electrons in the metal over the barrier E_b.

(2) The band to band excitation of electron-hole pairs within a diffusion length of the semiconductor depletion region.

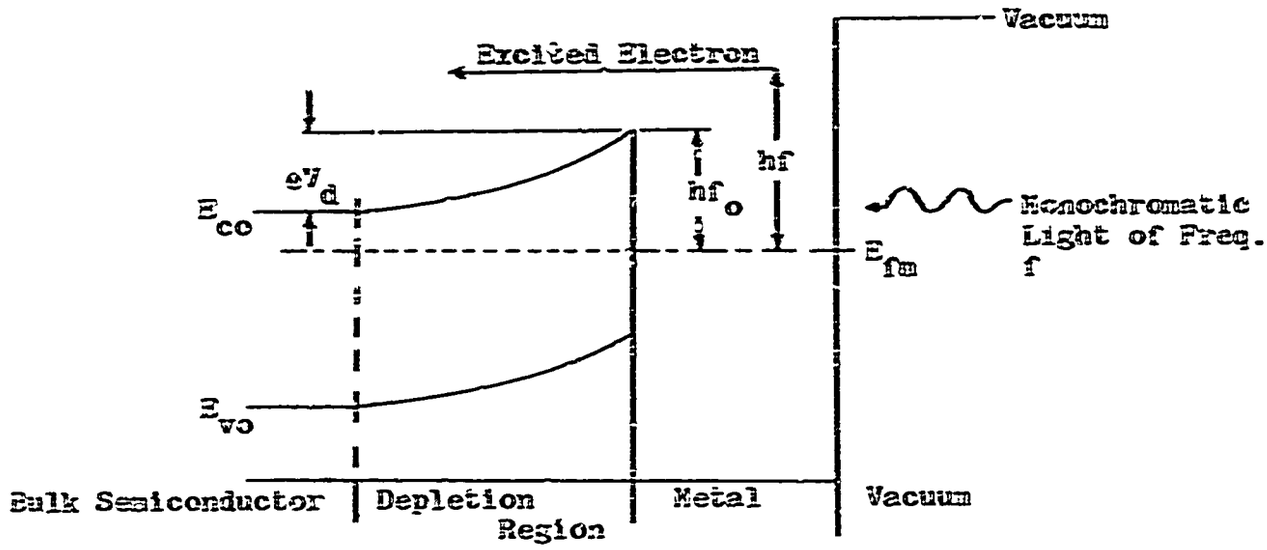

FIGURE 5.1: Energy Diagram of a Metal-Semiconductor Rectifying Contact Showing the Parameters Involved in the Measurement of E_b by the Photoexcitation Method.

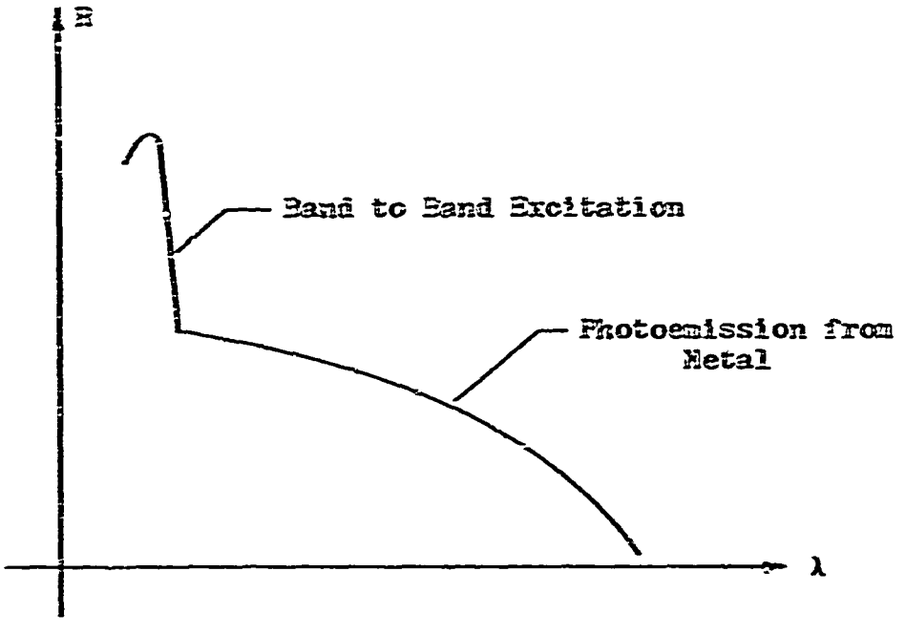

FIGURE 5.2: Spectral Response of a Metal-Semiconductor Rectifying Contact.[22]

The Fowler theory[23] of the photoelectric effect predicts that the dependence of the photocurrent (J_p) on photon energy, for photon energies exceeding E_b+3KT, may be expressed as[24]

$$J_p \propto (hf - hf_c)^2 \tag{5.1}$$

where

$$E_b = hf_c \tag{5.2}$$

as shown in Fig. 5.1. Thus, if one plots $R^{\frac{1}{2}}$ (which is defined to be proportional to J_p) versus the incident photon energy (hf),* a straight line would result, which in turn yields an extrapolated value for E_b, i.e., the intercept value on the hf axis. A plot of $R^{\frac{1}{2}}$ versus hf for an Au-CdSe contact is shown in Fig. 5.3. Figure 5.3 also illustrates quite clearly why it is necessary to have a very thin metal contact, since an accurate extrapolation for E_b becomes difficult for metal widths exceeding 900 Å.

The capacitance versus voltage technique for determining

---

*The values of R are taken from the longer wavelengths of f to insure data corresponding to the process of photoemission from the metal and not band to band excitation.

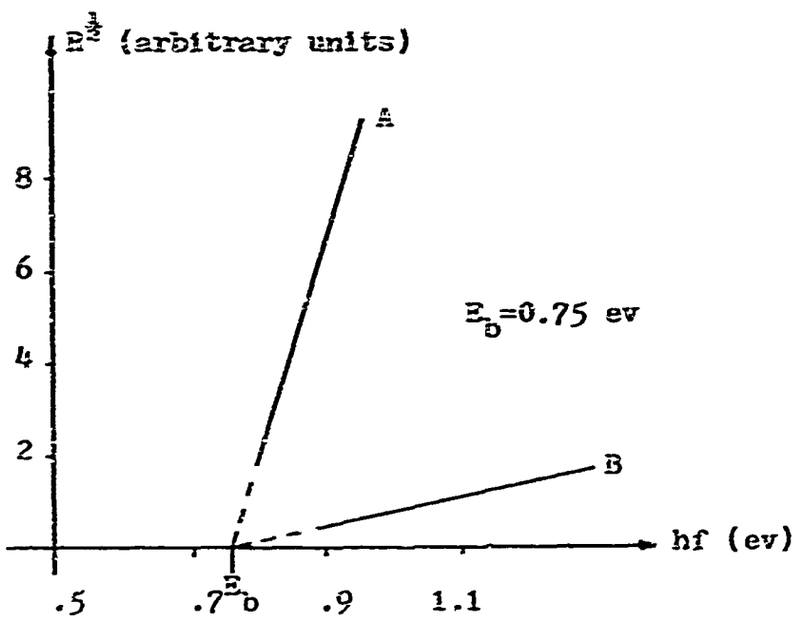

FIGURE 5.3: Photoresponse of a Au-CdSe Contact versus Photon Energy.[25] The Curve Labeled A if for a Metal Thickness of 300 Å and the Curve Labeled B is for a Metal Thickness of 900 Å.

the equilibrium diffusion potential (V_d), assuming an idealized contact, can also provide an indirect measurement of E_b, since E_b is related to V_d as follows:

$$E_b = eV_d + E_{fs} \tag{5.3}$$

which is evident from Fig. 2.5 with V_a=0. The quantity V_d is experimentally determined by plotting the square of the reciprocal of the junction capacitance per unit area (C_j) versus the reverse bias voltage (V_r). A plot of this form will allow one to extrapolate a value of V_d (the intercept value on the V_r axis) and once V_d is known, E_b may be calculated by using Eq. 5.3. The major difficulty encountered when using this method is that the theoretical expression for the junction capacitance (Eq.'s 3.28 and 4.39) is "model dependent" and the relation of the experimentally determined intercept voltage to V_d will reflect this dependence. This will become apparent in the discussion which follows.

First, consider the capacitance expression based on the Schottky model (Eq. 3.28). If this expression is squared and the reciprocal taken of the result, one obtains

$$\frac{1}{C_j^2} = \frac{2(V_d+V_r)}{e\varepsilon_s N_d} = \frac{1}{k_3^2}(y_o) \tag{5.4}$$

where

$$x_3 = \left(\frac{e^2 \varepsilon_s N_d}{2KT}\right)^{\frac{1}{2}} \tag{5.5}$$

and

$$y_o = \frac{e(V_d + V_r)}{KT} \tag{5.6}$$

Clearly, if $(1/C_j^2)$ versus y_o is plotted, a straight line will result and at the point where

$$V_o = -V_r = V_d \tag{5.7}$$

y_o is zero, or $(1/C_j^2)=0$. Also of interest is the slope, since it provides a means of determining the doping density (N_d). The slope can be calculated as follows:

$$m = \frac{d(1/C_j^2)}{dV_r} = \frac{2}{e\varepsilon_s N_d} \tag{5.8}$$

The doping concentration may then be expressed as

$$N_d = \frac{2}{em\varepsilon_s} \tag{5.9}$$

A typical experimental plot of $(1/C_j^2)$ versus V_r is shown in Fig. 5.4a, illustrating the experimentally determined values of V_o and N_d. For the purpose of comparison, Fig. 5.4b shows the photoresponse method used to determine E_b for the same diode.

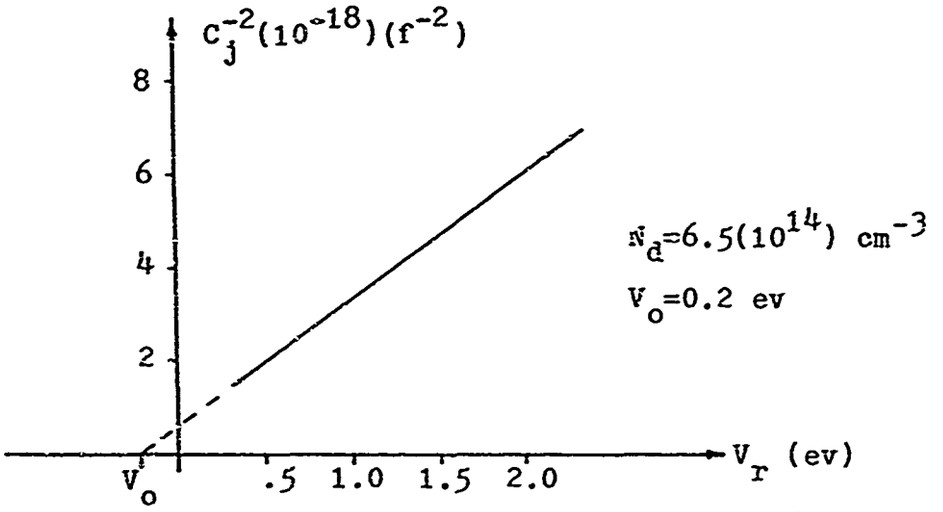

FIGURE 5.4a: C_j^{-2} versus V_r for an Au-Ge Contact.[26]

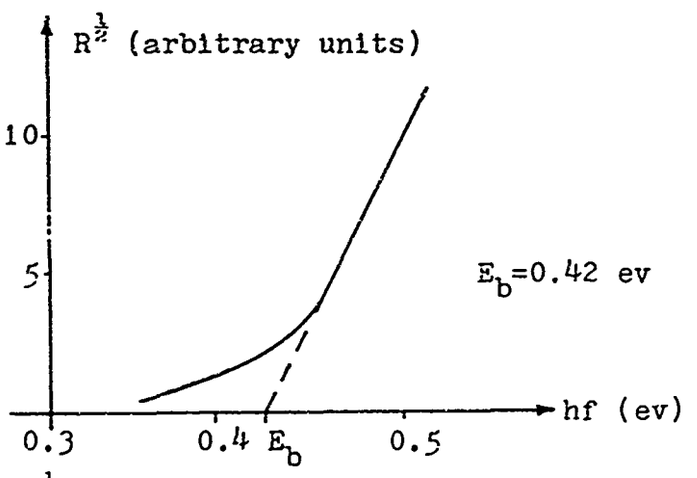

FIGURE 5.4b: $R^{\frac{1}{2}}$ versus hf for the same Au-Ge Contact as in Fig. 5.4a.[26]

Next, consider the capacitance expression derived on the basis of the more exact model of Chapter IV. Squaring Eq. 4.39 and taking the reciprocal yields

$$C_j^{-2} = \frac{1}{k_3^2}\left\{\frac{\ln[\gamma e^{y_o}+1-\gamma] + \gamma e^{-y_o} - \gamma}{\left\{\frac{1}{1 + (1/\gamma-1)e^{-y_o}} - \gamma e^{-y_o}\right\}^2}\right\} \tag{5.10}$$

in which

$$k_3 = \left(\frac{e^2\epsilon_s N_d}{2KT}\right)^{\frac{1}{2}} \tag{5.11}$$

This expression is considerably more complicated than the equivalent expression (Eq. 5.4) based on the Schottky model. However, for sufficient values of reverse bias $y_o \gg 1$, Eq. 5.10 may be approximated by

$$C_j^{-2} \approx k_3^{-2}\left\{\ln[\gamma e^{y_o}+1-\gamma] - \gamma\right\} \tag{5.12}$$

Expanding the logrithmic term by the power series

$$\ln(a+x) = \ln(a) + 2\left\{\frac{x}{2a+x} + \frac{1}{3}\left[\frac{x}{2a+x}\right]^3 + \frac{1}{5}\left[\frac{x}{2a+x}\right]^5 + \cdots\right\}_{x>0} \tag{5.13}$$

a further approximation may be made for $y_o \gg 1$,

yielding*

$$C_j^{-2} \approx k_3^{-2}[y_o + \ln(\gamma) - \gamma] \qquad (5.14)$$

One may now recognize the equation of a straight line if $(k_3/C_j)^2$ is plotted against y_o. The approximations leading to Eq. 5.14 can be easily justified by observing a plot of Eq. 5.10 for arbitrary values of y_o and γ. Such a plot is shown in Fig. 5.5. For values of $y_o > 4$ (approximately), Eq. 5.10 becomes a straight line and an extrapolation of these lines for each γ may be used to determine the intercept value of V_o. This intercept value of V_o is of primary importance since it will result in an expression for V_d. The quantity V_d can be obtained by noting that when $(k_3/C_j)^2=0$, the straight line approximation to Eq. 5.10 can be written as

---

*Dewald[27] has obtained the same limiting result for C_j^{-2}; however, his original expression for C_j^{-2} is not the same as Eq. 5.10 although both expressions produce the same limiting result as reverse bias becomes large. Furthermore, his derivation of a voltage dependent capacitance follows from an investigation of the distributions of charge and potential at a zinc oxide-electrolyte interface.

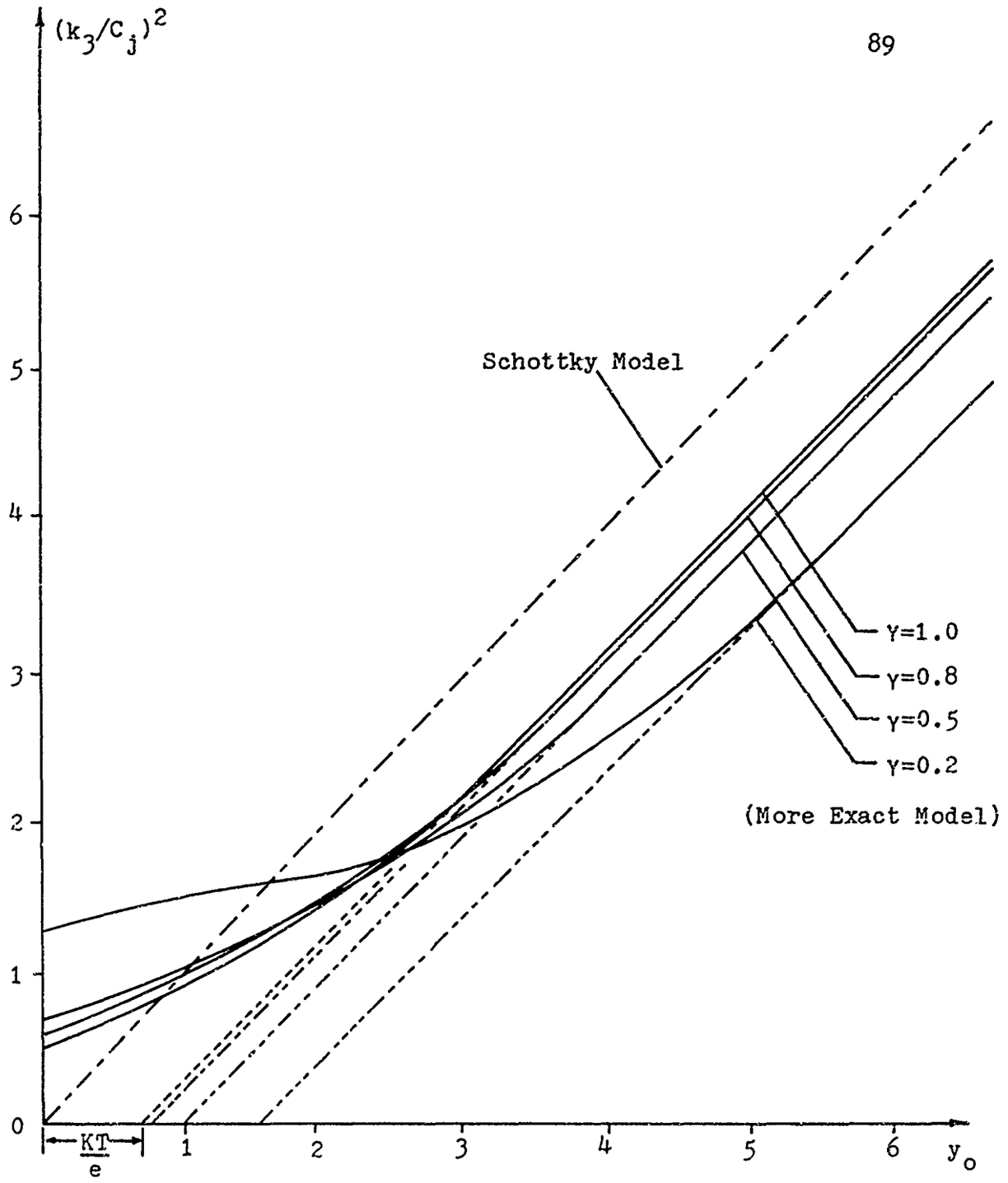

FIGURE 5.5: Normalized Junction Capacitance versus Normalized Bias Voltage (Eq. 5.10).

$$y_o + \ln(\gamma) - \gamma = 0 \tag{5.15}$$

or

$$\frac{e(V_d - V_o)}{KT} \approx \gamma - \ln(\gamma) \tag{5.16}$$

Rearranging yields

$$V_d \approx V_o + (KT/e)[\gamma - \ln(\gamma)] \tag{5.17}$$

It should be noted that the above expression for the equilibrium diffusion potential (V_d) has neglected the influence of image effects. If image effects were included, then y_o in Eq. 5.15 would be replaced by the effective barrier height near the contact, i.e., $y_o - y_b'$. However, since $y_o >> y_b'$ one would seem justified in neglecting y_b'. For this particular application the error introduced by neglecting y_b' is quite small and it will become even smaller as the bias voltage is increased. This may not be the case when considering the carrier transport properties of the contact since the magnitude of y_b' increases as the bias voltage is increased and quantum-mechanical effects are critically dependent on the barrier height and the electric field strength at the contact, which also increases with bias. Thus, one can safely neglect image effects for this particular application and Eq. 5.17 should give a reasonably

accurate relation between the intercept voltage and the equilibrium diffusion potential; however, when one considers the current-voltage properties of the contact image effects may become fairly important at higher reverse bias.

The slope of the straight line approximation for Eq. 5.10 reduces to the same slope as obtained using the Schottky expression for junction capacitance. This can be easily verified by taking the derivative of Eq. 5.14 with respect to voltage. In other words, the value for N_d predicted by the two models is exactly the same (Eq. 5.9) since the slopes agree for $y_o \gg 1$. This is shown quite clearly in Fig. 5.5.

By comparison of Eq.'s 5.7 and 5.17 one can see that there will be a significant difference between the diffusion potential predicted by the Schottky and more accurate model when using the capacitance versus voltage method to determine V_o. The exact disagreement between the two models will be the difference between the intercept values (V_o) as shown in Fig. 5.5, and will be influenced by the degree of ionization. Thus, one can expect the value of V_d predicted by the Schottky model to be in error by at least KT/e (from Eq. 5.17 with $\gamma=1$) and this error would increase as the degree of ionization decreases. Furthermore, the value of the doping concentration (N_d) obtained by the capacitance method will be independent of the model used, since the slope predicted by the Schottky model and the

straight line approximation to Eq. 5.10 are the same for sufficient values of reverse bias.

The conclusions drawn thus far are for an idealized contact and one will find that an application of the capacitance method to determine V_d for a "real" contact will involve many complications. Goodman[28] has made a comprehensive study of the complications involved in the measurement of barrier heights by the capacitance method for "real" metal-semiconductor contacts, and outlines a procedure to minimize many of these complications. He also examines the model dependence of the capacitance expression and concludes that "the true value of the barrier height is greater than the 'intercept value' by KT/e." However, there can be significant error in this conclusion for incomplete ionization, i.e., $\gamma<1$, as can be seen from Eq. 5.17.

Having determined the diffusion potential by experimentally determining V_o, one can calculate the barrier height as seen by electrons of the metal (E_b) by using Eq. 5.3. In order to use Eq. 5.3 the position of the Fermi level must be known for the bulk semiconductor and this may be calculated by using the following relation:[29]

$$E_{fs} = \tfrac{1}{2}(E_{co}+E_{vo}) + \frac{3KT}{4}\ln(m_h^*/m_e^*) + KT\ln\left\{\frac{N_d}{2n_i}\left\{1 + \left[1 + \left(\frac{2n_i}{N_d}\right)^2\right]^{\frac{1}{2}}\right\}\right\} \tag{5.18}$$

Equation 5.18 is an exact expression and all of the quantities are either known or material constants, with the possible exception of N_d which can be determined by Eq. 5.9. Thus, using Eq.'s 5.3, 5.17 and 5.18 (V_d by the more exact model) or 5.7 (V_d by the Schottky model) a value of E_b can be determined and a comparison can be made between E_b as measured by the photoresponse method and indirectly measured by the capacitance method. This comparison would be an indication of the degree of accuracy associated with the Schottky and more exact models; however, any comparison should be made with reservation since Goodman[28] has indicated that there may be many experimental errors associated with experimentally determining V_o.

CHAPTER VI

CURRENT-VOLTAGE CHARACTERISTICS OF A METAL-SEMICONDUCTOR RECTIFYING CONTACT

6.1 Current-Voltage Equation.

Before undertaking the development of the current-voltage equation of a metal-semiconductor contact it would be helpful to understand more clearly the basic mechanism by which rectification takes place. In the absence of an external voltage (Fig. 2.4d) the electrons of the metal are in dynamic equilibrium with the conduction electrons of the semiconductor. Under this condition the rates at which carriers transverse the barrier are equal from either direction and the probability of such a crossing taking place will depend on the number of electrons having thermal energies greater than E_b and moving in the right direction. Furthermore, this rate of carrier transfer will be an exponential function of the barrier height and would thus decrease rapidly as the barrier height is increased. Since the probability for electron transfer is the same for either direction, one would expect no net electron current to flow across the junction.

Next, consider the situation in which an external bias is introduced in such a way as to make the semiconductor

positive with respect to the metal (Fig. 2.5b). This would correspond to a reverse bias, since the effective barrier height to electron flow from the semiconductor into the metal has been increased. On a probability basis, the probability of electron transfer from the metal is still governed by $\exp(-E_b/KT)$ and must therefore remain unchanged with respect to the equilibrium condition. On the other hand, the probability of electron transfer from the conduction band of the semiconductor into the metal will be proportional to $\exp[-e(V_d+V_r)/KT]$ and must therefore be greatly reduced even for a small amount of reverse bias (V_r). The equilibrium condition of equal electron transfer can no longer be maintained and a small net current will cross the junction. This will be called the reverse saturation current (I_o) and represents an electron leakage current from the metal into the semiconductor under reverse bias. Here the term "leakage" is used to emphasize the fact that it is an unwanted current, since ideally I_o should be zero for perfect rectification.

Finally, consider the situation in which the polarity of the bias voltage is reversed, i.e., the metal is now made positive with respect to the semiconductor. This will correspond to a forward biased condition and is shown in Fig. 2.5a. Again equilibrium conditions cannot be maintained, since the probability of electron transfer from the conduction band of the semiconductor to the metal is greatly

increased, i.e., it must now be proportional to $\exp[-e(V_d-V_j)/KT]$. Furthermore, the rate at which electrons flow in the opposite direction remains unchanged since this transfer is still proportional to $\exp(-E_b/KT)$ and E_b remains constant (neglecting image effects). The result of this unbalance is a large net electron current flowing into the metal under the influence of a forward bias.

Thus, the character of rectification is exhibited through the unbalanced flow of electron current under forward and reverse bias conditions. In addition, one should note that for a metal-(N-Type)-semiconductor contact positive values of V_a correspond to a reverse bias and negative values of V_a to a forward bias. Furthermore, the current flowing under forward bias will be of much greater magnitude than under reverse bias conditions.

In order to calculate an expression which can predict the current-voltage relationship of a metal-semiconductor contact it is necessary to assume that the actual number of electrons constituting current flow across the contact is only a small fraction of the total free electron population of the semiconductor. This seems to be a reasonable assumption for effective barriers, i.e., $E_b \gg KT$, and allows one to assume that the electron concentration of the bulk semiconductor is constant and independent of the current flowing in the device. Furthermore, it is possible to distinguish two types of models for rectification on the

basis of barrier width. The most general case is to consider the width of the barrier within an energy increment of KT near the top as being large compared with the mean free path* (λ_e) of an electron in the semiconductor. This distance near the top of the barrier is used because it is necessary to compare the probability of an electron being stopped by a normal collision process and the probability of its reflection by the potential barrier itself. When the width within KT of the top of the barrier is large compared to the mean free path of an electron, the electrons crossing the barrier can be expected to suffer many collisions before reaching the other side and as a consequence current flow across the barrier must be by a diffusion process. When this width is small compared to λ_e, the probability of many collisions taking place is small and current flow can be thought of as an emission of electrons over the barrier.[30] The emission model is somewhat simpler than the diffusion model, but the diffusion model must be regarded as the most general since λ_e is on the order of 10^{-5} to 10^{-6} cm,[31] causing the model to be applicable to all but the thinnest barriers. A possible example of a thin barrier might be a point contact device, in which case λ_e could exceed the

---

*λ_e is defined as the average distance between two successive collisions of an electron with the lattice structure of the semiconductor.

width of the barrier near the top.

Under the assumption that diffusion theory is applicable and that the potential within the barrier is known from the model developed in Chapter IV, one may calculate the current-voltage relationship for the contact. Quantum-mechanical effects and image force will be neglected initially so that the current flow will be assumed to be strictly by a diffusion process. Furthermore, since the current in the barrier region depends on the local field as well as the local concentration gradient, a calculation of the current-voltage relation for a N-Type material must begin from the general diffusion equation of the form[32]

$$I_n = eAD_n\left[\frac{dn(x)}{dx} + \frac{eE(x)n(x)}{KT}\right] \qquad (6.1.1)$$

The diffusion of carriers against a retarding electric field will occur across the barrier if a difference in electron density occurs, and with the aid of Fig. 6.1 this difference in respective densities can be easily shown. The minimum value of electron concentration will ocur at the junction, i.e.,

$$n(0) = \gamma N_d \exp(-eV_d/KT) \qquad (6.1.2)$$

One should note that this density will be independent of the applied voltage since the electron concentration in the

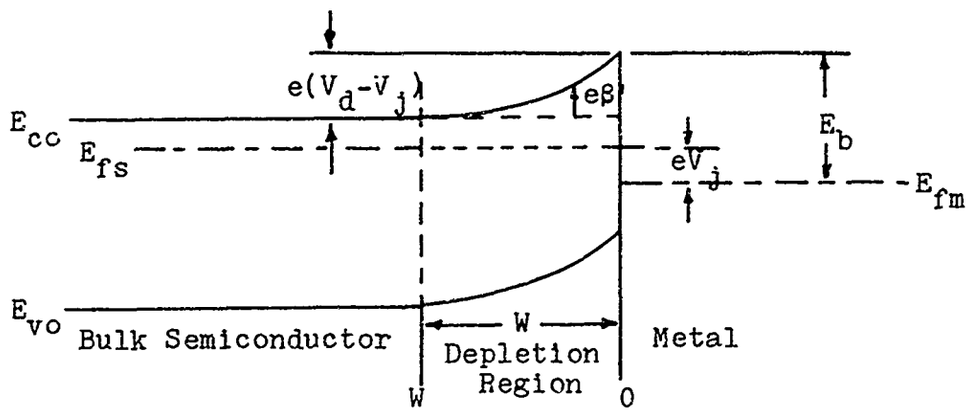

FIGURE 6.1: Energy Diagram for a Metal-Semiconductor Barrier Under Forward Bias Conditions; Image Force Neglected.

metal and the barrier height E_b have constant values (neglecting image effects). Furthermore, n(x) will increase as x increases until it reaches a maximum at x=W where

$$n(W) = n_o = \gamma N_d \tag{6.1.3}$$

and may also be regarded as constant since it was originally assumed that the equilibrium concentration of electrons in the bulk semiconductor is not appreciably disturbed by current flow in the device. Thus, a difference in electron densities between opposite sides of the barrier is apparent and one can expect a diffusion of electrons in the direction of the metal through the potential barrier. Electron diffusion constitutes an electron current (I_n) and if one adopts the convention that positive current flows in the negative x direction the calculation of I_n may proceed as follows:

(1) Equation 6.1.1 is multiplied by $\exp[-e\beta'(x)/KT]$ and upon substitution of $E(x)=-d\beta'(x)/dx$ yields

$$I_n \exp[-e\beta'(x)/KT] = eAD_n\left[\frac{dn(x)}{dx} - \frac{e}{KT}\cdot\frac{d\beta'(x)}{dx}\cdot n(x)\right]\exp[-e\beta'(x)/KT] \tag{6.1.4}$$

(2) Noting that

$$\frac{d}{dx}\exp[-e\beta'(x)/KT] =$$

$$-\frac{e}{KT}\cdot\frac{d\beta'(x)}{dx}\cdot\exp[-e\beta'(x)/KT] \tag{6.1.5}$$

the right side of Eq. 6.1.4 may be expressed in terms of a derivative, or

$$I_n\exp[-e\beta'(x)/KT] =$$

$$eAD_n\left\{\frac{d}{dx}\left\{n(x)\exp[-e\beta'(x)/KT]\right\}\right\} \tag{6.1.6}$$

(3) Multiplying both sides of Eq. 6.1.6 by dx and integrating over the depletion width yields

$$\int_0^W I_n\exp[-e\beta'(x)/KT] =$$

$$eAD_n\left\{n(x)\exp[-e\beta'(x)/KT]\right\}\Big|_0^W \tag{6.1.7}$$

(4) The right side of Eq. 6.1.7 may be evaluated by noting the following boundary conditions:

(a) $n(W)\exp[-e\beta'(W)/KT] = \gamma N_d\exp[-e(V_d-V_j)/KT]$ (6.1.8)

(b) $n(0)\exp[-e\beta'(0)/KT] = \gamma N_d \exp[-eV_d/KT]$ (6.1.9)

(5) Finally, I_n may be regarded as a constant if recombination is neglected in the depletion region. Thus, I_n may be expressed as

$$I_n = \frac{eAD_n\gamma N_d \exp[-eV_d/KT][\exp(eV_j/KT) - 1]}{\int_0^W \exp[-e\beta'(x)/KT]dx} \qquad (6.1.10)$$

Equation 6.1.10 takes the form of the familiar diode equation and may be rewritten in a shortened form as follows:

$$I_n = I_o[\exp(eV_j/KT) - 1] \qquad (6.1.11)$$

where

$$I_o = eAD_n\gamma N_d\left[\exp(-eV_d/KT)\right] \cdot \left\{\int_0^W \exp[-e\beta'(x)/KT]\right\}^{-1} \qquad (6.1.12)$$

Upon closer examination of the integral which appears in

Eq. 6.1.12, one finds that after the variable transformation used in Chapter IV (Eq.'s 4.25 and 4.26) I_o may be expressed as

$$I_o = e^2 A D_n \gamma N_d^{3/2} (KT\epsilon_s)^{-\frac{1}{2}} \cdot \left[\exp(-eV_d/KT)\left(\int_0^W e^{-y} du\right)^{-1}\right] \tag{6.1.13}$$

and the integral could be evaluated by using numerical techniques similar to those used to evaluate y. This is pointed out because a numerical evaluation of $\int e^{-y} du$ would be a simple matter of inserting several statements into the computer program which has already been used to calculate the normalized electron potential and space charge density (Appendix F). However, since each evaluation of $\int e^{-y} du$ would depend on the initial value of y (a function of bias) and the degree of ionization (Eq. D.7), one must conclude that Eq. 6.1.13, and thus Eq. 6.1.12 already appear in their most general form.

Thus, if one neglects quantum-mechanical and image effects, the I-V characteristic may be stated in its most general form as follows:

$$I_n = I_o[\exp(eV_a/KT) - 1] \tag{6.1.14}$$

where I_o is given by either Eq. 6.1.13 (in normalized form)

or by Eq. 6.1.12. Inherent in Eq. 6.1.14 is the assumption that the magnitude and polarity of V_a is consistent with the assumptions on which the diffusion model is based.

6.2 Influence of Tunneling and Quantum-Mechanical Reflection on the I-V Characteristic.

In the previous section quantum-mechanical effects were neglected in forming the diffusion model for current transport at a metal-semiconductor contact. Clearly, the discussion as presented in Section 2.6 would indicate that the effects of tunneling and QMR may exert considerable influence on the overall I-V characteristic of the contact.

The effects of tunneling and QMR can be incorporated into the diffusion model by introducing a factor f_q which represents the ratio of total current flow (I_t) predicted considering quantum-mechanical effects to the diffusive current flow neglecting these effects (I_n). Stated mathematically,

$$I_t = f_q I_n \tag{6.2.1}$$

Furthermore, a numerical value for f_q may be calculated by averaging the QMTC over the complete kinetic energy spectrum associated with the electrons incident on the potential barrier (corrected for image effects). If the kinetic energy associated with an incident electron is denoted by

E_e and it is assumed that E_e is governed by a Maxwellian distribution, then f_q may be computed as follows:

$$f_q = \frac{1}{KT}\int_{-\infty}^{\infty}(QMTC)\exp(-E_e/KT)dE_e \qquad (6.2.2)$$

Crowell and Sze[33] have used numerical techniques to compute f_q for Au-GaAs, Au-Ge, and Au-Si N-Type contacts as a function of the electric field at the contact (E_o) for selected temperatures.* A plot of f_q versus E_o is shown in Fig. 6.2 using the curves of the QMTC shown in Fig. 2.9 for an Au-GaAs (N-Type) contact for selected temperatures. For this particular contact quantum-mechanical effects may be seen to exert considerable influence on the total current flow as predicted by the diffusion model since tunneling becomes excessive for electric fields exceeding 10^5 v/cm. Similar results are found for the Au-Si contact over the same range of E_o; however, for the Au-Ge contact f_q approaches a very low value at $E_o > 10^5$ v/cm ($f_q \approx 0.01$). This would indicate that reflection predominates in the germanium contact at relatively high electric fields.

An alternate approach to calculating f_q for a contact

---

*They have assumed the approximate form of E_b' as $E_b' \approx e\left[\frac{eE_o}{4\pi\epsilon_s'}\right]^{\frac{1}{2}}$.

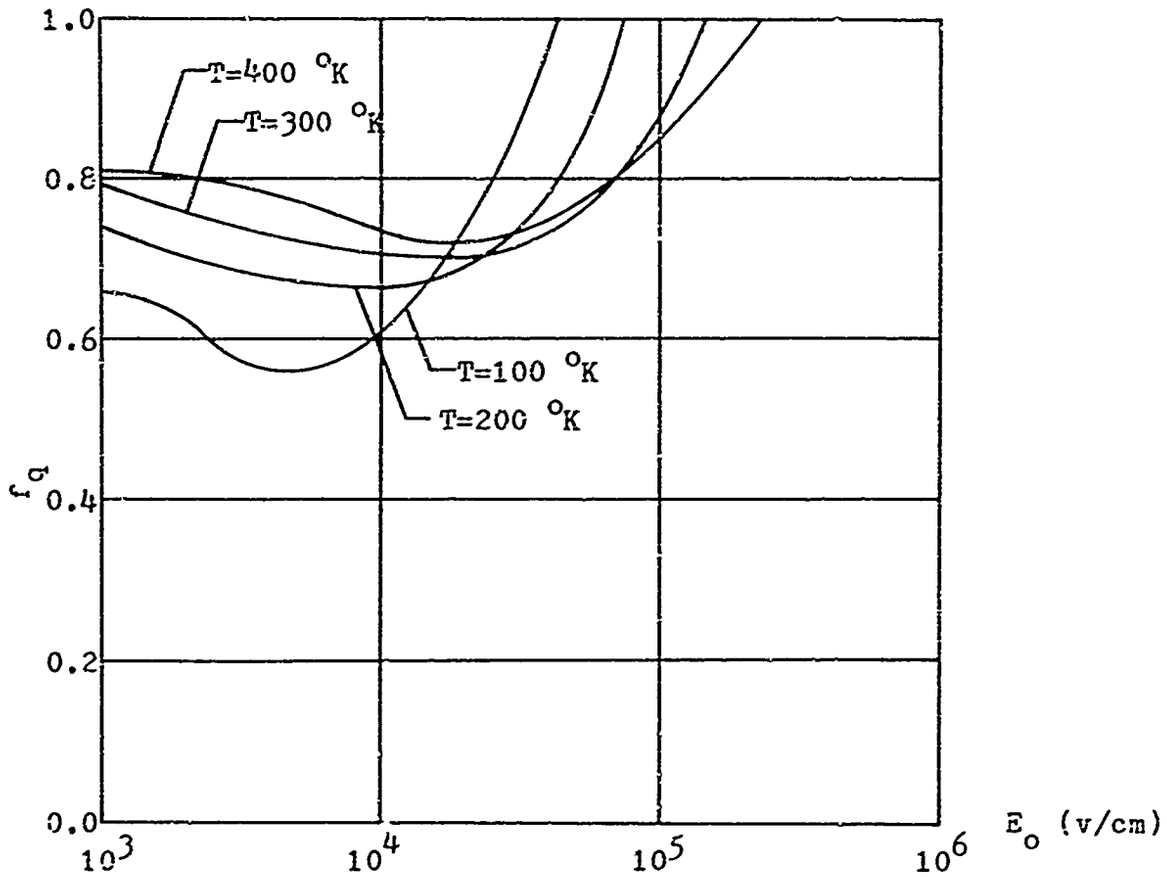

FIGURE 6.2: Quantum-Mechanical Transmission Coefficient, f_q, Averaged over a Maxwellian Distribution of Electrons Incident on the Potential Energy Maximum of an Au-GaAs (N-Type) Contact as a Function of the Electric Field (E_o) for Selected Temperatures, Assuming a Smooth Merging of the Conduction Band Edge in the Semiconductor into the Conduction Band Edge of the Metal.[34]

barrier would be to adopt the approximate expressions given by Kemble[19] (Appendix C) for the QMTC and average these approximate expressions assuming a Maxwellian distribution in electron energy. However, a calculation of this type would also require numerical techniques because of the complexity of the expressions for the QMTC.

Still another approach is available if one is willing to approximate a QMTC plot by simple analytic expressions in order to allow the average value of f_q to appear in closed form. In order to illustrate this technique the QMTC will be approximated by a single straight line whose slope has been adjusted to obtain the best agreement possible. A plot of this form is shown in Fig. 6.3. This would certainly represent a crude approximation, but increased accuracy would be obtained by using additional straight lines, higher order analytic expressions, or a combination of both. Using the single straight line approximation the calculation of f_q would proceed as follows:

(1) $$f_q = \frac{1}{KT}\int_{-\infty}^{\infty}(\mathrm{QMTC})\exp(-E_e/KT)dE_e \qquad (6.2.3)$$

(2) In terms of the straight line approximation for the QMTC, f_q may be expressed as

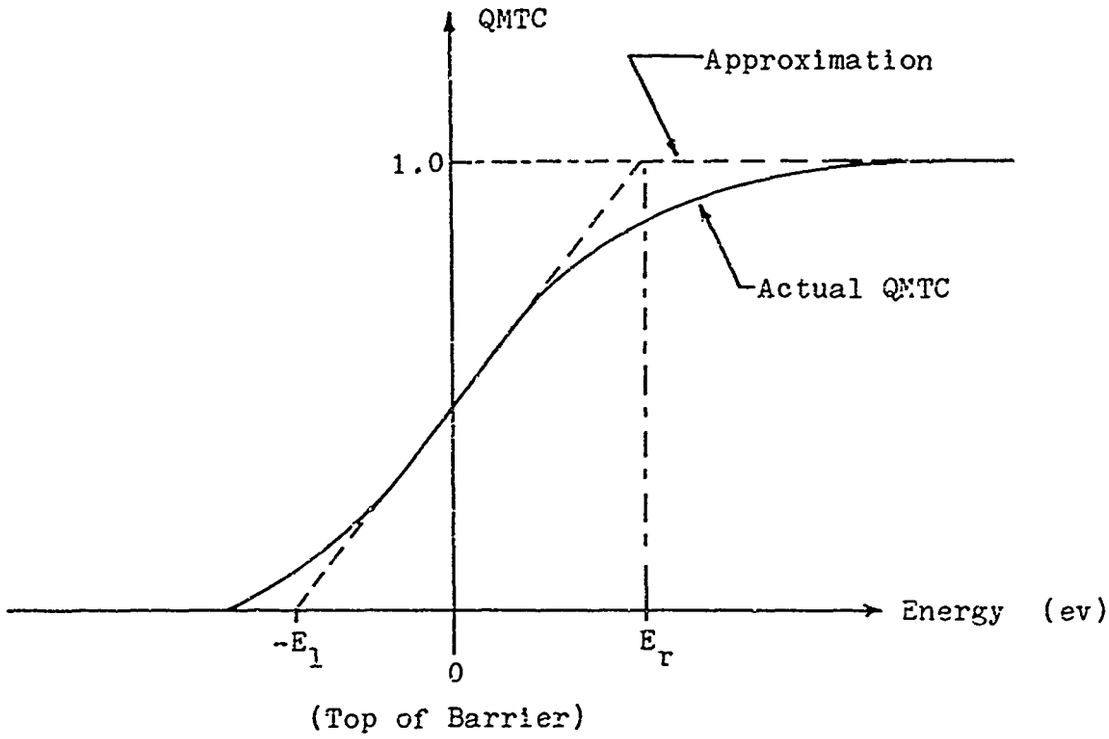

$$QMTC = \begin{cases} 0 & E_e < -E_l \\ \dfrac{E_l + E_e}{E_l + E_r} & -E_l < E_e < E_r \\ 1 & E_e > E_r \end{cases}$$

FIGURE 6.3: Single Straight Line Approximation for the QMTC.

$$f_q = \frac{1}{KT}\int_{-\infty}^{-E_1}(0)\exp(-E_e/KT)dE_e + \frac{1}{KT}\int_{-E_1}^{E_r}\frac{E_1 + E_e}{E_1 + E_r}\exp(-E_e/KT)dE_e + \frac{1}{KT}\int_{E_r}^{\infty}(1)\exp(-E_e/KT)dE_e \qquad (6.2.4)$$

(3) Integration with respect to E_e and substitution of the limits yields

$$f_q = \frac{KT}{E_1 + E_r}\left[\exp(E_1/KT) - \exp(-E_r/KT)\right] \qquad (6.2.5)$$

(4) Since plots of the QMTC reveal that $E_r > E_1$, a reasonable approximation would be

$$f_q = \frac{KT\exp(E_1/KT)}{E_1 + E_r} \qquad (6.2.6)$$

Thus, using this form of approximation for the QMTC, f_q may be expressed in terms of the end-point energies E_r and E_1. One should also note that these end-point energies are rather strong functions of E_o, and thus a function of the applied bias. In addition, if more accurate approximations are used for the QMTC then f_q would become a more complicated expression involving more characteristic energies.

6.3 Influence of Image Effects on the I-V Characteristic.

The sample calculation presented at the end of Chapter IV indicated that the normalized correction to the barrier

height due to image effects (y_b') was quite small in comparison to the uncorrected, normalized barrier height at the contact (y_o). However, the importance of image effects should not be overlooked since a small change in the barrier height has significant influence on the QMTC. This can be seen from Fig. 2.9 in which the QMTC changed significantly for small changes in the kinetic energy associated with an incident electron when the kinetic energy is referenced to the top of the barrier corrected for image effects. Furthermore, y_b' is voltage dependent so that greater influence may be expected at higher bias voltages. As it turns out y_b' exerts greater influence at higher reverse bias, but due to large currents flowing under forward bias ($e^{eV_f/KT} >> 1$) the influence of y_b' may go completely unnoticed.

In order to include the influence of image effects in the I-V characteristic predicted by the diffusion model the original assumption that n(0) was independent of bias (assuming E_b was independent of bias, Eq. 6.1.12) must be modified to include the influence of image effects. This can be done by replacing V_d by an effective diffusion potential (V_{dso}) which includes image effects. Stated mathematically,

$$V_{dso} = V_d - \alpha_b(V_a) \qquad (6.3.1)$$

in which $\alpha_b(V_a)=E'(V_a)/e$ and represents the voltage dependent reduction in the diffusion potential due to image effects. Furthermore, $\alpha_b(V_a)$ may be written in the form

$$\alpha_b(V_a) = \alpha_{bo}\alpha_b' \tag{6.3.2}$$

in which α_{bo} is independent of bias voltage and α_b' contains the voltage dependence. Expressions for α_{bo} and α_b' may be found by writing Eq. 3.3.4 in the form*

$$\alpha_b(V_a) = \left[\frac{e^3N_d}{8\pi^2(\epsilon_s'\epsilon_s^o)^2\epsilon_s}\right]^{\frac{1}{4}}(V_d - V_a)^{\frac{1}{4}} \tag{6.3.3}$$

so that α_{bo} may be expressed as

$$\alpha_{bo} = \left[\frac{e^3N_dV_d}{8\pi^2(\epsilon_s'\epsilon_s^o)^2\epsilon_s}\right]^{\frac{1}{4}} \tag{6.3.4}$$

and

$$\alpha_b'(V_a) = (1 - V_a/V_d)^{\frac{1}{4}} \tag{6.3.5}$$

It should also be noted that the inclusion of image effects will alter the integral expression in Eq. 6.1.12 since $\beta'(x)$ must now be replaced by the total electron

---

*Recalling that $V_a=-V_r$ for reverse bias and $V_a\approx V_f$ for small forward bias.

potential $\beta(x)$ where $\beta(x)$ is given by

$$\beta(x) = \beta'(x) - \frac{e}{16\pi\epsilon_s' x} \qquad (x>0) \qquad (6.3.6)$$

6.4 Complete I-V Characteristic for a Metal-Semiconductor Contact.

The complete expression for the I-V characteristic for an idealized metal-semiconductor contact, assuming the diffusion model is applicable, may be summarized as follows:

$$I_t = I_o' \exp(-eV_d/KT)[\exp(eV_a/KT) - 1] \qquad (6.4.1)$$

where

$$I_o' = \frac{eAD_n\gamma N_d f_q \exp(-\alpha_{bo}\alpha_b'/KT)}{\int_0^W \exp[-e\beta(x)]dx} \quad , \qquad (6.4.2)$$

$$f_q = \frac{1}{KT}\int_{-\infty}^{\infty} (QMTC)\exp(-E_e/KT)dE_e \quad , \qquad (6.4.3)$$

$$\alpha_{bo} = \left[\frac{e^3 N_d V_j}{8\pi^2(\epsilon_s'\epsilon_s^o)^2\epsilon_s}\right]^{\frac{1}{4}} \quad , \qquad (6.4.4)$$

$$\alpha_b' = (1 - V_a/V_d)^{\frac{1}{4}} \quad , \tag{6.4.5}$$

$$\beta(x) = \beta'(x) - \frac{e}{16\pi\epsilon_s' x} \quad , \tag{6.4.6}$$

and

$$\beta'(x) \text{ is the solution to Eq. 4.24} \tag{6.4.7}$$

6.5 Breakdown Mechanisms for a Metal-Semiconductor Contact.

At large applications of reverse bias, junction breakdown may occur by anyone of the following mechanisms:

(1) The barrier becomes so thin and the electric field so large that current flow due to tunneling may become excessive.

(2) Electrons can travel to the conduction band by tunneling from deep lying traps or directly from the valence band (Zener breakdown).

(3) The electron velocity becomes so large that electron-hole pairs can be generated through collisions. These in turn are again accelerated by the electric field so that additional electron-hole pairs are created. As a consequence

a single carrier can produce an avalanche of electron-hole pairs (avalanche breakdown).

Junction breakdown by tunneling can be expected to be one of the chief breakdown mechanisms in the reverse biased metal-semiconductor diode. This fact becomes apparent by examining Fig. 6.2 for large electric fields at the contact. I_o is greatly increased due to f_o and breakdown of the junction may occur.

Junction breakdown by the Zener effect is less likely to occur in metal-semiconductor devices than in P-N junctions. This is due to the fact that current flow in the metal-semiconductor device is chiefly, if not exclusively, by majority carriers. Since $\phi_m - X_e$ is typically much less than E_g (the original assumption on which the approximation that $p \approx 0$ is based) tunneling by the Zener mechanism is greatly reduced for a majority carrier device.

Junction breakdown by the avalanche mechanism is also of prime importance for a metal-semiconductor contact under large reverse bias. At very large reverse biases it may happen that an electron emitted over the barrier from the metal into the semiconductor may gain more energy due to the high electric field during collisions that it loses because of a collision. Thus, the kinetic energy of the electron will continue to increase until it exceeds E_g. At this point a collision can generate electron-hole pairs, which in turn may produce additional electron-hole pairs

and the avalanche process has begun. Under this condition the reverse current I_{so} (reverse current prior to breakdown) is greatly increased by the addition of free carriers, i.e.,

$$I_o^m = MI_{so} \tag{6.5.1}$$

in which M is the avalanche multiplication factor. At a certain field strength, which is constant for a given semiconducting material, M becomes infinite and breakdown occurs. Empirically it is found that M may be expressed as

$$M = \frac{1}{1 - [(V_d - V_r)/V_{br}]^N} \tag{6.5.2}$$

in which V_{br} is the reverse voltage at which breakdown occurs and N is a relatively large (5 to 6) constant dependent on the particular semiconducting material.[35]

6.6 Qualitative Comparisons Between the Theoretical I-V Characteristic and Experimental Measurements.

The complete theoretical expression for the I-V characteristic was summarized in Section 6.4 for an idealized metal-semiconductor contact. Although the complete expression would be quite difficult to evaluate, it could conceivably be done and result in a theoretical plot of the I-V characteristic by assuming the necessary constants and evaluating the various expressions by appropriate numerical

techniques. However, without making a direct comparison between a theoretical plot of this type and an experimentally determined characteristic, it is possible to make certain qualitative comparisons between experimental measurements and the general form of Eq. 6.4.1. This type of comparison will be undertaken in this section in hopes of justifying at least the form of the theoretical expression.

In Fig. 6.4 an experimentally determined I-V characteristic is shown for a Pt-Si (N-Type) contact. For this particular application it is convenient to plot $\ln(I_t)$ versus V_a. Using Eq. 6.4.1, $\ln(I_t)$ becomes

$$\ln(I_t) = \ln[I_o'\exp(-eV_d/KT)] + \ln[\exp(eV_a/KT)-1] \quad (6.6.1)$$

which under forward bias conditions may be written as

$$\ln(I_t) = \ln[I_o'\exp(-eV_d/KT)] + eV_f/KT \quad (6.6.2)$$

since $\exp(eV_f/KT) \gg 1$. Thus, if $\ln(I_t)$ is plotted against V_f a straight line should result with slope

$$m_y = e/KT \quad (6.6.3)$$

Experimentally it is found that for this particular contact

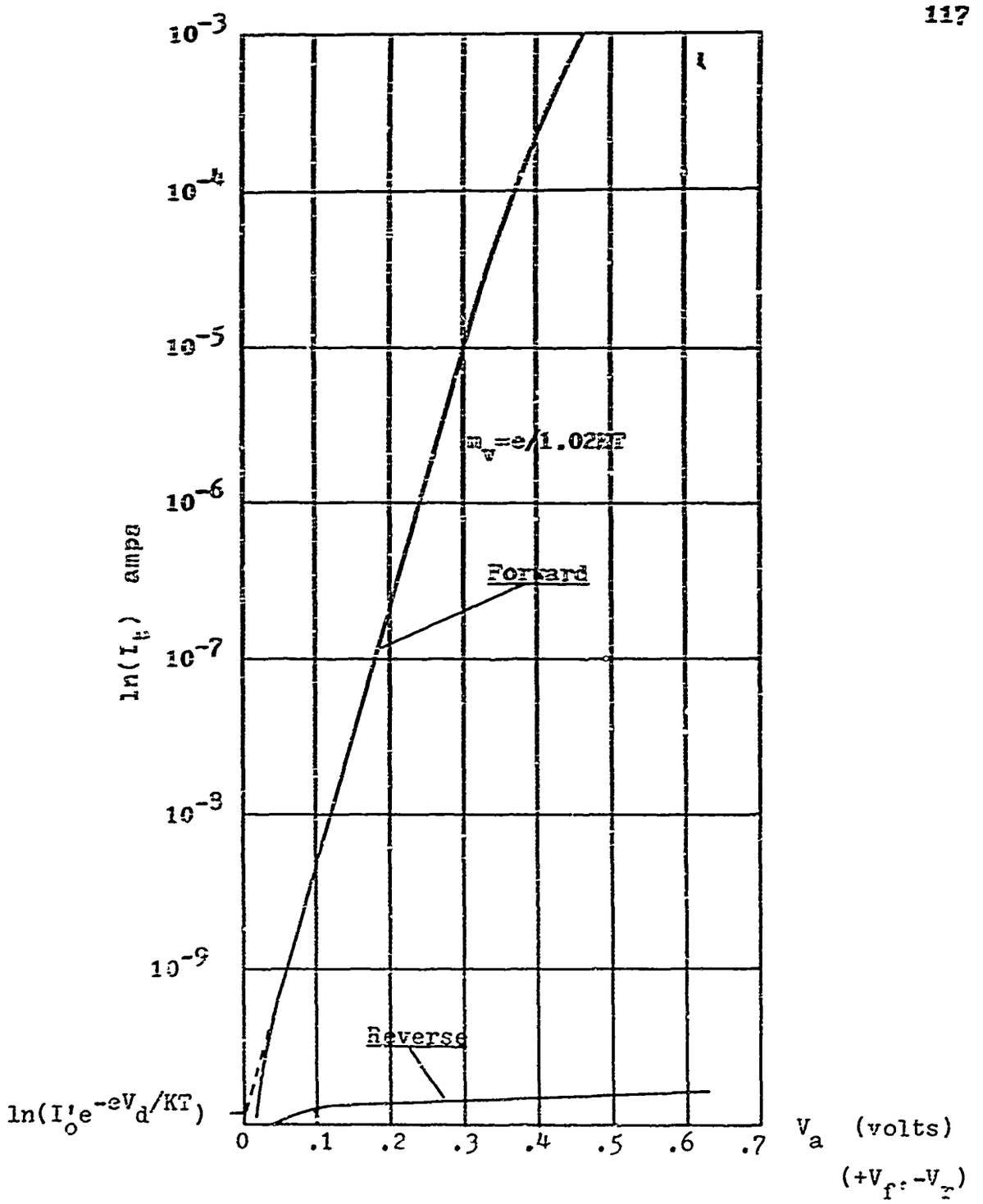

FIGURE 6.4: Current-Voltage Characteristic for a Pt-Si (N-Type) Contact.[36] Diam.=1.54(10^{-2}) cm.

that

$$m_v = \frac{e}{\delta KT} \tag{6.6.4}$$

in which $\delta = 1.02$. This small deviation from the slope as predicted by Eq. 6.6.3 can be attributed to the nonideal nature of the contact, or more specifically to the presence of a thin interfacial layer of foreign material and/or nonuniform contact between the metal and semiconductor.[37] In general, δ is usually included in the expression for the I-V characteristic to account for the nonideal nature of the contact and can be expected to be slightly different for each device. If δ is included, it may be determined by the following relation:

$$\delta = \frac{e}{KT}\frac{dV_f}{d\ln(I_t)} \quad (V_f \text{ sufficiently large}) \tag{6.6.5}$$

The deviation from the constant slope (m_v) at higher current [$\ln(I_t) > 10^{-4}$ amps] can be attributed to the series resistance associated with the bulk semiconductor. Also, by examining Eq. 6.6.2 a means of determining $I_o'\exp(-eV_d/KT)$ becomes apparent. This parameter may be determined by an extrapolation of the $\ln(I_t)$ versus V_f curve until intersection occurs at the $\ln(I_t)$ axis ($V_f = 0$) as shown in Fig. 6.4.

The exponential dependence of $I_o'\exp(-eV_d/KT)$ on the

equilibrium diffusion potential (V_d) can be shown by a plot of the type shown in Fig. 6.5. Here $\ln(I_o' e^{-eV_d/KT})$ is plotted against V_d for several metal-Si (N-Type) contacts, showing a constant slope of approximately e/KT. Although exact agreement is not shown, the deviation can be attributed to inaccuracies in the measurement of V_d.[39]

The temperature dependence of $I_o' \exp(-eV_d/KT)$ can be shown by a plot of the type shown in Fig. 6.6. Here $\ln(I_o' e^{-eV_d/KT})$ versus 1/T is plotted under forward bias for a Au-Si (N-Type) contact with eV_d=0.08. The slope is constant and equal to

$$E_a = -e(V_d - V_f) = 0.799 \text{ ev} \qquad (6.6.6)$$

E_a is usually referred to as the thermal activation energy for the contact.

The voltage dependence of the I-V characteristic at high reverse bias is shown by Fig. 6.7. Here $\ln(I_r)$ versus V_r is plotted, where

$$I_r = I_{or} \exp(y_b') \qquad (6.6.7)$$

and y_b' is given by Eq. 4.47. I_r is interpreted as the effective reverse current flowing in this region (large reverse bias) of operation and I_{or} is the effective saturation value of I_r. For silicon $\epsilon_s'=11.7\epsilon_o$[42], and good agreement is shown between the theoretical value predicted by image effects and the data shown in Fig. 6.7.

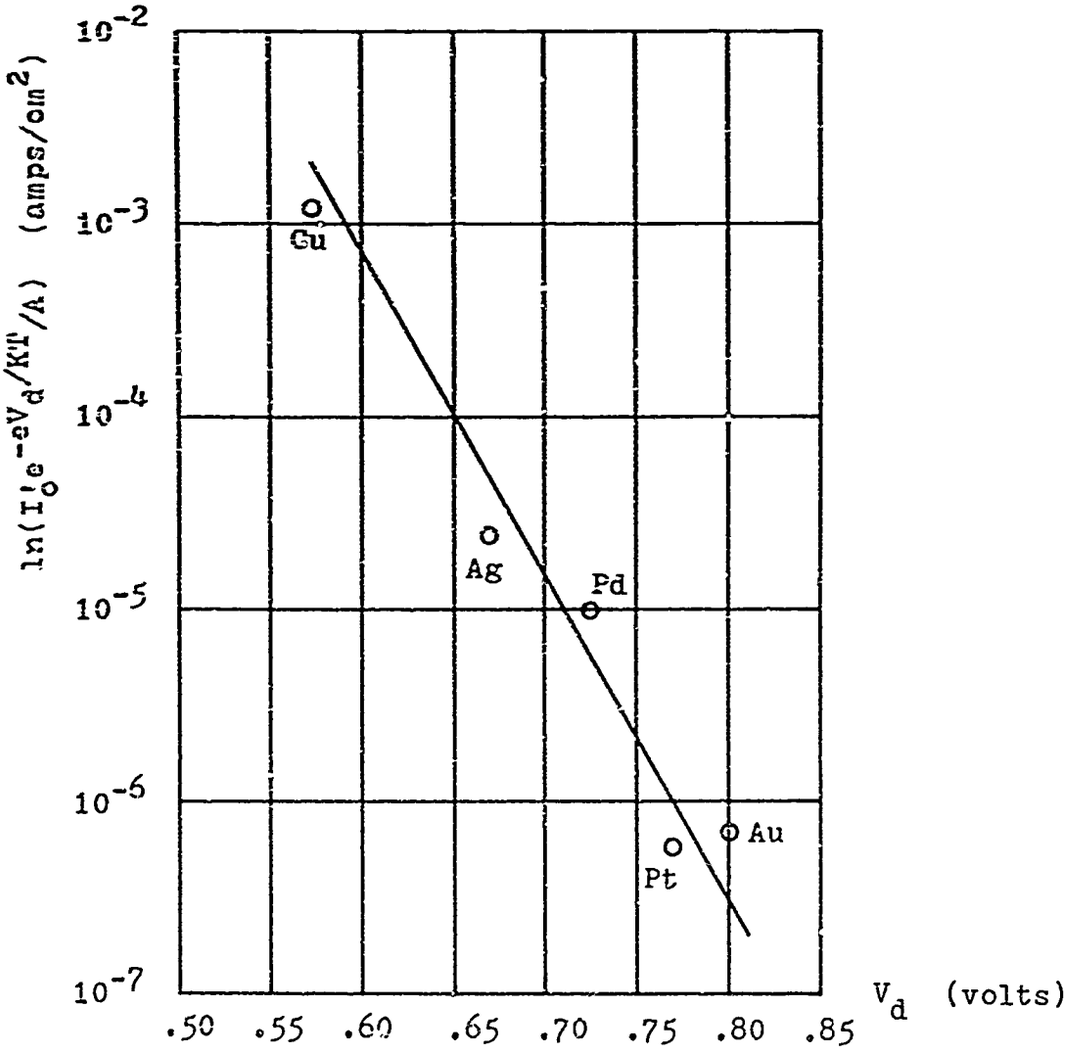

FIGURE 6.5: Dependence of the Saturation Current Density on the Equilibrium Diffusion Potential (V_d) for Several Metal-Si (N-Type) Contacts.[39]

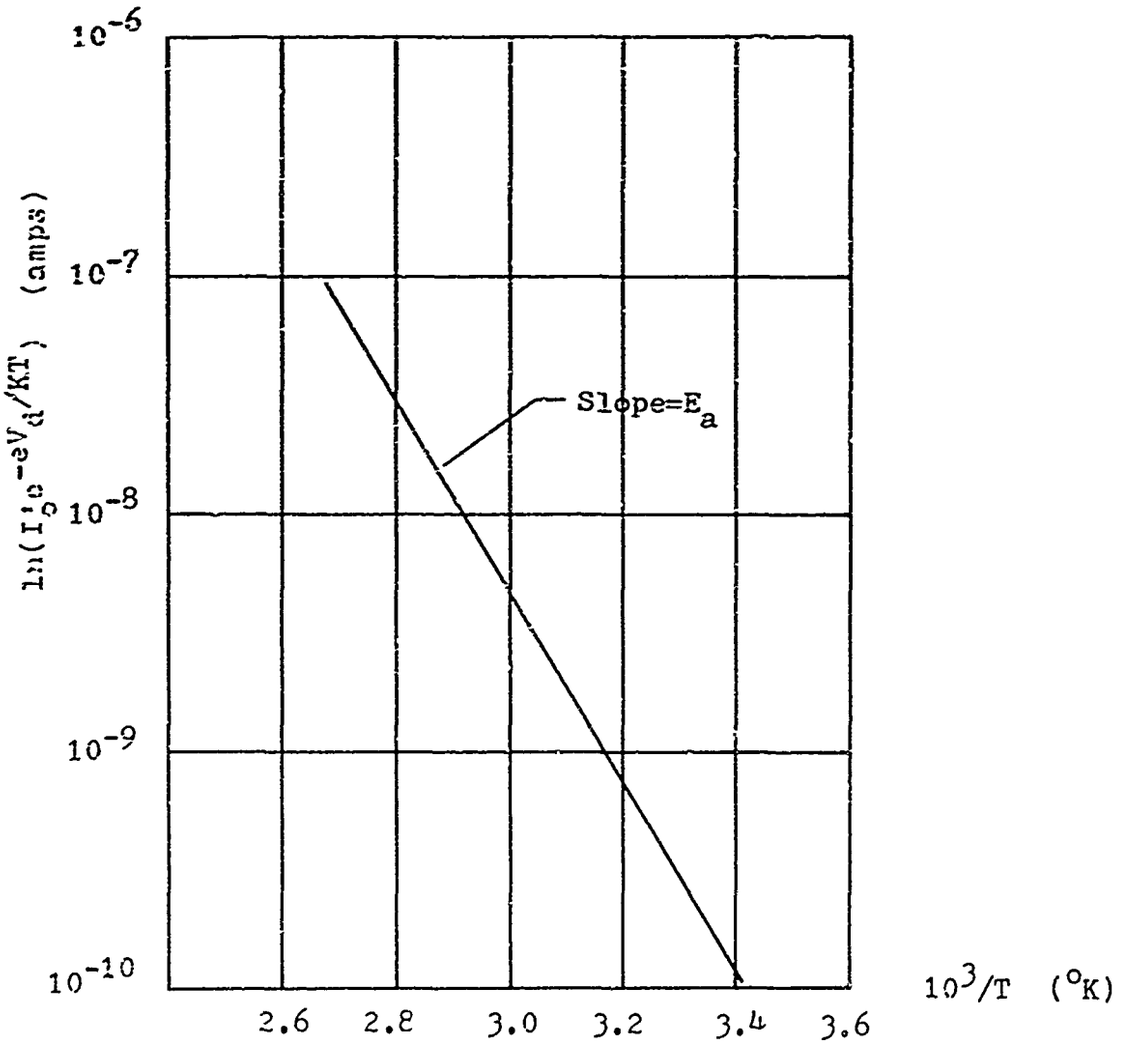

FIGURE 6.6: Temperature Dependence of the Saturation Current Under Forward Bias for a Au-Si (N-Type) Contact.[40] (eV_d=0.08 ev and E_a=0.799 ev)

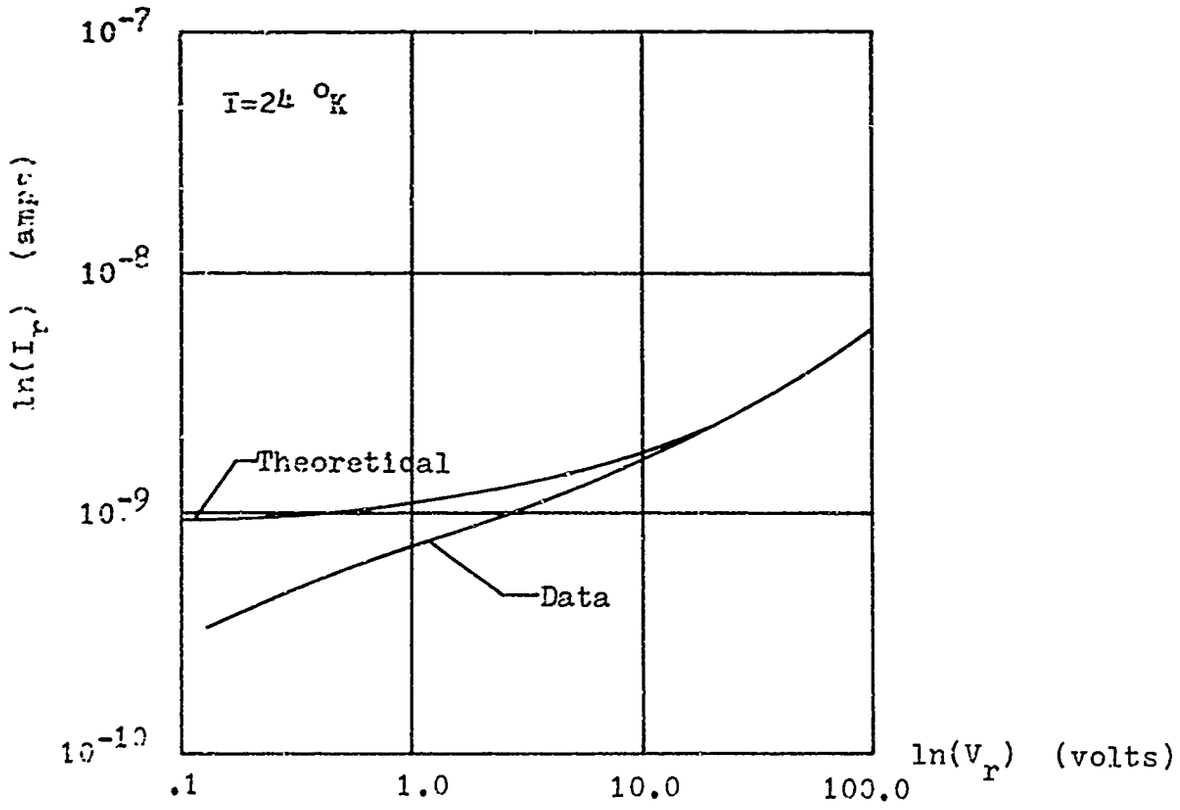

FIGURE 6.7: Reverse Current-Voltage Characteristic of an Au-Si (N-Type) Contact Compared with the Theoretical Voltage Dependence due to Image Effects.[41]

CHAPTER VII

SUMMARY, CONCLUSIONS AND RECOMMENDATIONS FOR FURTHER STUDY

This study originated as an effort to answer the question of why the experimental method of measuring capacitance as a function of reverse bias could be used to accurately predict the doping concentration and yet could not be expected to give a reliable measure of the equilibrium diffusion potential, even though both quantities resulted from an interpretation of the same data. Since the capacitance technique is based on the Schottky model for the contact, the most logical approach to explaining this apparent inconsistency was to examine more closely the theoretical expression for junction capactiance, or more basically the Schottky model itself, while paying particular attention to any approximations which could limit accuracy.

The Schottky model is based on the assumption that the space charge associated with the depletion region formed at a metal-semiconductor contact is constant and due entirely to the uniform and complete ionization of donor impurities within the depletion region. Outside the depletion region charge compensation due to the presence of free electrons is complete so that the net space charge is

zero. A more accurate model for space charge in the depletion region is developed in Chapter IV which considers the possibility of incomplete and nonuniform donor ionization and the partial compensation to positive space charge due to the presence of free electrons in the immediate vicinity of the depletion region edge. Once the space charge density is known as a function of distance in the depletion region, Poisson's equation (this study assumes a one-dimensional application) can be used to solve for expressions for the electric field and potential variation within this region. A comparison between the solutions based on both models shows that the Schottky model is quite accurate in the region near the contact; however, there may be significant error in the region near the depletion region edge. Furthermore, this error increases as the degree of ionization decreases.

Even though there may be large differences between the electric field and potential plots for the two models on a point by point basis, a comparison between the two space charge density plots reveals quite clearly why the Schottky model can give accurate results for certain applications. A comparison of this type shows that the Schottky model represents a fairly accurate estimate for the effective space charge density since the error predicted by the more exact model on a point by point basis is compensating and the overall difference between the two models can be quite small,

if the degree of ionization is fairly close to unity. This is equivalent to saying that the areas under the two space charge density plots (Fig.'s 4.2b and 4.3b) are approximately the same.

In Chapter V the differential capacitance technique for measuring the equilibrium diffusion potential was examined in detail. Using the expressions for junction capacitance (C_j^{-2}) based on both models the diffusion potential and intercept voltage are related as follows:

$$V_d = V_o \qquad \text{(Schottky Model)} \qquad (7.1)$$

$$V_d = V_o + \frac{KT}{e}(\gamma - \ln\gamma) \qquad \text{(More Exact Model)} \qquad (7.2)$$

Comparing these two expressions one can expect the diffusion potential predicted by Eq. 7.1 to be in error by at least KT/e (using Eq. 7.2 with $\gamma=1$) and this error will increase as the degree of ionization decreases. For $\gamma=0.05$ the error is approximately 3(KT/e); however, this is not a true representation of the actual error since the temperature must also decrease as γ decreases.

Another interpretation of the data from a capacitance (C_j^{-2}) versus reverse bias voltage plot results in an expression for the doping concentration. In Chapter V

N_d was shown to be proportional to the slope and the predicted slopes from both models were identical for sufficient reverse bias (y_o>4). The theoretical expression for N_d for both models is given by

$$N_d = \frac{2}{\frac{e\epsilon_s d(C_j^{-2})}{dV_r}} \qquad (y_o>4) \qquad (7.3)$$

and is known to agree quite well with results obtained by other means of measuring N_d. Why the apparent inconsistency between N_d and V_d using the differential capacitance method based on the Schottky model? The inaccurate measurement of V_d by interpreting V_d as equal to V_o is not the fault of the model, but results from a false interpretation of V_o. The experimental method of determining V_o is by extrapolating a C_j^{-2} versus V_r plot, which is linear as shown in Eq. 7.3, to a point where it intersects the V_r axis, i.e., V_o. This straight line passes through a region of small reverse bias and the eventual value of V_o falls in the region of negative V_r (see Fig. 5.4a). The apparent assumption is that the capacitance (C_j^{-2}) remains linear in this region and this is contrary to fact as shown in Fig. 5.5. The non-linear variation in capacitance (C_j^{-2}) at small values of reverse bias can be explained quite easily by examining the term corresponding to the free electron concentration in Eq. 4.23, or

$$n(x) = n_c \exp(-y) \qquad (0<x<W) \qquad (7.4)$$

Under a fairly large reverse bias y_o is large and y is increased so that $n(x) \approx 0$, which is consistent with the assumption on which the Schottky model is based; however, as V_r is decreased, y_o becomes smaller and eventually a point is reached at which one may no longer neglect the free electron population at the depletion region edge. This value of y_o can be interpreted from the capacitance (C_j^{-2}) versus voltage plot as shown in Fig. 5.5. Since the capacitance (C_j^{-2}) becomes nonlinear for all values of y_o less than four ($V_d + V_r \approx 0.104$ volts) and all values of γ, then one may interpret this as the point at which the Schottky model assumption that the depletion region is free of electrons is no longer valid. There is a small variation in this point due to γ, which is consistent with this line of reasoning since n_c in Eq. 7.4 is a function of γ, i.e., $n_c = \gamma N_d$. Thus, if γ decreases the free electron population at the depletion region edge will also decrease and the cut off value of y_o can be expected to increase. This is shown quite clearly in Fig. 5.5.

Since the interpretation of V_o is based on the intercept value of a linear plot, the value of V_o may be in error and the plot can still predict the correct slope. This is pointed out by Fig. 5.5 in which the Schottky and more exact

models predict the same slope for $y_o>4$, but there is significant difference in the values predicted for V_o. Furthermore, the slope is independent of γ ($y_o>4$) and the intercept value of V_o is not. The reason is again due to the correct interpretation of the components of space charge for different degrees of ionization. If all donor atoms are assumed to be ionized and $y_o>4$, then the slopes of the Schottky and more exact model are in complete agreement; however, if $\gamma<1$ then the positive space charge furnished by positive donor sites is reduced and one would expect an increasing disagreement between the two models for space charge density as γ decreases. This is shown in Fig.'s 4.2b and 4.3b. Furthermore, since the effective depletion width is reduced for smaller values of γ one would expect larger values of capacitance (assuming a constant value of bias) for lower values of γ (see Fig. 5.5). Since a lower value of γ implies a larger value of capacitance for the same bias voltage, one would also expect the intercept value of V_o (based on a linear estrapolation) to be γ dependent, with V_o increasing as γ decreases. This is also evident from Fig. 5.5.

The agreement between the two models in predicting N_d for $y_o>4$ stems from the fact that the two models are completely equivalent in this range of bias with regard to capacitance. The voltage dependence of the junction capacitance arises from the change in stored charge within the depletion region with and incremental change ($C_j=dQ/dV$) in the

applied bias and this addition and subtraction of charge will be independent of the initial stored charge (proportional to γ) as long as the depletion region is free of charge compensating electrons. For the region of bias voltage in which the free electron population at the depletion region edge can no longer be neglected ($y_o<4$), the change in capacitance (C_j^{-2}) associated with a change in bias is no longer constant since the density of compensating electrons varies exponentially (Eq. 7.3). Furthermore, the electron population is dependent on γ so that the slope can be expected to be altered by an additive constant due to the influence of γ. In addition, the change in capacitance (C_j^{-2}) caused by a change in γ will eventually reverse itself in this region, i.e., higher values of γ will produce lower values of capacitance (assuming the same value of bias) since the electron population at low values of y is more strongly influenced by γ than by y (y approaches a minimum value which is proportional to V_d). The above conclusions are illustrated quite well in Fig. 5.5.

In conclusion, the inaccuracy introduced by using Eq. 7.1 to interpret the diffusion potential from a capacitance (C_j^{-2}) versus voltage plot is due to the misrepresentation of the Schottky model. The Schottky model assumes that the depletion region is free of electrons and y_o has a minimum value for compliance with this assumption. Since capacitance (C_j^{-2}) is a nonlinear function of bias

below this minimum, a linear extrapolation for V_o produces significant error in V_d. However, if Eq. 7.2 is used to interpret V_o, then one may expect an accurate value for the equilibrium diffusion potential.

The influence of image effects on the accuracy of Eq. 7.2 was also considered in Chapter V and the conclusion drawn that image effects may be safely neglected for this particular application. This is due to the fact that the reduction in barrier height caused by image effects is quite small in comparison to the barrier height (neglecting image effects) at the contact, i.e., $y_o - y_b' \approx y_o$ at all values of bias even though y_b' increases with bias.

This study has also considered a theoretical development of the current-voltage characteristic of an idealized contact based on a diffusion model. Although justification for the accuracy of the I-V model developed on a quantitative basis has not been attempted, a qualitative comparison between the model and experimental measurements have produced favorable results. The model is able to predict the correct slope for the forward characteristic within a small multiplicative constant and this deviation can be attributed to the nonideal nature of the contact. Furthermore, the forward characteristic shows the correct temperature dependence and the reverse saturation current agrees well with the experimentally observed exponential dependence on the equilibrium diffusion potential. Also, the model is

able to predict a voltage dependence of the reverse characteristic which agrees well with experiment. This dependence arises from the increasing importance of image effects at large reverse biases. The theoretical model predicts a high probability of breakdown due to tunneling which is also consistent with experimental results. In short, although the theoretical I-V model would require fairly sophisticated numerical techniques for evaluation, it should agree quite well with experimental results on a quantitative basis.

Since the results of this study are quite conclusive with respect to the use of the differential capacitance technique for determining the diffusion potential and doping concentration, this method should compare favorably with values of V_d measured by the photoresponse technique. Thus, an experimental study of this type would warrant consideration. Also, it would be interesting, although the practicality may be questioned, to pursue a complete numerical evaluation of the theoretical current-voltage characteristic for the purpose of comparing the results with experimental measurements.

REFERENCES

REFERENCES

1. H. K. Henisch, Rectifying Semi-Conductor Contacts (Oxford University Press, New York, 1957), p. 7.

2. Henisch, p. 8.

3. A. H. Wilson, Proc. Roy. Soc. (London), 133, 458 (1931).

4. Henisch, p. 194.

5. B. Davydov, J. Tech. Phys. USSR, 5, 87 (1938).

6. L. Waibel and W. Schottky, Naturwiss, 20, 297 (1932).

7. N. F. Mott, Proc. Camb. Phil. Soc., 34, 568 (1938).

8. W. Schottky, Z. Phys., 113, 367 (1939).

9. W. Schottky, Z. Phys., 118, 539 (1942).

10. H. A. Bethe, Mass. Inst. Technol. Rept. #43-12 (1942). (Copy available from Publications Board, Dept. of Comm., Wash., D.C.).

11. J. Bardeen, Phys. Rev., 71, 717 (1947).

12. W. Schockley, Bell Syst. Tech. J., 28, 435 (1949).

13. J. Lindmayer and C. Wrigley, Fundamentals of Semiconductor Devices (D. Van Nostrand Co., Inc., Princeton, N. J., 1965), p. 101.

14. C. A. Mead, Solid-State Elect., 1027 (1966).

15. C. A. Mead and W. G. Spitzer, Phys. Rev. Lett., 10, 471 (1963).

16. A. van der Ziel, Solid State Physical Electronics (Prentice-Hall, Inc., Englewood Cliffs, N. J., 1968), p. 142.

17. Henisch, p. 186.

18. L. V. Azaroff and J. J. Brophy, Electronic Processes in Materials (McGraw-Hill Book Co., Inc., New York, 1963), p. 309.

19. E. C. Kemble, The Funadmental Principals of Quantum Mechanics (McGraw-Hill Book Co., Inc., New York, 1937), pp. 108-12.

20. C. R. Crowell and S. M. Sze, J. Appl. Phys., 37, No. 7, 2683 (1966).

21. D. M. Chang, Defense Documentation Center Report No. AD639568, 24 (1966).

22. C. A. Mead, Solid-State Elect., 9, 1026 (1966).

23. R. H. Fowler, Phys. Rev., 38, 45 (1931).

24. C. A. Mead, Solid-State Elect., 9, 1026 (1966).

25. G. Kano, J. Nakai and S. Mihara, Japan J. Appl. Phys., 3, 32 (1964).

26. Kano and others, pp. 32-3.

27. J. F. Dewald, Bell Syst. Tech. J., 39, 615 (1960).

28. A. M. Goodman, J. Appl. Phys., 31, No. 2, 329 (1963).

29. Lindmayer and Wrigley, p. 215.

30. Van der Ziel, p. 266.

31. Van der Ziel, p. 266.

32. Lindmayer and Wrigley, p. 13.

33. C. R. Crowell and S. M. Sze, J. Appl. Phys., 37, No. 7, 2683 (1966).

34. C. R. Crowell and S. M. Sze, Solid-State Elect., 9, 1042 (1966).

35. Van der Ziel, p. 281.

36. Chang, p. 16.

37. C. R. Crowell and S. M. Sze, J. Appl. Phys., 37, No. 7, 2865 (1966).

38. Chang, p. 18.

39. Chang. p. 17.

40. Chang, p. 19.

41. Chang, p. 23.

42. C. R. Crowell and S. M. Sze, Solid-State Elect., 9, 1041 (1966).

43. Lindmayer and Wrigley, p. 210.

44. Lindmayer and Wrigley, p. 225.

45. Azaroff and Brophy, p. 245.

APPENDIXES

APPENDIX A

THE MOTT MODEL OF A METAL-SEMICONDUCTOR RECTIFYING CONTACT

The Mott model[7] for a metal-(N-Type)-semiconductor contact will not be discussed in as much detail as the Schottky and Bethe models since its application is limited to only a very thin barrier. Furthermore, it represents a special case of the Schottky model which is discussed in Chapter III. The model and equations based on the model are included only for completeness, although its importance should not be overlooked since it was one of the first successful models which could predict and mathematically account for the rectification phenomena observed at a metal-semiconductor contact.

The potential distribution for the Mott barrier is shown in Fig. A.1. The barrier is defined as a barrier which extends throughout the N-Type semiconductor, or in other words joins both metal contacts of the device. The left-hand contact is regarded as ohmic since the barrier at $x=W$ offers very little opposition to current flow. The basic assumption of the Mott model is that due to the nature of the barrier too few impurities of the semiconductor are ionized to disturb the electric field in the semiconductor.

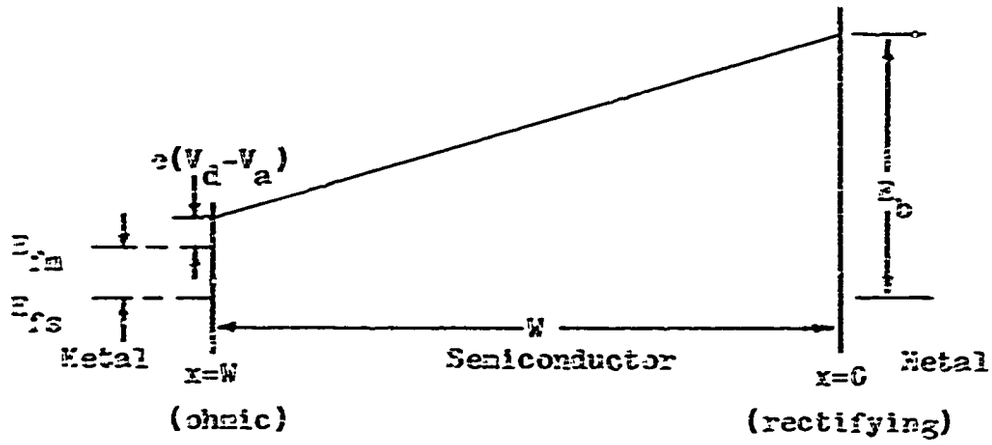

FIGURE A.1: The Mott Model for a Metal-Semiconductor Rectifying Contact.

Since the charge associated with the system must be assumed by the metal surfaces, the electric field is constant in the semiconductor and the potential function is thus linear. Stated mathematically, Poisson's equation takes the form

$$\frac{d^2V}{dx^2} = 0 \qquad (0 \leq x \leq W) \tag{A.1}$$

since there is no space charge associated with the semiconductor. Upon integration and evaluation at the boundaries one obtains an expression for the electric field, or

$$\frac{dV}{dx} = -E(x) = \frac{V_d - V_a}{W} \tag{A.2}$$

A second integration yields an expression for the potential distribution of the semiconductor, or

$$V(x) = \frac{V_d - V_a}{W} + C \tag{A.3}$$

in which C may be evaluated by noting that

$$V(0) = -E_b/e = -V_b \tag{A.4}$$

Thus, the potential is linear and may be expressed as

$$V(x) = \frac{V_d - V_a}{W} x - V_b \tag{A.5}$$

One could also develop an expression for capacitance and the current-voltage characteristic based on this model, but because of its limited applicability this will not be undertaken.

APPENDIX B

THE BETHE MODEL OF A METAL-SEMICONDUCTOR RECTIFYING CONTACT

The Bethe model[10] for a metal-semiconductor contact is shown in Fig. B.1. The assumptions used to model the contact are identical to those of the Schottky model with the additional assumption that the interface is an insulating layer of thickness r, seperating the metal from the semiconductor. The model is particularly applicable to a semiconducting oxide layer, which may have been deliberately applied to the semiconductor before forming the metal contact, or may have resulted from the process of applying the metal contact. In either case the semiconducting oxide forms a thin insulating layer and the model assumes the transition from the oxide to the pure semiconductor is abrupt.

Under the above assumptions Poisson's equation takes the following form for a planar contact:

$$\frac{d^2V(x)}{dx^2} = 0 \qquad (0<x<r) \qquad (B.1)$$

for the region of the insulator, and

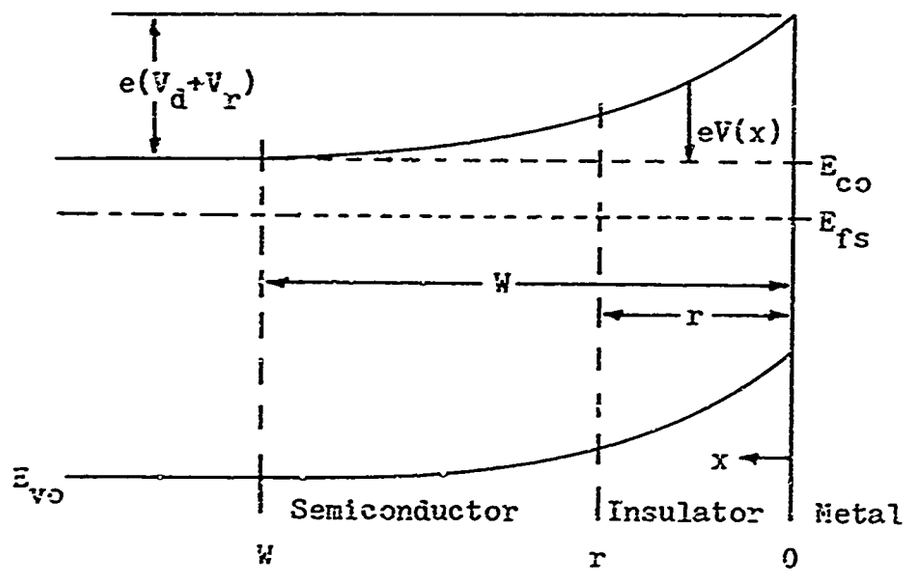

FIGURE B.1: Bethe Model for a Metal-Semiconductor Rectifying Contact.

$$\frac{d^2V(x)}{dx^2} = -\frac{eN_d}{\epsilon_s} \qquad (r<x<W) \qquad (B.2)$$

for the region of the pure semiconductor with completely ionized donor concentration N_d. The potential within the barrier may be found by solution of Poisson's equation, subject to the following boundary conditions:

$$(1) \quad V(W) = V_d + V_r \qquad (B.3)$$

$$(2) \quad V(0) = 0 \qquad (B.4)$$

$$(3) \quad \frac{dV(x)}{dx} = 0 \quad \text{at } x=W \qquad (B.5)$$

with the potential and electric field continuous at x=r. The solution may be written as

$$V(x) = \frac{eN_d}{\epsilon_s}(W-r)x \qquad (0<x<r) \qquad (B.6)$$

$$V(x) = \frac{eN_d}{2\epsilon_s}[W^2-r^2-(W-x)^2] \qquad (r<x<W) \qquad (B.7)$$

The Bethe model gives the following result for the barrier width W:

$$W^2 = r^2 + \frac{2\varepsilon_s}{eN_d}(V_d+V_r) \qquad (B.8)$$

Since the Bethe model neglects electrons and holes as part of the space charge of the barrier, the charge per unit area is given by

$$Q(W+r) = eN_d(W-r) \qquad (B.9)$$

giving the following result for barrier capacitance:

$$C_j = \frac{\varepsilon_s}{W} = \frac{\varepsilon_s}{\left[r^2 + \frac{2\varepsilon_s}{eN_d}(V_d+V_r)\right]^{\frac{1}{2}}} \qquad (B.10)$$

One should note that the conditions of the problem as stated in Poisson's equation make the solutions physically valid only for values of the barrier width equal to, or greater than the thickness of the insulating layer.

As a means of comparing the Bethe and Schottky models the junction capacitance versus reverse bias voltage is shown in Fig. B.2. The extrapolation indicated in Fig. B.2 illustrates how one may theoretically estimate the thickness of the insulating layer through the intercept on the voltage axis. For an applied forward bias voltage exceeding the equilibrium diffusion potential (V_d), the barrier should behave as an ordinary capacitance with a dielectric layer of thickness r. This would correspond to the region of the

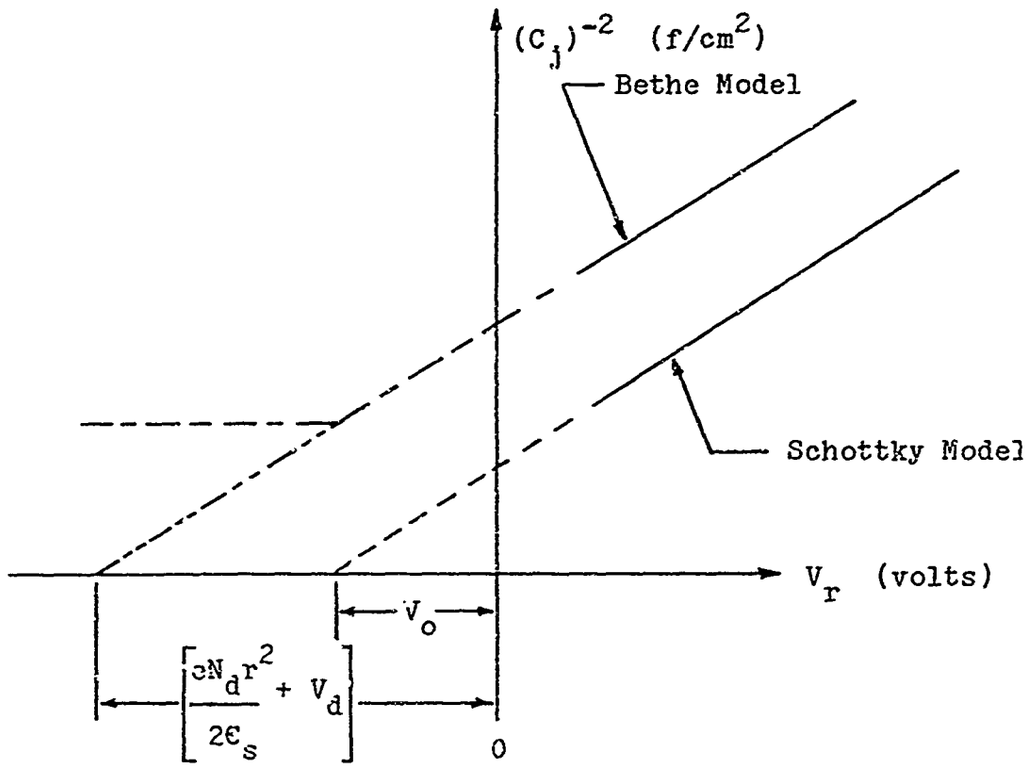

FIGURE B.2: Comparison of the Bethe and Schottky Model Plots of C_j^{-2} versus V_r.

horizontal dashed line in Fig. B.2. However, the diffusion of charge carriers into and beyond the barrier does not attain a steady state condition until a certain time has elapsed and this time may be on the order of time needed to charge the barrier. This would have the effect of either causing the measured capacitance to fall below or above the constant value indicated in Fig. B.2.

APPENDIX C

AN APPROXIMATION FOR THE QMTC OF A PARABOLIC POTENTIAL BARRIER

Kemble[19] has approximated the transmission coefficient (QMTC) for electrons of momentum s incident on a parabolic potential barrier with the presence of an image force and with reference to Fig. C.1 his results are as follows:

$$\text{Case I:} \quad \text{QMTC} = \frac{1}{1 + \exp(2\mu)} \qquad (E_n' < \beta_m) \qquad (C.1)$$

$$\text{Case II:} \quad \text{QMTC} = \frac{1}{1 + \exp(-2\mu)} \qquad (E_n' > \beta_m) \qquad (C.2)$$

$$\text{Case III:} \quad \text{QMTC} = \tfrac{1}{2} \qquad (E_n' = \beta_m) \qquad (C.3)$$

where

$$\mu = -\frac{2\pi}{h}\int_{x_1}^{x_2} \left|s\right| \left|dE_n'\right| \qquad (C.4)$$

$$s(x) = \left\{2m_e^*[E_n' - \beta(x)]\right\}^{\frac{1}{2}} \qquad (C.5)$$

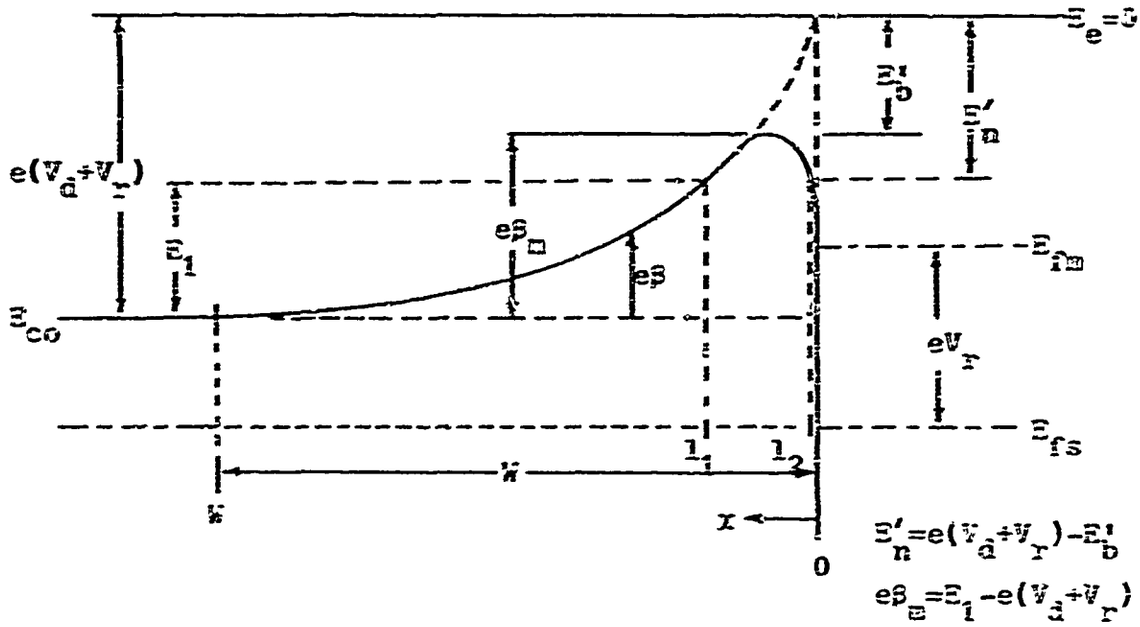

FIGURE C.1: Energy Diagram for the Calculation of the Transmission Coefficient for a Parabolic Potential Barrier with Image Force.

and

$$\beta_m = e(V_d+V_r) - E_b' \qquad (C.6)$$

Case I, $E_n'<\beta_m$, is shown in Fig. C.1; for Case II, l_1 and l_2 are the complex roots of

$$E_n' - \beta(x) = 0 \qquad (C.7)$$

For Case III, $l_1=l_2$ and $\beta(x)=\beta_m$ so that the QMTC becomes equal to $\frac{1}{2}$. One should note that for this application E_n' is measured from the top of the barrier without correction for image force and also that $\beta(x)$ contains the corrective term for image force lowering, i.e.,

$$\beta(x) = \beta'(x) + \beta''(x) \qquad (C.8)$$

APPENDIX D

ADDITIONAL COMMENTS ON THE DEGREE OF IONIZATION (γ)

In view of the calculations of Chapter IV, the importance of the degree of ionization of donor impurities has become apparent in determining the normalized electron potential and space charge density as predicted by the more exact model for the metal-semiconductor contact (Fig.'s 4.2 and 4.3). In addition the results of Chapter V (Fig. 5.4 and Eq. 5.17) would indicate that γ is of prime importance in determining the equilibrium diffusion potential (V_d) by the capacitance method. In light of these results, the degree of ionization becomes an important parameter for the metal-semiconductor contact and would warrant further discussion.

Equation 4.14 defines γ as the ratio of the number of free electrons furnished by ionized donor impurities (n_c) to the total impurity density (N_d) in the bulk semiconductor. In order to gain a better perspective of the dependence of γ with respect to temperature and material properties one can reexamine Eq. 4.15, or

$$\exp(E_i/KT) = \frac{(N_c/N_d)(1-\gamma)}{2\gamma^2} \tag{D.1}$$

Equation D.1 can be arranged to form a quadratic equation in γ, or

$$a\gamma^2 + b\gamma - c = 0 \tag{D.2}$$

where

$$a = 2\exp(E_i/KT) \tag{D.3}$$

and

$$b = c = N_c/N_d \tag{D.4}$$

Using the standard quadratic formula, the principal value of γ may be expressed as follows:

$$\gamma = \frac{N_c\left(-1 + \left[1 + 8(N_c/N_d)\exp(E_i/KT)\right]\right)^{\frac{1}{2}}}{4N_d\exp(E_i/KT)} \tag{D.5}$$

The effective density of states for the conduction band (N_c) may be expressed as[43]

$$N_c = \frac{4\sqrt{2}(\pi m_e^* KT)^{3/2}}{h^3} \tag{D.6}$$

and upon substitution into Eq. D.5, γ becomes

$$\gamma = \frac{\sqrt{2}(\pi m_e^* KT)^{3/2}}{N_d \exp(E_i/KT)} h^{-3} \left\{ -1 + \left[\frac{(\pi m_e^* KT)^{3/2} + \sqrt{2} N_d h^3 \exp(E_i/KT)}{(\pi m_e^* KT)^{3/2}} \right]^{\frac{1}{2}} \right\} \tag{D.7}$$

Although Eq. D.7 is a fairly complicated expression, it allows one to calculate γ for a particular device if N_d, T, m_e^*, and E_i are known. It should be noted that, in general, when a particular semiconductor material is specified E_i, N_d, and m_e^* are known so that γ is essentially a function of temperature.

Since a quantitative evaluation of γ would make it necessary for one to assume a particular material, dopant, doping density and temperature, no general conclusions could be made from taking this approach. However, as an alternate approach, one could make the following qualitative observations by examining Eq. D.7:

(1) Since (E_i/KT) appears as the argument of an exponential, it should be regarded as the most influencial factor in determining γ. In addition, since E_i is a constant for a specific material, one would expect γ to be a strong function of temperature. If one assumes a specific temperature, then γ will be strongly influenced by the ionization energy E_i. As an illustrative example, it could be shown that at room temperature using the normal dopants

(P, As, and Sb) to produce N-Type silicon and germanium, essentially all impurities will be ionized. This is due to the relatively low ionization energies associated with these dopants, ranging from 0.001 to 0.055 ev.[44] However, if one considers P-Type SiC using Al doping, $E_i \approx 0.25$ ev[45] and ionization of impurities is relatively incomplete at room temperature.

(2) The doping density (N_d) and the effective electron mass (m_e^*) also influence the character of γ, although this influence may go unnoticed because of the importance of E_i and T. However, one may draw the general conclusion that γ is proportional to the effective mass and inversely proportional to the doping concentration.

APPENDIX E

VERIFICATION OF EQUATION 4.32 AS THE SOLUTION OF EQUATION 4.27

In order to show that Eq. 4.32 is a solution of Eq. 4.27 it must be shown that Eq. 4.32 satisfies the differential equation (Eq. 4.27) and meets the boundary condition of Eq. 4.30. This result can be shown quite easily by performing the following differentiations:

$$(1) \quad \frac{d^2y}{du^2} = \left(\frac{d}{du}\right)\left(\frac{dy}{du}\right) = -\frac{\sqrt{2}}{2}z^{-\frac{1}{2}}\left(\frac{dz}{dy}\right)\left(\frac{dy}{du}\right) \qquad (E.1)$$

$$(2) \quad \frac{dz}{dy} = \frac{\gamma e^{y}}{\gamma e^{y} + 1 - \gamma} - \gamma e^{-y} \qquad (E.2)$$

$$(3) \quad \frac{dy}{du} = -\sqrt{2}z^{\frac{1}{2}} \qquad (E.3)$$

$$= -\sqrt{2}\left\{\ln[\gamma e^{y} + 1 - \gamma] + \gamma e^{-y} - \gamma\right\}^{\frac{1}{2}}$$

Upon substitution of E.2 and E.3 into E.1 one obtains

$$\frac{d^2y}{du^2} = \frac{1}{1 + (1/\gamma - 1)e^{-y}} - \gamma e^{-y} \qquad (E.4)$$

which is identical to Eq. 4.27. Thus, Eq. 4.32 satisfies the differential equation.

Next, considering the boundary condition:

$$\frac{dy}{du} = 0 \quad \text{at } y=0 \qquad (E.5)$$

and

$$\left.\frac{dy}{du}\right|_{y=0} = -\sqrt{2}[\ln(\gamma e^{0} + 1 - \gamma) + \gamma e^{0} - \gamma]^{\frac{1}{2}} \qquad (E.6)$$

or

$$\left.\frac{dy}{du}\right|_{y=0} = -\sqrt{2}[\ln(1) + \gamma - \gamma]^{\frac{1}{2}} = 0 \qquad (E.7)$$

so that Eq. 4.32 satisfies the boundary condition of Eq. 4.30. Thus, since Eq. 4.32 meets both requirements as stated above it must be considered a valid solution to Eq. 4.27 subject to the boundary condition of Eq. 4.30.

<u>q.e.d.</u>

APPENDIX F

THE RUNGE-KUTTA METHOD FOR NUMERICAL INTEGRATION

The solution of Eq. 4.32 is accomplished by a numerical integration employing the Runge-Kutta technique. In general, this technique takes the interval (θ_n, θ_{n+1}) and breaks it into two or more subintervals. The integral of the function $f(\theta, \Delta)$ over the whole interval is then calculated as the sum of the integrals over the subintervals. The function is taken to be constant over each subinterval and by judicious choice of the points at which the function is evaluated a low truncation error can be obtained. In addition, when using the Runge-Kutta method only one initial point (θ_o, Δ_o) is needed for the iteration process to begin. The chief disadvantage of this method is that it requires several evaluations of $f(\theta, \Delta)$ for each point of integration which makes it somewhat slower than other methods.

The specific Runge-Kutta method used for the solution of this problem is of order four, or the interval (Ω) is divided into four subintervals. The integration is then given by the following system of equations:

$$\Sigma_0 = \Omega f(\theta_n, \Delta_n) \tag{F.1}$$

$$\Sigma_1 = \Omega f(\theta_n + \alpha_1\Omega, \Delta_n + \beta_{10}\Sigma_0) \tag{F.2}$$

$$\Sigma_2 = \Omega f(\theta_n + \alpha_2\Omega, \Delta_n + \beta_{20}\Sigma_0 + \beta_{21}\Sigma_1) \tag{F.3}$$

$$\Sigma_3 = \Omega f(\theta_n + \alpha_3\Omega, \Delta_n + \beta_{30}\Sigma_0 + \beta_{31}\Sigma_1 + \beta_{32}\Sigma_2) \tag{F.4}$$

$$\Delta_{n+1} = \Delta_n + (a\Sigma_0 + b\Sigma_1 + c\Sigma_2 + d\Sigma_3) \tag{F.5}$$

Although a large number of parameters appear in Eq.'s F.1 through F.5 they may be determined, at least in part, by equating Eq. F.5 to the Taylor-series expansion of Δ_{n+1} about the point (θ_n, Δ_n). This can be done so as to achieve agreement through terms in Ω^4, yielding solutions that have an error of approximately (Ω^5).

One possible solution is

$$\Sigma_0 = \Omega f(\theta_n, \Delta_n) \tag{F.6}$$

$$\Sigma_1 = \Omega f(\theta_n + \Omega/2, \Delta_n + \Omega/2) \tag{F.7}$$

$$\Sigma_2 = \Omega f(\theta_n + \Omega/2, \Delta_n + \Omega/2) \tag{F.8}$$

$$\Sigma_3 = \Omega f(\theta_n + \Omega, \Delta_n + \Sigma_2) \tag{F.9}$$

$$\Delta_{n+1} = \Delta_n + 1/6(\Sigma_0 + 2\Sigma_1 + 2\Sigma_2 + \Sigma_3) \tag{F.10}$$

where $d\Delta/d\theta = f(\theta, \Delta)$ with the initial starting point specified as (θ_o, Δ_o). Here the interval Ω is divided into subintervals of $\Omega/6$, $\Omega/3$, $\Omega/3$, and $\Omega/6$. The function is evaluated at the left-hand side first, then twice at extrapolated center points, and finally at the extrapolated right-hand side.

The complete computer program used to integrate Eq. 4.32

by the Runge-Kutta method of order four follows. In addition to calculating the normalized electron potential, the program is designed to calculate the space charge density based on both models and present the results in a normalized form for comparison purposes. Also incorporated into the program is a plot subroutine which allows the data generated to appear in a more useful form. The program is written in Fortran-IV for use in the GE-225 computer and takes approximately three minutes running time for each parameter change.

```
      SUBROUTINE PLOTT (N,NP,X,Y1,Y2,Y3)
      DIMENSION X(100),Y1(100),Y2(100),Y3(100)
      DIMENSION A(100),PLOT(100)
      COMMON G,BLNK,PRD,STAR,EQ,PLUS,COM,EXE
    7 FORMAT(1X,2E10.3,4X,95A1)
    8 FORMAT(1X,3E10.3,4X,85A1)
    9 FORMAT(1X,4E10.3,4X,75A1)
  300 FORMAT(1H1,45X,16HPLOT SUBROUTINE )
  310 FORMAT(1H ,22X,I3,43H VALUES OF DY/DU(*), V(=), W(+) ARE
     1 PLOTTED,8H AGAINST,I3,31H VALUES OF U(.)  SCALE FACTOR
     2 =,E10.3)
      NP=NP
      DO 5 I=1,95
    5 PLOT(I)=BLNK
      XM=0.0
      XMU=0.0
      DO 10 I=1,NP
   10 A(I)=Y1(I)
      MSW=2
      GO TO 60
   40 DO 50 I=1,NP
   50 A(I)=Y2(I)
      MSW=3
   60 DO 90 I=1,NP
      IF(A(I)-XM) 70,75,75
   70 IF(A(I)-XMI) 80,90,90
   80 XMI=A(I)
```

```
      GO TO 90
   75 XM=A(I)
   90 CONTINUE
      IF(MSW-(N-1)) 20,40,100
  100 NRA=94-(N-1)*10
      RA=NRA
      SF=(XM-XMI)/RA
      REF=ABSF(XMI/(XM-XMI))*RA+1.0
      NR=REF
      PRINT 300
      PRINT 310,NP,NF,SF
      GO TO (320,330,340),N
  320 PRINT 325
  325 FORMAT(7X,4HX(.),5X,5HY1(*))
      GO TO 4
  330 PRINT 335
  335 FORMAT(7X,4HX(.),5X,5HY1(*),5X,5HY2(=))
      GO TO 4
  340 PRINT 345
  345 FORMAT(7X,4HX(.),5X,5HY1(*),5X,5HY2(=),5X,5HY3(+))
    4 PRINT 350
  350 FORMAT(1X,116H.....................................
     1.............................................
     2......................)
      DO 290 I=1,NP
      PLOT(NR)=PRD
      L=Y1(I)/SF+REF
```

```
      PLOT(L)=STAR
      GO TO (140,110,110),N
  110 K=Y2(I)/SF+REF
      PLOT(K)=EQ
      IF(N-2) 150,150,120
  120 J=Y3(I)/SF+REF
      PLOT(J)=PLUS
      GO TO 160
  140 PRINT 7,X(I),Y1(I),(PLOT(J),J=1,95)
      PLOT(L)=BLNK
      GO TO 290
  150 PRINT 8,X(I),Y1(I),Y2(I),(PLOT(J),J=1,85)
      PLOT(L)=BLNK
      PLOT(K)=BLNK
      GO TO 290
  160 PRINT 9,X(I),Y1(I),Y2(I),Y3(I),(PLOT(J),J=1,75)
      DO 165 NO=1,95
  165 PLOT(NO)=BLNK
  290 CONTINUE
      RETURN
      END
```

```
SUBROUTINE FNCT (X,Y,F)
COMMON G,BLNK,PRD,STAR,EQ,PLUS,COM,EXE
AA=SQRTF(2.0)
BB=LOGF(G*EXPF(Y)+1.0-G)+G*EXPF(-Y)-G
CC=SQRTF(BB)
F=-AA*CC
RETURN
END
```

```
C  ********** RUNGE-KUTTA METHOD FOR SOLUTION OF D.E. USING GE415
C  ********** H. ALLEN LINDSEY, NOVEMBER 1968
C  ********** THE FOLLOWING VARIABLES ARE USED:
        **** A AND B ARE THE INTERVAL LIMITS
        **** H IS THE STEP SIZE
        **** Y IS THE INITIAL VALUE OF THE SOLUTION
        **** DELTA IS THE INCREMENT AT WHICH THE SOLUTION IS
                IS TO BE PRINTED OUT
        **** G IS THE DEGREE OF IONIZATION
      DIMENSION NEQ(80),P(1)
      DIMENSION X1(200),Y1(200),Y2(200),Y3(200)
      DIMENSION X11(70),Y11(70),Y22(70),Y33(70)
      COMMON G,BLNK,PRD,STAR,EQ,PLUS,COM,EXE
  999 FORMAT (80A1)
  998 FORMAT (//5X,19H ON THE INTERVAL U=,F8.4,6H TO U=,F8.4,
     1   17H WITH STEP SIZE =, F9.7/)
  997 FORMAT (5X,51H THE TOTAL NUMBER OF INTERVALS FOR THIS
      PROBLEM IS ,
     1   I6/)
  996 FORMAT (5X,48H THE DEGREE OF IONIZATION FOR THIS
      PROBLEM IS G=,
     1   F8.4/)
  995 FORMAT (5X,48H THE EXPECTED ERROR FOR THIS PROBLEM
      IS E=(+OR-),
     1   E16.8/)
  994 FORMAT (8X,2H U,13X,2H Y,15X,2H V//)
  993 FORMAT (5X,F12.7,3X,F13.8)
```

```
992 FORMAT (5X,F12.7,3X,F13.8,3X,F13.8)
991 FORMAT (6F10.3)
990 FORMAT (//////)
989 FORMAT (2X,1A1,2X,1A1,2X,1A1,2X,1A1,2X,1A1)
988 FORMAT (5X,37H U=NORMALIZED DISTANCE FROM JUNCTION /
   1   5X,33H Y=NORMALIZED ELECTRON POTENTIAL /
   2   5X,35H V=NORMALIZED SPACE CHARGE DENSITY /
   3   5X,32H W=SCHOTTKY APPROXIMATION FOR V ////)
    READ 989,PRD,STAR,EQ,PLUS,BLNK
    N1=3
C  ********** MAIN PROGRAM
  1 READ 991,A,B,DELTA,H,Y,G
C  ********** CHECK FOR EOF
    IF (H) 2,100,2
  2 NH=(B-A)/H
    PRINT 990
    READ 999,(NEQ(I),I=1,80)
    E=H**5.0
    P(1)=SQRTF(2.0*Y)
C  ********** PRINT HEADINGS
    PRINT 999,NEQ
    PRINT 998,A,B,H
    PRINT 996,G
    PRINT 995,E
    PRINT 988
    PRINT 994
    PRINT 993,A,Y
```

```
C  ********** INITIALIZATION
   10 X=A
      I=1
      J=0
C  ********** COMPUTATION OF THE NUMBER OF PRINT INTERVALS
      N=DELTA/H
      NN=N+1
   15 YO=Y
C  ********** EVALUATION OF THE FUNCTION FOR RUNGE-KUTTA FORMULA
   30 CALL FNCT (X,YO,F)
      ZK1=F
      XH=X+H/2.0
      YO=Y+H*ZK1/2.0
      CALL FNCT (XH,YO,F)
      ZK2=F
      YO=Y+H*ZK2/2.0
      CALL FNCT (XH,YO,F)
      ZK3=F
      XH=X+H
      YO=Y+H*ZK3
      CALL FNCT (XH,YO,F)
      ZK4=F
   50 Y=Y+H*(ZK1+2.0*(ZK2+ZK3)+ZK4)/6.0
      D=1.0+(1.0/G-1.0)*EXPF(-Y)
      V= 1.0/D-G*EXPF(-Y)
C  ********** INCREMENT ARGUMENT AND COUNTERS
      Z=I
```

```
      X=A+Z*H
      I=I+1
C  ********** TEST FOR PRINT INCREMENT
      IF (I-NN) 30,70,70
   70 PRINT 992,X,Y,V
      J=J+1
      Y1(J)=Y
      Y2(J)=V*Y1(1)
      IF (X-P(1)) 76,76,78
   76 Y3(J)=Y1(1)
      GO TO 79
   78 Y3(J)=0.0
   79 X1(J)=X
C ********** TEST FOR FINAL COMPUTATION
      IF (NN-(NH+1)) 80,90,90
   80 NN=N+NN
      GO TO 15
   90 S=(1.0/DELTA)*B
      MN=S
      IF (S-58.0) 96,96,92
   92 SCALE=S/58.0+1.0
      NM=SCALE
      L=MN/NM
      K=-2*NM
      DO 94 JJ=1,L,1
      K=K+NM
      Y11(JJ)=Y1(K+NM+1)
```

```
      Y22(JJ)=Y2(K+NM+1)
      Y33(JJ)=Y3(K+NM+1)
   94 X11(JJ)=X1(K+NM+1)
      NP=L
      GO TO 98
   96 CONTINUE
      DO 97 J1=1,MN,1
      Y11(J1)=Y1(J1)
      Y22(J1)=Y2(J1)
      Y33(J1)=Y3(J1)
   97 X11(J1)=X1(J1)
      NP=MN
   98 CALL PLOTT (N1,NP,X11,Y11,Y22,Y33)
      GO TO 1
  100 CALL EXIT
      END
```

APPENDIX G

A TYPICAL COMPUTER SOLUTION

```
* * * * * * * * * * * * * * * * * *
*  DEPARTMENT.....EE              *
*  USER NAME......ALLENLINDSEY    *
*  USER NUMBER....                *
* * * * * * * * * * * * * * * * * *
```

```
      SUBROUTINE PLOTY(N,NP,X,Y1,Y2,Y3)
      DIMENSION X(100),Y1(100),Y2(100),Y3(100)
      DIMENSION A(100), PLOT(100)
      COMMON G,BLNK,PRD,STAR,EQ,PLUS,COM,EXE
    7 FORMAT(1X,2E10.3,4X,95A1)
    8 FORMAT(1X,3E10.3,4X,85A1)
    9 FORMAT(1X,4E10.3,4X,75A1)
  300 FORMAT(1H1,45X,16HPLOT SUBROUTINE )
  310 FORMAT(1H ,22X,I3,43H VALUES OF DY/DU(*), V(*), W(+) ARE PLOTTED
     1,8H AGAINST,I3,31H VALUES OF U(.)  SCALE FACTOR =,E10.3)
      NP=NP
      DO 5 I=1,95
    5 PLOT(I)=BLNK
      XM=0.
      XMU=0.
      DO 10 I=1,NP
   10 A(I)=Y1(I)
      MSW=1
      GO TO 60
   20 DO 30 I=1,NP
   30 A(I)=Y3(I)
      MSW=2
      GO TO 60
   40 DO 50 I=1,NP
   50 A(I)=Y2(I)
      MSW=3
   60 DO 90 I=1,NP
      IF(A(I)-XM) 70,75,75
   70 IF(A(I)-XMI)80,90,90
   80 XMI=A(I)
      GO TO 90
   75 XM=A(I)
   90 CONTINUE
      IF(MSW-(N-1))20,40,100
  100 NRA=94-(N-1)*10
      RA=NRA
      SF=(XM-XMI)/RA
      REF=ABSF(XMI/(XM-XMI))*RA+1.0
      NR=REF
      PRINT 300
      PRINT 310,NP,NP,SF
      GO TO(320,330,340),N
  320 PRINT 325
  325 FORMAT(7X,4HX(.),5X,5HY1(*))
      GO TO 4
  330 PRINT 335
  335 FORMAT(7X,4HX(.),5X,5HY1(*),5X,5HY2(=))
      GO TO 4
  340 PRINT 345
  345 FORMAT(7X,4HU(.),2X,8HDY/DU(*),4X,4HV(=),4X,4HW(+))
    4 PRINT 350
  350 FORMAT(1X,116H.......................................................
     1.......................................................
      DO 290 I=1,NP
      PLOT(NR)=PRD
```

```
      L=Y1(I)/SF+REF
      PLOT(L)=STAR
      GO TO (140,110,110),N
  110 K=Y2(I)/SF+REF
      PLOT(K)=EQ
      IF(N-2) 150,150,120
  120 J=Y3(I)/SF+REF
      PLOT(J)=PLUS
      GO TO 160
  140 PRINT 7,X(I),Y1(I),(PLOT(J),J=1,95)
      PLOT(L)=BLNK
      GO TO 290
  150 PRINT 8,X(I),Y1(I),Y2(I),(PLOT(J),J=1,85)
      PLOT(L)=BLNK
      PLOT(K)=BLNK
      GO TO 290
  160 PRINT 9,X(I),Y1(I),Y2(I),Y3(I),(PLOT(J),J=1,75)
      DO 165 NO=1,95
  165 PLOT(NO)=BLNK
  290 CONTINUE
      RETURN
      END
 02070, 17745

PLOTT  0000012
N   1000012
NP  1000013
X   1000014 0020144
Y1  1000015 0020144
Y2  1000016 0020144
Y3  1000017 0020144
A   0000036 0020144
PLOT   0000346 0020144
G   0017764
BLNK   0017762
PRD 0017760
STAR   0017756
EQ  0017754
PLUS   0017752
COM 0017750
EXE 0017746
/00007 0000661
/00008 0000670
/00009 0000677
/00300 0000706
/00310 0000720
I   0000656
+00001 0000657
-00096 0000775
/00005 0001025
XM  0001000
0.  0001002
XMU 0001004
/00010  001046
-00002 0001006
MSW 0001 10
/00060 0001153
/00020 0001074
/00030 0001076
+00002 0001011
```

```
/00040 0001124
/00050 0001126
+00013 0001012
/00070 0001167
/00075 0001121
XMI 0001014
/00080 0001201
/00090 0001216
/00100 0001240
NRA 0001016
+00094 0001017
+00010 0001021
RA  0001022
SF  0001254
REF 0001261
ABSF    141262  EXT PROG
1.0 0001266
NR  0001270
/00320 0001355
/00330 0001372
/00340 0001413
/00325 0001361
/00064 0001437
/00335 0001376
/00345 0001417
/00350 0001443
L   0001271
/00140 0001632
/00110 0001560
K   0001273
/00150 0001700
/00120 0001610
J   0001274
/00160 0001763
/00290 0001056
-00086 0001275
-00076 0001276
AO  0001277
/00165  02042
```

```
      SUBROUTINE FNCT (X,Y,F)
      COMMON G,BLNK,PRD,STAR,EQ,PLUS,COM,EXE
      AA=SQRTF(2.0)
      BB=LOGF(G*EXPF(Y)+1.0-G)+G*EXPF(-Y)-G
      CC=SQRTF(BB)
      F=-AA*CC
      RETURN
      END
 00113, 17745

FNCT   0000012
X   1000012
Y   1000013
F   1000014
G   0017764
BLNK   0017762
PRD 0017760
STAR   0017756
EQ  0017754
PLUS   0017752
COM 0017750
EXE 0017746
AA  0000014
SQRTF  0140026  EXT PROG
2.0 0000030
BB  0000032
LOGF   0140034  EXT PROG
EXPF   0140036  EXT PROG
1.0 0000042
CC  0000046
```

```
C  ********** RUNGE-KUTTA METHOD FOR SOLUTION OF O.D.E. USING GE225
C  ********** H. ALLEN LINDSEY, NOVEMBER 1968
C  ********** THE FOLLOWING VARIABLES ARE USED
C          *** A AND B ARE THE INTERVAL LIMITS
C          *** H IS THE STEP SIZE
C          *** Y IS THE INITIAL VALUE OF THE SOLUTION
C          *** DELTA IS THE INCREMENT AT WHICH THE SOLUTION
C                 IS TO BE PRINTED OUT
C          *** G IS THE DEGREE OF IONIZATION
      DIMENSION NEQ(80),P(1)
      DIMENSION X1(200),Y1(200),Y2(200),Y3(200)
      DIMENSION X11(70),Y11(70),Y22(70),Y33(70)
      COMMON G,BLNK,PRD,STAR,EQ,PLUS,COM,EXE
  999 FORMAT (80A1)
  998 FORMAT (//5X,19H ON THE INTERVAL U=,F8.4,6H TO U=,F8.4,
     1   17H WITH STEP SIZE =,F9.7/)
  997 FORMAT (5X,51H THE TOTAL NUMBER OF INTERVALS FOR THIS PROBLEM IS
     1   I6/)
  996 FORMAT (5X,48H THE DEGREE OF IONIZATION FOR THIS PROBLEM IS G=,
     1   F8.4/)
  995 FORMAT (5X,48H THE EXPECTED ERROR FOR THIS PROBLEM IS E=(+OR-),
     1   E16.8/)
  994 FORMAT (8X,2H U,13X,2H Y,15X,2H V//)
  993 FORMAT (5X,F12.7,3X,F13.8)
  992 FORMAT (5X,F12.7,3X,F13.8,3X,F13.8)
  991 FORMAT (6F10.3)
  990 FORMAT (//////)
  989 FORMAT (2X,1A1,2X,1A1,2X,1A1,2X,1A1,2X,1A1)
  988 FORMAT (5X,37H U=NORMALIZED DISTANCE FROM JUNCTION /
     1   5X,33H Y=NORMALIZED ELECTRON POTENTIAL /
     2   5X,35H V=NORMALIZED SPACE CHARGE DENSITY /
     3   5X,32H W=SCHOTTKY APPROXIMATION FOR V ////)
      READ 989,PRD,STAR,EQ,PLUS,BLNK
      N1=3
C  ********** MAIN PROGRAM
    1 READ 991,A,B,DELTA,H,Y,G
C  ********** CHECK FOR EOF
      IF (H) 2,100,2
    2 NH=(B-A)/H
      PRINT 990
      READ 999,(NEQ(I),I=1,80)
      E=H**5.0
      P(1)=SQRTF(2.0*Y)
C  ********** PRINT HEADINGS
      PRINT 999,NEQ
      PRINT 998,A,B,H
      PRINT 997,NH
      PRINT 996,G
      PRINT 995,E
      PRINT 988
      PRINT 994
      PRINT 993,A,Y
C  ********** INITIALIZATION
   10 X=A
      I=1
      J=
C  ********** COMPUTATION OF THE NUMBER OF PRINT INTERVALS
      N=DELTA/H
```

```
      NN=N+1
   15 YO=Y
C     ********** EVALUATION OF THE FUNCTION FOR RUNGE-KUTTA FORMULA
   30 CALL FNCT (X,YO,F)
      ZK1=F
      XH=X+H/2.0
      YO=Y+H*ZK1/2.0
      CALL FNCT (XH,YO,F)
      ZK2=F
      YO=Y+H*ZK2/2.0
      CALL FNCT (XH,YO,F)
      ZK3=F
      XH=X+H
      YO=Y+H*ZK3
      CALL FNCT (XH,YO,F)
      ZK4=F
   50 Y=Y+H*(ZK1+2.0*(ZK2+ZK3)+ZK4)/6.0
      D=1.0+(1.0/G-1.0)*EXPF(-Y)
      V=1.0/D-G*EXPF(-Y)
C     ********** INCREMENT ARGUMENT AND COUNTERS
      Z=I
      X=A+Z*H
      I=I+1
C     ***(****** TEST FOR PRINT INCREMENT
      IF (I-NN) 30,70,70
   70 PRINT 992,X,Y,V
      J=J+1
      Y1(J)=Y
      Y2(J)=V*Y1(1)
      IF (X-P(1)) 76,76,78
   76 Y3(J)=Y1(1)
      GO TO 79
   78 Y3(J)=0.0
   79 X1(J)=X
C     ********** TEST FOR FINAL COMPUTATION
      IF (MN-(NH+1)) 80,90,90
   80 NN=N+NN
      GO TO 15
C     *********  STORAGE / SCALE FOR PLOT SUBROUTINE
   90 S=(1.0/DELTA)*R
      MN=S
      IF (S-58.0) 96,96,92
   92 SCALE=S/58.0+1.0
      NM=SCALE
      L=MN/NM
      K=-2*NM
      DO 94 JJ=1,L,1
      K=K+NM
      Y11(JJ)=Y1(K+NM+1)
      Y22(JJ)=Y2(K+NM+1)
      Y33(JJ)=Y3(K+NM+1)
   94 X11(JJ)=X1(K+NM+1)
      NP=L
      GO TO 98
   96 CONTINUE
      DO 97 J1=1,MN,1
      Y11(J1)=Y1(J1)
      Y22(J1)=Y2(J1)
      Y33(J1)=Y3(J1)
   97 X11(J1)=X1(J1)
```

```
C  ********** RUNGE-KUTTA METHOD FOR SOLUTION OF O.D.E. USING GE225
C  ********** H. ALLEN LINDSEY, NOVEMBER 1968
C  ********** THE FOLLOWING VARIABLES ARE USED
C          *** A AND B ARE THE INTERVAL LIMITS
C          *** H IS THE STEP SIZE
C          *** Y IS THE INITIAL VALUE OF THE SOLUTION
C          *** DELTA IS THE INCREMENT AT WHICH THE SOLUTION
C                IS TO BE PRINTED OUT
C          *** G IS THE DEGREE OF IONIZATION
      DIMENSION NEQ(80),P(1)
      DIMENSION X1(200),Y1(200),Y2(200),Y3(200)
      DIMENSION X11(70),Y11(70),Y22(70),Y33(70)
      COMMON G,BLNK,PRD,STAR,EQ,PLUS,COM,EXE
  999 FORMAT (80A1)
  998 FORMAT (//5X,19H ON THE INTERVAL U=,F8.4,6H TO U=,F8.4,
     1   17H WITH STEP SIZE =,F9.7/)
  997 FORMAT (5X,51H THE TOTAL NUMBER OF INTERVALS FOR THIS PROBLEM IS
     1   I6/)
  996 FORMAT (5X,48H THE DEGREE OF IONIZATION FOR THIS PROBLEM IS G=,
     1   F8.4/)
  995 FORMAT (5X,48H THE EXPECTED ERROR FOR THIS PROBLEM IS E=(+OR-),
     1   E16.8/)
  994 FORMAT (8X,2H U,13X,2H Y,15X,2H V//)
  993 FORMAT (5X,F12.7,3X,F13.8)
  992 FORMAT (5X,F12.7,3X,F13.8,3X,F13.8)
  991 FORMAT (6F10.3)
  990 FORMAT (//////)
  989 FORMAT (2X,1A1,2X,1A1,2X,1A1,2X,1A1,2X,1A1)
  988 FORMAT (5X,37H U=NORMALIZED DISTANCE FROM JUNCTION /
     1   5X,33H Y=NORMALIZED ELECTRON POTENTIAL /
     2   5X,35H V=NORMALIZED SPACE CHARGE DENSITY /
     3   5X,32H W=SCHOTTKY APPROXIMATION FOR V ////)
      READ 989,PRD,STAR,EQ,PLUS,BLNK
      N1=3
C  ********** MAIN PROGRAM
    1 READ 991,A,B,DELTA,H,Y,G
C  ********** CHECK FOR EOF
      IF (H) 2,100,2
    2 NH=(B-A)/H
      PRINT 990
      READ 999,(NEQ(I),I=1,80)
      E=H**5.0
      P(1)=SQRTF(2.0*Y)
C  ********** PRINT HEADINGS
      PRINT 999,NEQ
      PRINT 998,A,B,H
      PRINT 997,NH
      PRINT 996,G
      PRINT 995,E
      PRINT 988
      PRINT 994
      PRINT 993,A,Y
C  ********** INITIALIZATION
   10 X=A
      I=1
      J=
C  ********** COMPUTATION OF THE NUMBER OF PRINT INTERVALS
      N=DELTA/H
```

```
      NN=N+1
   15 YO=Y
C     ********** EVALUATION OF THE FUNCTION FOR RUNGE-KUTTA FORMULA
   30 CALL FNCT (X,YO,F)
      ZK1=F
      XH=X+H/2.0
      YO=Y+H*ZK1/2.0
      CALL FNCT (XH,YO,F)
      ZK2=F
      YO=Y+H*ZK2/2.0
      CALL FNCT (XH,YO,F)
      ZK3=F
      XH=X+H
      YO=Y+H*ZK3
      CALL FNCT (XH,YO,F)
      ZK4=F
   50 Y=Y+H*(ZK1+2.0*(ZK2+ZK3)+ZK4)/6.0
      D=1.0+(1.0/G-1.0)*EXPF(-Y)
      V=1.0/D-G*EXPF(-Y)
C     ********** INCREMENT ARGUMENT AND COUNTERS
      Z=I
      X=A+Z*H
      I=I+1
C     ***(****** TEST FOR PRINT INCREMENT
      IF (I-NN) 30,70,70
   70 PRINT 992,X,Y,V
      J=J+1
      Y1(J)=Y
      Y2(J)=V*Y1(1)
      IF (X-P(1)) 76,76,78
   76 Y3(J)=Y1(1)
      GO TO 79
   78 Y3(J)=0.0
   79 X1(J)=X
C     ********** TEST FOR FINAL COMPUTATION
      IF (NN-(NH+1)) 80,90,90
   80 NN=N+NN
      GO TO 15
C     **********  STORAGE / SCALE FOR PLOT SUBROUTINE
   90 S=(1.0/DELTA)*R
      MN=S
      IF (S-58.0) 96,96,92
   92 SCALE=S/58.0+1.0
      NM=SCALE
      L=MN/NM
      K=-2*NM
      DO 94 JJ=1,L,1
      K=K+NM
      Y11(JJ)=Y1(K+NM+1)
      Y22(JJ)=Y2(K+NM+1)
      Y33(JJ)=Y3(K+NM+1)
   94 X11(JJ)=X1(K+NM+1)
      NP=L
      GO TO 98
   96 CONTINUE
      DO 97 J1=1,MN,1
      Y11(J1)=Y1(J1)
      Y22(J1)=Y2(J1)
      Y33(J1)=Y3(J1)
   97 X11(J1)=X1(J1)
```

```
      NP=MN
   98 CALL PLOTT (N1,NP,X11,Y11,Y22,Y33)
      GO TO 1
  100 CALL EXIT
      END
 05616, 17745

,KP (00.03)
NEQ 000 003 0020120
P   000 124 0020001
X1  000 126 0020310
Y1  000 746 0020310
Y2  0001566 0020310
Y3  0002436 0020310
X11 0003226 0020106
Y11 0003442 0020106
Y22 0003656 0020106
Y33 0004872 0020106
G   0017764
BLNK     17762
PRD 0017760
STAR     17756
EQ  0017754
PLUS     17752
COM 0017750
EXE 0017746
/00999   04321
/00998    4324
/00997   04356
/00996   04404
/00995   04431
/00994   04457
/00993   04471
/00992   04509
/00991    4512
/00990   04515
/00989   04528
/00988   04535
N1  0004306
+00003   04307
/00001   04644
A   0004310
B   0004312
DELTA     4314
H   0004316
Y   000466
/00002   0472
/00100   05614
NH  0004662
I   0004666
-00001    4667
-00001    4467
E   0004672
5.0 0004674
,IR 0144676  EXT PROG
SQRTF   144700  EXT PROG
2.0 0004712
,AY 0104704  EXT PROG
/00010   05032
X   0005 34
```

```
J    0005136
+00000    05037
N    0005140
NN   0005141
/00015    05100
YO   0005142
/00030    05102
FNCT     105044   EXT PROG
F    0005146
ZK1  0005150
XH   0005152
ZK2  0005154
ZK3  0005156
ZK4  0005160
/00050    05165
6.0  0005200
D    0005202
1.0  0005204
EXPF     145206   EXT PROG
V    0005210
Z    0005214
/00070    05304
/00076    05337
/00078    05346
/00079    05354
0.0  0005220
/00080    05373
/00090    05377
S    0005222
MN   0005224
58.0      05410
/00096    05551
/00092    05446
SCALE     05412
NM   0005414
L    0005415
K    0005416
-00002    05417
JJ   0005420
/00094    05524
NP   0005422
/00098    05604
J1   0005423
/00097    05565
PLOTT    105424   EXT PROG
EXIT     105426   EXT PROG
```

```
PLOTT          04300
FNCT           06370
,KP            06504
EXIT           14320
SQRTF          14340
,IR            14410
ABSF           14476
LOGF           14516
EXPF           14604
,AY            14762
,ST            15100
.LOAD LIMITS 15145,    17745
```

ON THE INTERVAL U= 0.0000 TO U= 20.0000 WITH STEP SIZE =0.200000

THE TOTAL NUMBER OF INTERVALS FOR THIS PROBLEM IS 100

THE DEGREE OF IONIZATION FOR THIS PROBLEM IS G= 0.0500

THE EXPECTED ERROR FOR THIS PROBLEM IS E=(+OR-) 0.31999996E-03

U=NORMALIZED DISTANCE FROM JUNCTION
Y=NORMALIZED ELECTRON POTENTIAL
V=NORMALIZED SPACE CHARGE DENSITY
W=SCHOTTKY APPROXIMATION FOR V

U	Y	V
.0000000	60.00000000	
.2000000	57.88544110	1.00000000
.4000000	55.81088220	1.00000000
.6000000	53.77632340	1.00000000
.8000000	51.78176450	1.00000000
1.0000000	49.82720570	1.00000000
1.2000000	47.91264680	1.00000000
1.4000000	46.03808800	1.00000000
1.6000000	44.20352910	1.00000000
1.8000000	42.40897030	1.00000000
2.0000000	40.65441140	1.00000000
2.2000000	38.93985260	1.00000000
2.4000000	37.26529380	1.00000000
2.6000000	35.63073500	1.00000000
2.8000000	34.03617610	1.00000000
3.0000000	32.48161730	1.00000000
3.2000000	30.96705850	1.00000000
3.4000000	29.49249970	1.00000000
3.6000000	28.05794090	1.00000000
3.8000000	26.66338200	1.00000000
4.0000000	25.30882320	1.00000000
4.2000000	23.99426440	1.00000000
4.4000000	22.71970560	1.00000000
4.6000000	21.48514680	0.99999999
4.8000000	20.29058800	0.99999997
5.0000000	19.13602920	0.99999991
5.2000000	18.02147040	0.99999972
5.4000000	16.94691150	0.99999917
5.6000000	15.91235270	0.99999766
5.8000000	14.91779380	0.99999368
6.0000000	13.96323460	0.99998357
6.2000000	13.04867470	0.99995899
6.4000000	12.17411300	0.99990167
6.6000000	11.33954720	0.99977349
6.8000000	10.54497190	0.99949875
7.0000000	9.79037563	0.99893456
7.2000000	9.07573494	0.99782523
7.4000000	8.40100406	0.99573872
7.6000000	7.76609726	0.99198973
7.8000000	7.17086121	0.98556724
8.0000000	6.61503444	0.97510387
8.2000000	6.09819286	0.95894403
8.4000000	5.61968424	0.93536874
8.6000000	5.17856088	0.90299029
8.8000000	4.77352563	0.86123036

9.0000000	4.40291005	0.81068663
9.2000000	4.06469852	0.75317845
9.4000000	3.75659978	0.69140161
9.6000000	3.47615281	0.62833644
9.8000000	3.22084401	0.56666858
10.0000000	2.98821345	0.50842300
10.2000000	2.77593549	0.45485896
10.4000000	2.58186948	0.40655608
10.6000000	2.40408354	0.36358749
10.8000000	2.24085804	0.32570041
11.0000000	2.09067604	0.29246392
11.2000000	1.95220643	0.26337331
11.4000000	1.82428385	0.23791585
11.6000000	1.70588840	0.21560783
11.8000000	1.59612629	0.19601236
12.0000000	1.49421241	0.17874544
12.2000000	1.39945500	0.16347535
12.4000000	1.31124229	0.14991866
12.6000000	1.22903122	0.13783483
12.8000000	1.15233777	0.12702043
13.0000000	1.08072879	0.11730378
13.2000000	1.01381513	0.10853994
13.4000000	0.95124584	0.10060648
13.6000000	0.89270322	0.09339975
13.8000000	0.83789873	0.08683184
14.0000000	0.78656939	0.08082791
14.2000000	0.73847484	0.07532408
14.4000000	0.69339474	0.07026562
14.6000000	0.65112660	0.06560544
14.8000000	0.61148387	0.06130290
15.0000000	0.57429433	0.05732273
15.2000000	0.53939867	0.05363422
15.4000000	0.50664927	0.05021051
15.6000000	0.47590910	0.04702801
15.8000000	0.44705078	0.04406591
16.0000000	0.41995577	0.04130575
16.2000000	0.39451362	0.03873111
16.4000000	0.37062127	0.03632733
16.6000000	0.34818255	0.03408124
16.8000000	0.32710756	0.03198099
16.9999999	0.30731226	0.03001585
17.2000000	0.28871801	0.02817610
17.4000000	0.27125119	0.02645290
17.6000000	0.25484284	0.02483815
17.8000000	0.23942836	0.02332445
18.0000000	0.22494717	0.02190502
18.2000000	0.21134246	0.02057358
18.3999999	0.19856097	0.01932438
18.6000000	0.18655271	0.01815206
18.8000000	0.17527077	0.01705170
18.9999999	0.16467112	0.01601869
19.2000000	0.15471242	0.01504879
19.4000000	0.14535586	0.01413802
19.6000000	0.13656501	0.01328268
19.8000000	0.12830563	0.01247934
19.9999999	0.12054558	0.01172476

PLOT SUBROUTINE

50 VALUES OF DY/DU[+], V[=], W[+] ARE PLOTTED AGAINST 50 VALUES OF U[.] SCALE FACTOR =

0.782E+00

U[.]	DY/DU[+]	V[=]	W[+]
0.200E+00	0.579E+02	0.579E+02	0.579E+02
0.600E+00	0.538E+02	0.579E+02	0.579E+02
0.100E+01	0.498E+02	0.579E+02	0.579E+02
0.140E+01	0.460E+02	0.579E+02	0.579E+02
0.180E+01	0.424E+02	0.579E+02	0.579E+02
0.220E+01	0.389E+02	0.579E+02	0.579E+02
0.260E+01	0.356E+02	0.579E+02	0.579E+02
0.300E+01	0.325E+02	0.579E+02	0.579E+02
0.340E+01	0.295E+02	0.579E+02	0.579E+02
0.380E+01	0.267E+02	0.579E+02	0.579E+02
0.420E+01	0.240E+02	0.579E+02	0.579E+02
0.460E+01	0.215E+02	0.579E+02	0.579E+02
0.500E+01	0.191E+02	0.579E+02	0.579E+02
0.540E+01	0.169E+02	0.579E+02	0.579E+02
0.580E+01	0.149E+02	0.579E+02	0.579E+02
0.620E+01	0.130E+02	0.579E+02	0.579E+02
0.660E+01	0.113E+02	0.579E+02	0.579E+02
0.700E+01	0.979E+01	0.578E+02	0.579E+02
0.740E+01	0.840E+01	0.576E+02	0.579E+02
0.780E+01	0.717E+01	0.570E+02	0.579E+02
0.820E+01	0.610E+01	0.555E+02	0.579E+02
0.860E+01	0.518E+01	0.523E+02	0.579E+02
0.900E+01	0.440E+01	0.469E+02	0.579E+02
0.940E+01	0.376E+01	0.400E+02	0.579E+02
0.980E+01	0.322E+01	0.328E+02	0.579E+02
0.102E+02	0.278E+01	0.263E+02	0.579E+02
0.106E+02	0.240E+01	0.210E+02	0.579E+02
0.110E+02	0.209E+01	0.169E+02	0.000E+00
0.114E+02	0.182E+01	0.138E+02	0.000E+00
0.118E+02	0.160E+01	0.113E+02	0.000E+00
0.122E+02	0.140E+01	0.946E+01	0.000E+00
0.126E+02	0.123E+01	0.798E+01	0.000E+00
0.130E+02	0.108E+01	0.679E+01	0.000E+00
0.134E+02	0.951E+00	0.582E+01	0.000E+00
0.138E+02	0.838E+00	0.503E+01	0.000E+00
0.142E+02	0.738E+00	0.436E+01	0.000E+00
0.146E+02	0.651E+00	0.380E+01	0.000E+00
0.150E+02	0.574E+00	0.332E+01	0.000E+00
0.154E+02	0.507E+00	0.291E+01	0.000E+00
0.158E+02	0.447E+00	0.253E+01	0.000E+00
0.162E+02	0.395E+00	0.224E+01	0.000E+00
0.166E+02	0.348E+00	0.197E+01	0.000E+00
0.170E+02	0.307E+00	0.174E+01	0.000E+00
0.174E+02	0.271E+00	0.153E+01	0.000E+00
0.178E+02	0.239E+00	0.135E+01	0.000E+00
0.182E+02	0.211E+00	0.119E+01	0.000E+00
0.186E+02	0.187E+00	0.105E+01	0.000E+00
0.190E+02	0.165E+00	0.927E+00	0.000E+00
0.194E+02	0.145E+00	0.818E+00	0.000E+00
0.198E+02	0.128E+00	0.722E+00	0.000E+00

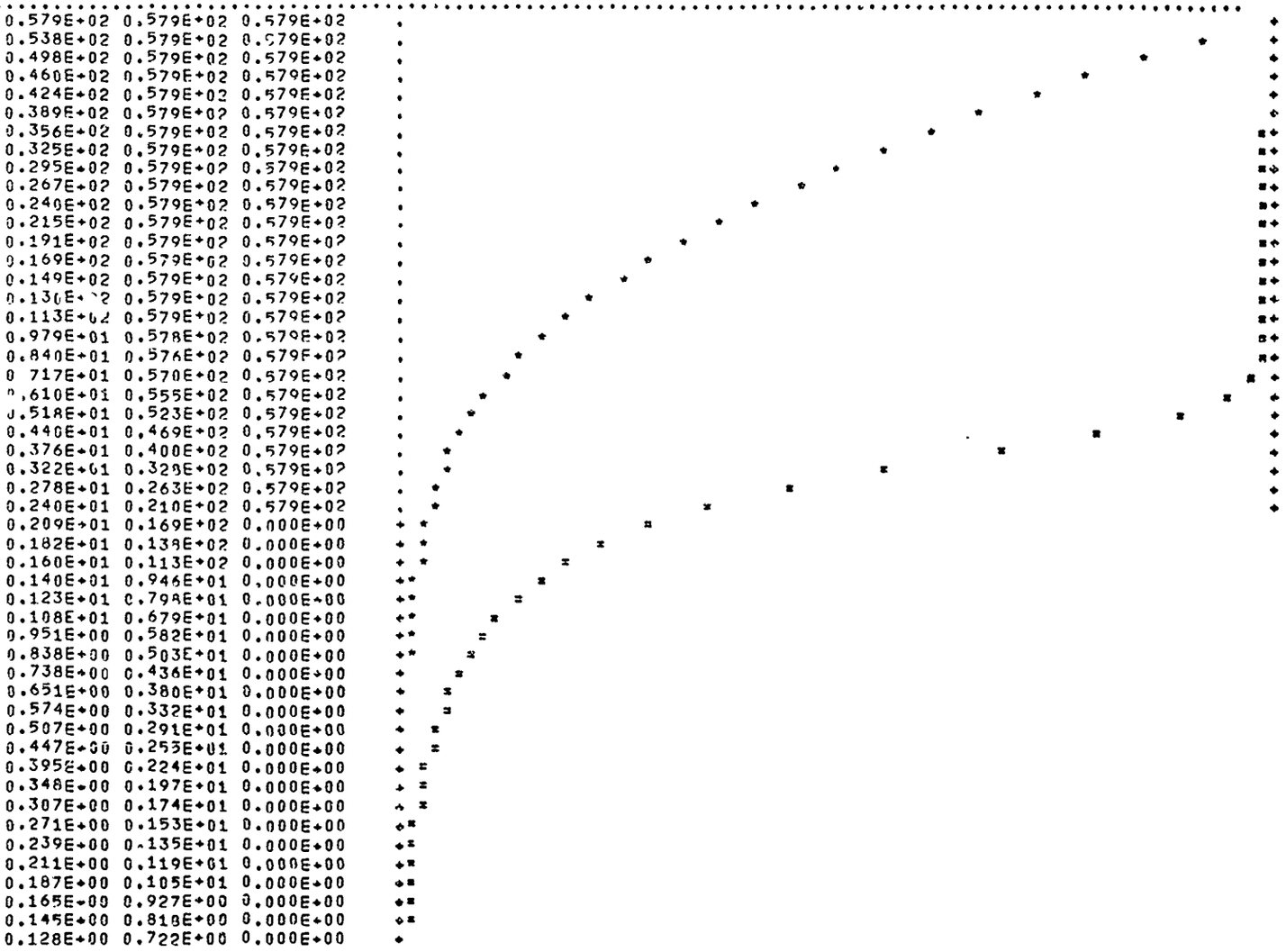

SOLUTION TO DY/DU=F

UNCLASSIFIED

Security Classification

DOCUMENT CONTROL DATA - R & D

(Security classification of title, body of abstract and indexing annotation must be entered when the overall report is classified)

1. ORIGINATING ACTIVITY (Corporate author)
Arizona State University
Electrical Engineering Department
Tempe, Arizona 85281

2a. REPORT SECURITY CLASSIFICATION
UNCLASSIFIED

2b. GROUP

3. REPORT TITLE

A STUDY OF THE METAL-SEMICONDUCTOR (N-TYPE) RECTIFYING CONTACT

4. DESCRIPTIVE NOTES (Type of report and inclusive dates)
Scientific Interim

5. AUTHOR(S) (First name, middle initial, last name)
Bryn Allen Lindsey
Thomas A DeMassa

6. REPORT DATE
May 1969

7a. TOTAL NO. OF PAGES
181

7b. NO. OF REFS
45

8a. CONTRACT OR GRANT NO. F44620-69-C-0025

b. PROJECT NO. 7921-01

c. 6144501F

d. 681314

9a. ORIGINATOR'S REPORT NUMBER(S)
Technical Report No. 1

9b. OTHER REPORT NO(S) (Any other numbers that may be assigned this report)
AFOSR 69-1224TR

10. DISTRIBUTION STATEMENT
1. This document has been approved for public release and sale; its distribution is unlimited.

11. SUPPLEMENTARY NOTES
TECH, OTHER

12. SPONSORING MILITARY ACTIVITY
AF Office of Scientific Research (SREE)
1400 Wilson Boulevard
Arlington, Virginia 22209

13. ABSTRACT

A theoretical study of metal-semiconductor (N-type) rectifying contacts is developed. This study begins by first analyzing previous models for this type of junction. Particular attention is given to the Schottky model and to the approximations it contains. This model is then improved upon by taking into account nonuniform impurity ionization and the free electron concentration in the depletion region. Using this more exact model a theoretical expression for the differential junction capacitance is calculated. The results indicate that the junction capacitance as a function of reverse bias can be used to accurately predict the doping concentration in the semiconductor material, but does not yield a correct measurement of the equilibrium diffusion potential or barrier height.

The current voltage characteristic for this type of contact is also discussed. An expression for the I-V characteristic of this junction is derived based upon a diffusion model. This expression is then improved upon by accounting for tunneling and quantum-mechanical reflection of carriers at the junction.

DD FORM 1 NOV 65 1473

UNCLASSIFIED

Security Classification

UNCLASSIFIED

Security Classification

14 KEY WORDS	LINK A ROLE	LINK A WT	LINK B ROLE	LINK B WT	LINK C ROLE	LINK C WT
Semiconductor						
N-Type Metal Contacts						
Junction Capacitance						
Metal Contact Model						

Security Classification